Heparan sulfates as regulators of articular cartilage integrity and cell-matrix interactions

Inaugural Dissertation

for the

Doctoral Degree

Dr. rer. nat.

from the Faculty of Biology

at the University of Duisburg-Essen

submitted by

Ann-Christine Severmann

from Kamen

August, 2020

The experiments underlying the present work were conducted at the Department of Developmental Biology, Centre for Medical Biotechnology, University of Duisburg-Essen.

1. Examiner: Prof. Andrea Vortkamp
2. Examiner: Prof. Perihan Nalbant
3. Examiner: Prof. Brian Johnstone

Chair of the Board of Examiners: Prof. Gero Hilken

Date of the oral examination: 05.02.2021

DOI: 10.17185/duepublico/74077
URN: urn:nbn:de:hbz:465-20240325-123623-7

Table of Contents

List of Abbreviations

AC	articular cartilage
ACLT	anterior cruciate ligament transection
ADAMTS	A Disintegrin and Metalloproteinase with Thrombospondin motifs
AMOT	Angiomotin
APS	Ammonium Peroxide di-Sulfate
Arp	Actin related Protein
BSA	Bovine Serum Albumin
BMP	Bone Morphogenetic Protein
CHO	Chinese Hamster Ovary
Col1	collagen type I
Col10	collagen type X
Col2	collagen type II
CS	chondroitin sulfate
d	days
DAPI	4′,6-diamidino-2-phenylindole
DMEM	Dulbecco’s Modified Eagle’s Medium
DMM	destabilisation of the medial meniscus
DMSO	Di-methylsulfoxide
dNTPs	Deoxyribonucleotide triphosphates
DPBS	Dulbecco's Phosphate-Buffered Saline
DS	dermatan sulfate
DTT	Dithioerythritol
E	embryonic day
ECM	extracellular matrix
EDTA	Ethylendiamintetraacetate
ERK	Extracellular signal-Regulated Kinase
EtOH	Ethanol
EXT	Exostosin Glycosyltransferase
EXTL	Exostosin Like Glycosyltransferase
FA	Focal Adhesion
FAK	Focal Adhesion Kinase
FC	Focal Complex
FCS	Fetal calf serum
FGF	Fibroblast Growth Factor

FGF-R	FGF Receptor
FH	Femoral Head
GAG	glycosaminoglycan
Gal	galactose
GalNAc	N-acetylgalactosamine
GlcA	glucuronic acid
Glce	glucuronic acid-C5-epimerase
GlcNAc	N-acetylglucosamine
GP	growth plate
h	hour
HDI	highest density interval
Hh	Hedgehog
HS	Heparan Sulfate
HS2St	heparan sulfate 2O-sulfotransferase
HS3St	heparan sulfate 3O-sulfotransferase
HS6St	heparan sulfate 6O-sulfotransferase
IdoA	iduronic acid
Ihh	Indian Hedgehog
kgbw	kg body weight
KS	keratan sulfate
LATS	Large tumour suppressor kinase
LP	link protein
LRP-1	Low Density Lipoprotein Receptor-related Protein 1
m	months
MAPK	Mitogen-Activated Protein Kinase
MEF	Murine Embryonic Fibroblast
MHCII	Myosin Heavy Chain Type II
min	minute
MMP	Matrix Metalloprotease
MO	Multiple Osteochondroma Syndrome
MT-MMP	membrane-type matrix metalloproteinase
NDST	N-deacetylase/sulfotransferase
OA	osteoarthritis
oN	over night
P	post-natal day

PBS	Phosphate Buffered Saline
PCR	Polymerase Chain Reaction
PFA	Paraformaldehyde
PG	proteoglycan
Prg4	Proteoglycan 4
qPCR	quantitative polymerase chain reaction
RA	retinoic acid
RT	Room Temperature
Sdc	Syndecan
SDS	Sodium dodecyl sulfate
SF	stress fibre
SN	supernatant
Sox9	sex determining region - box transcription factor 9
Src	Sarcoma Proto-Oncogene Non-Receptor Tyrosine Kinase
Sulf	Sulfatase
Surfen	bis-2-methyl-4-amino-quinolyl-6-carbamide
TAE	Tris Acetatae EDTA buffer
TBS	Tris Buffered Saline
TEMED	Tetra-methylethylendiamin
TIMP	tissue inhibitor of metalloproteinases
TPS	Total Protein Staining
VE	purified water
w	weeks
YAP	Yes-Associated Protein

List of Figures

List of Tables

In the context of this study the following article was published, containing Figures 9, 10 and 11 or similar images.

Severmann, A.C., Jochmann, K., Feller, K., Bachvarova, V., Piombo, V., Holzer, T., Brachvogel, B., Stange, R., Pap, T., Esko, J. D., Hoffmann, D., Vortkamp, V., 2020, *An altered heparan sulfate structure in the articular cartilage protects against osteoarthritis*, Osteoarthritis and Cartilage

Author contributions:

Conception - 5%: This study was originally designed by AV, VP and KJ. The experiment for Figure 4E was outlined by ACS.

Conduction of experimental work - 10%: Most experiments were done by KJ. The immunostaining for Figure 1E was conducted by ACS, and one repetition each of the experiments shown in Figure 4C and 4F were performed by ACS. Additionally, the qPCR for Mmp2 in Figure 3 was conducted by Yvonne Krause under the supervision of ACS and the zymogrammes for Figure 4E were done by KF under the supervision of ACS.

Data analysis - 15%: The data obtained from experiments conducted by KJ were analysed by KJ. Experiments conducted by YK, KF and ACS were assessed by ACS.

Statistical analysis - 30%: All statistical calculations were performed by DH. The collected data was assembled for statistical analysis by ACS and all presented graphs were arranged by ACS.

Writing the manuscript - 80%: The original draft of the manuscript was written by ACS and improved by AV. All Figures and Tables were prepared by ACS.

Revision of the manuscript - 40%: All authors proof-read the manuscript. Critical alterations were made by AV and ACS.

1. Introduction

The vertebrate skeleton executes numerous functions: It enables longitudinal growth, is the location of adult haematopoiesis, serves calcium- and phosphate metabolism, supports and protects internal organs and, at the same time, enables movement. Therefore, the regulation of bone development, growth and remodelling is crucial for the viability of vertebrate organisms. The skeleton is comprised of more than 200 individual bones which are interconnected by ligaments, tendons and muscles. It is subdivided in craniofacial skeleton, including the bones of skull and face, axial skeleton, consisting of spine and rib cage, and appendicular skeleton, containing the bony elements of limbs, shoulders and pelvic girdle (Clarke, 2008).

During embryonic development, bones are created by two distinct processes. The craniofacial skeleton and parts of the clavicle are formed by intramembranous ossification. During this process, osteoblasts are derived directly from mesenchymal progenitors. In contrast, the bones of the axial and appendicular skeleton are formed by endochondral ossification. Mesenchymal progenitor cells condensate as well, but differentiate into chondrocytes and give rise to a cartilaginous template which is later replaced by bone (Benninghoff & Zeneker, 1994).

1.1. Endochondral Ossification and Chondrocyte Differentiation

The transcription factor sex determining region - box transcription factor 9 (Sox9) Sox9 is considered a master regulator of chondrocyte differentiation. Sox9-deficient cells (*Sox9*$^{-/-}$) cannot be incorporated into cartilage anlagen *in vivo* (Bi *et al.*, 1999) and limb-specific loss of Sox9 function in *Prx1-Cre;Sox9*$^{fl/fl}$ mice fully abrogates the formation of cartilage anlagen (Akiyama *et al.*, 2002). At embryonic day 11.5 (E11.5) of murine development mesenchymal cells expressing Sox9 start to condensate (Fig. 1, a) (Kozhemyakina *et al.*, 2015). Cells from the outer layer of the condensation become fibroblastoid and form the perichondrium, while cells within the condensation differentiate into chondrocytes (Fig. 1, b). In these cells, Sox9 induces the expression of cartilage-specific *collagen type II* (*Col2*). Towards the centre of the cartilage anlage the chondrocytes undergo further differentiation. By E15.5 five functionally different populations of chondrocytes can be distinguished morphologically: distal resting chondrocytes, round proliferating chondrocytes, columnar fast-proliferating

chondrocytes, pre-hypertrophic and hypertrophic chondrocytes (Fig. 1, c). In the prospective diaphysis of the cartilage anlage hypertrophic chondrocytes exit the cell cycle and become post-mitotic. They produce a mineralised matrix containing collagen type X (Col10) that serves as a template for the disposition of bone matrix. Additionally, proteases degrading the chondrocyte-specific ECM, such as the collagenase Matrix Metalloprotease 13 (Mmp13) are expressed and degrade the cartilaginous matrix. Most hypertrophic chondrocytes undergo apoptosis and thus make room for osteoblasts, which produce bone matrix containing collagen type I (Col1). Osteoblasts can be derived through trans-differentiation from hypertrophic chondrocytes or brought into the anlage by invading blood vessels (Fig. 1, d). In addition to the primary ossification centre established at E15.5, secondary ossification centres arise at the epiphyseal ends of the cartilage template around post-natal day 7 (P7). Between the two ossified regions a cartilaginous zone remains, which is called the growth plate (GP). It is comprised of the described chondrocyte populations and enables longitudinal growth of the skeletal element by cell proliferation and matrix deposition (Fig. 1, e) (Kozhemyakina *et al.*, 2015; Ortega *et al.*, 2004; Wuelling and Vortkamp, 2011).

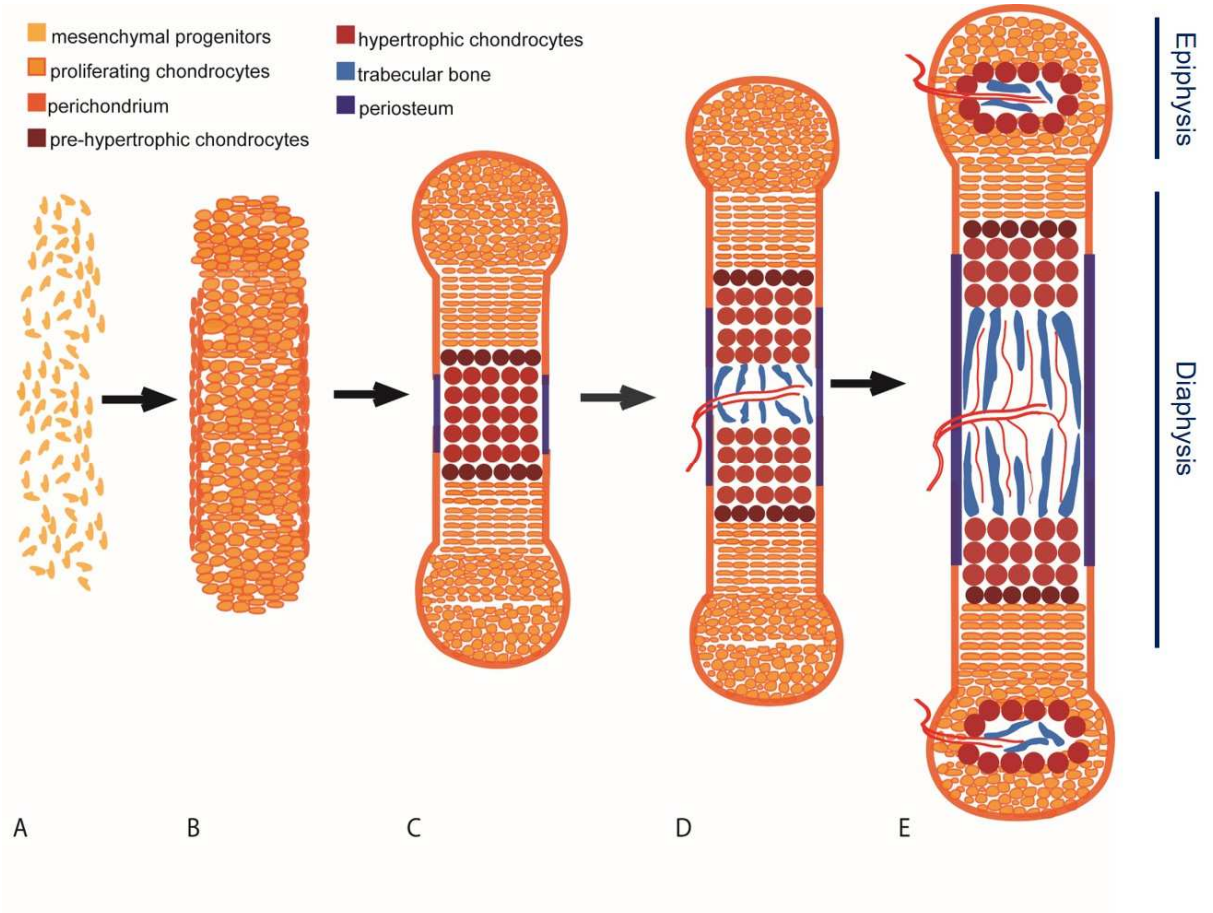

Figure 1: Sequence of endochondral ossification during murine development At E11.5 mesenchymal progenitor cells condense (A) and give rise to chondrocytes and perichondrial cells (B). Starting at E13.5, chondrocytes undergo differentiation in the prospective diaphysis. Morphologically distinct chondrocyte populations of different differentiation stages can be identified: distal resting chondrocytes (C). In centre of the anlage the cartilage template is replaced by bone forming the primary ossification centre around E15.5 (D). Secondary ossification centres are established postnatally at the epiphyseal ends of the cartilage anlage. Between the ossified regions a cartilaginous GP remains, enabling longitudinal growth of the skeletal element (E). Modified from (Severmann and Vortkamp, 2015).

1.2. Synovial Joints

In addition to the GP, another cartilage population persists covering bone surfaces in synovial joints. In general, three types of joints can be distinguished regarding the degree of allowed movement. Synarthroses, such as the sutures of the vertebrate skull, allow little movement and consist of closely connected bone elements typically linked by fibrous tissue. In amphiarthroses, the bone elements are connected by cartilaginous tissue and slight movement is permitted, for example in intervertebral discs. Lastly, diarthroses are freely movable joints composed of a fibrous joint

capsule lined by the synovial membrane, a joint cavity filled with synovial fluid and cartilage-covered epiphyseal bone surfaces (Benninghoff & Zenker, 1994).

The largest diarthrosis of the vertebrate skeleton is the knee joint (*Articulatio genus*), which is comprised of two distinct articulations: the femoro-patellar and the femoro-tibial joint, of which the latter is weight bearing (Figure 2). Two femoral condyles articulate with respective tibial plateaus. The four contact faces are covered with articular cartilage (AC), which acts as an absorber for sheering stress and shocks. Between the joint surfaces, two fibrocartilaginous menisci are found, providing additional pressure resistance. The medial meniscus is connected to an intercondylar position on the tibia by the medial menisco-tibial ligament while the lateral meniscus is held in place by the lateral menisco-tibial ligament. The stability of the femoro-tibial joint is ensured by the connection of its bone elements by ligaments. The anterior cruciate ligament (*Ligamentum cruciatum anterius*) links a lateral posterior position on the femur with an anterior medial position on the tibia. The posterior cruciate ligament (*Ligamentum cruciatum posterius*) proceeds from superior anterior medial towards inferior posterior lateral. The two cruciate ligaments prevent a displacement of femur and tibia along the dorso-ventral axis. Additionally, the femur is connected to the fibula by the lateral collateral ligament (*Ligamentum collaterae laterale*) and to the tibia by its medial counterpart (*Ligamentum collaterate mediale*) detaining shifts along the medio-lateral axis. Anatomically, the tibio-fibular joint is also part of the knee, although it is enclosed by a separate joint capsule (Hunziker *et al.*, 1992) (Benninghoff & Zenker, 1994).

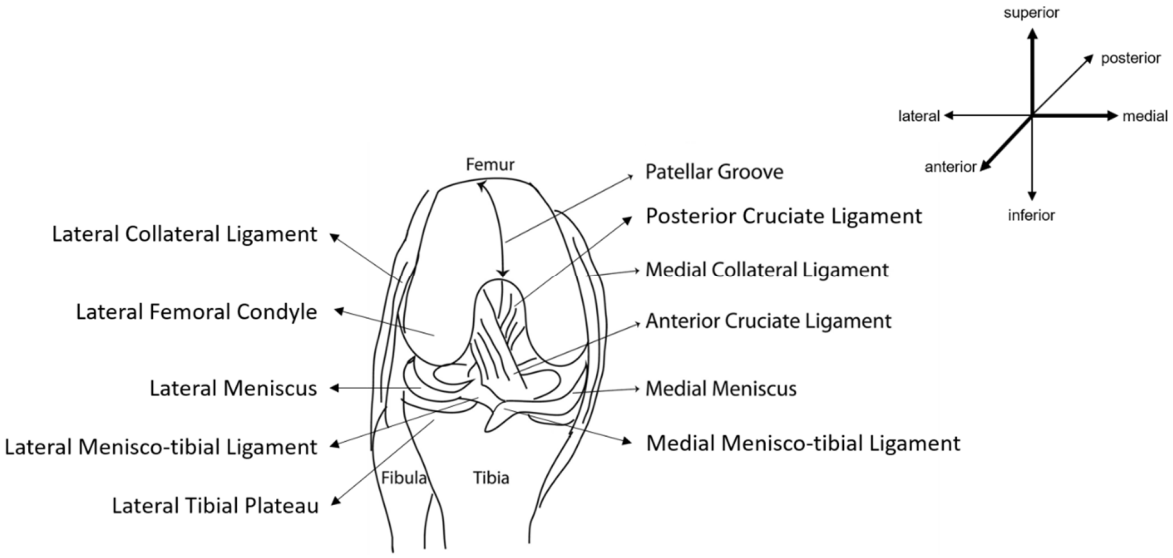

Figure 2: Anatomy of the knee joint The knee comprises three individual articulations: The tibio-fibular, the femoro-patellar and the femoro-tibial joint, of which the latter is weight bearing. Within the femoro-tibial joint two femoral condyles articulate with respective tibial plateaus, all of which are covered with AC. In the weightbearing areas, fibro-cartilaginous menisci are found, which are connected to the tibia by the medial and lateral menisco-tibial ligaments. In the centre of the joint femur and tibia are connected by the cruciate ligaments, prohibiting translational movement along the dorso-ventral body axis. Along the medio-lateral axis, the knee joint is stabilised by the medial and lateral collateral ligaments. Modified from (Piombo, 2017).

1.3. Articular Cartilage

Cartilaginous tissue is aneural and avascular. It contains a relatively low cell number but a high amount of extracellular matrix (ECM), giving it low regenerative capacity. Cartilage ECM is mainly composed of collagen fibres, providing tensile strength, and proteoglycans (PGs). The PGs content generates a high osmotic pressure binding water within the tissue and an elastic gel is created giving the cartilage its compressive features. Cartilage tissue can be divided into three subtypes: Elastic cartilage contains not only Col2 but also a high amount of elastic fibres giving it great flexibility. It can be found in structures that undergo repeated bending such as larynx or outer ear. Fibrocartilage is a mixture of fibrous and cartilaginous tissue and is rich in Col1 and 2 fibres, making it the most stable cartilage type. It is present in places with high exposure to compressive loads, e.g intervertebral discs and menisci. Hyaline cartilage is less abundant in fibres and constitutes the cartilage anlagen of endochondral bones and the AC in synovial joints (Benninghoff & Zenker, 1994; Lüllmann-Rauch, 2009) (Fox *et al.*, 2009).

Morphologically distinct layers can be distinguished within the AC, termed superficial, middle and deep zone (Figure 3). The articular surface is not covered by a

perichondrium, but the superficial layer is in direct contact to the synovial fluid. This zone contains small, flattened chondrocytes synthetizing Proteoglycan 4 (Prg4), which lubricates the articular surface. Col2 and 9 fibres are aligned parallel to the surface making this zone particularly sheer resistant. Below, the middle or transitional zone is found, which contains a low density of spherical chondrocytes and more randomly organised collagen fibres. This zone comprises a higher PG content making it more pressure resistant and it bridges the superficial to the deep zone, which is the most pressure resistant zone of the AC. The deep zone contains collagen fibres of higher diameter which are radially distributed. The chondrocytes are typically organised in columns along these fibres and thus perpendicular to the joint surface. Below the deep zone the tide mark can be identified, which marks the transition from hyaline to calcified cartilage matrix and anchors the cartilaginous tissue to the subchondral bone plate. This zone contains few but relatively large chondrocytes (Decker *et al.*, 2014; Fox *et al.*, 2009).

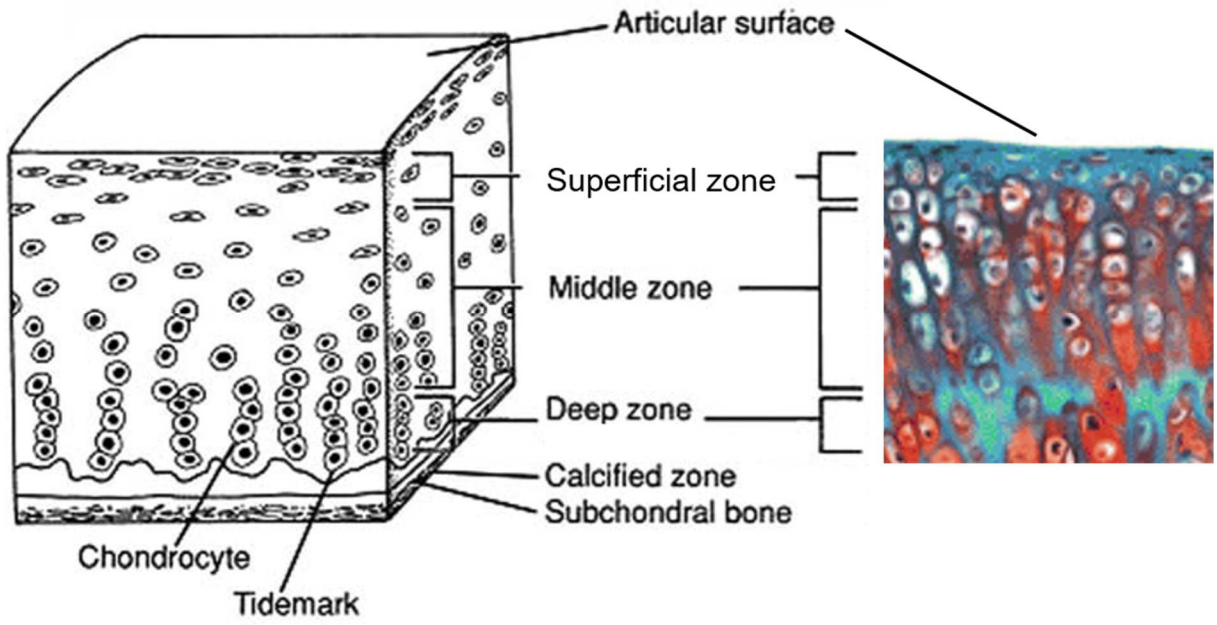

Figure 3: Articular cartilage structure The AC is comprised of morphologically and functionally distinct regions. The superficial zone is in contact with the synovial fluid of the joint cavity. It contains flattened chondrocytes producing Prg4 to reduce surface friction. The middle zone contains few, spherical chondrocytes and higher amounts of PGs, as highlighted by Safranin O staining, making it more pressure resistant. Within the deep zone, few but large chondrocytes are found. This zone contains thicker collagen fibres and is the most pressure resistant zone of the AC. Below, the tide mark is found, designating the transition from hyaline to calcified cartilage matrix. It bridges the cartilaginous tissue to the subchondral bone plate. Modified from (Decker *et al.*, 2015; Fox *et al.*, 2009).

1.4. Osteoarthritis

Osteoarthritis (OA) is a degenerative disorder of synovial joints. It is characterised by an accumulating deterioration of the AC, which was originally thought to be induced by trauma or age-related wear-and-tear. The degeneration of the AC may ultimately lead to a complete loss of joint function accompanied by severe chronic pain. Although it is the most prevalent degenerative joint disease worldwide, the underlying molecular mechanisms of OA pathogenesis are not completely understood and there is no causal treatment available. Currently, the patients' symptoms are relieved using analgesic or anti-inflammatory medication, physiotherapy or joint replacement surgery. The pathological changes seen in OA not only comprise abrasion of the AC but also inflammation of the synovial tissue and joint capsule, damage to menisci, ligaments, muscles and tendons of the joint, alterations of subchondral bone structure and the emergence of osteophytes, bony outgrowths compensatorily increasing the articular surface (Figure 4). OA is most commonly seen in highly loaded joints within hands, feet, hips or knees, but can potentially occur in any diarthrosis. Patients may have one or several joints affected. Known risk factors for OA are age, obesity, trauma and joint malformations (Loeser *et al.*, 2012; Wieland *et al.*, 2005). After menopause, women are more often affected than men, suggesting a role of endocrine, sex-dependent factors in the development of OA (Stevens-Lapsley and Kohrt, 2010).

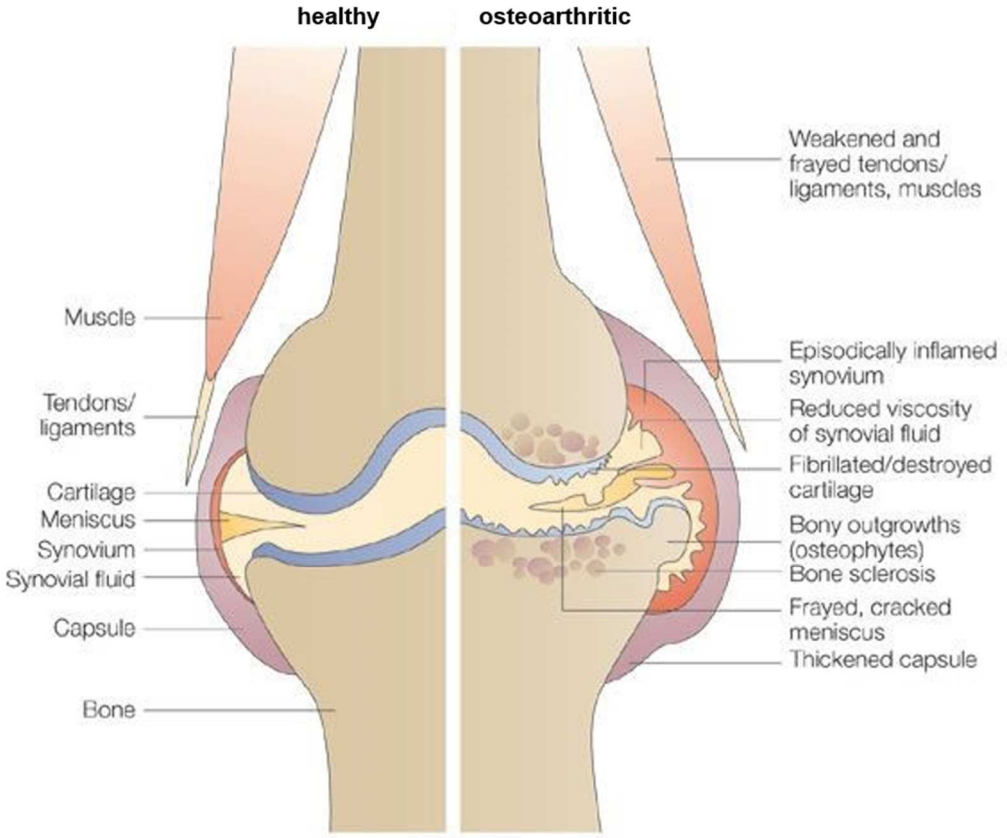

Figure 4: Pathological changes in osteoarthritic joints OA is considered a disease of the whole joint and all anatomical structures participating in the joint can be affected. This includes abrasion of the menisci and AC, especially in weight bearing areas, structural alterations of the subchondral bone plate, ligaments, tendons and muscles affiliated to the joint, formation of osteophytes, thickening of the joint capsule, inflammation of the synovial membrane and an aberrant composition of the synovial fluid. Modified from (Wieland *et al.*, 2005).

1.4.1. Mouse Models of Osteoarthritis

Animal models are commonly used to investigate the processes taking place during OA development. The anatomy of the knee joints of lager laboratory animals, such as pig or sheep, is rather similar to that of human knees, but those animals do not allow the generation of genetically modified strains. Transgenic mice enable the investigation of OA not only under physiological conditions but also give insight into the role of specific factors. Numerous strategies have been developed to analyse OA progression in mouse models. Since age is a known risk factor for the development of OA, the most straight-forward approach is to analyse joints of aged mice. Still, even if the life span of a mouse is limited, this requires an extensive time period. Forced exercise can be administered to accelerate the natural onset of the disease,

but mild to moderate exercise has also been shown to be protective against OA, so the exercise scheme must be carefully chosen. OA may also be triggered by intra-articular injection of factors increasing matrix degradation or joint inflammation. To model the post-traumatic onset of OA, several surgical models have been proposed resulting in different degrees of severity. Since the knee joint is the largest and best accessible diarthrosis of the vertebrate skeleton, it is targeted in surgical approaches allowing precise operation procedures in mice. For example, destabilisation of the medial meniscus (DMM) by dissection of the medial menisco-tibial ligament results in mild to moderate OA in the weight bearing region of the joint. In contrast, the transection of the anterior cruciate ligament and the medial collateral ligament in the anterior cruciate ligament transection (ACLT) model results in moderate to severe OA (Fang and Beier, 2014; Piombo, 2017; Thysen *et al.*, 2015).

1.4.2. Molecular Mechanisms Underlying the Progression of Osteoarthritis

Under physiological conditions cartilage matrix undergoes slow but constant remodelling. In OA, the balance between anabolic and catabolic processes is shifted towards degradation. ECM components can be digested by members of the A Disintegrin and Metalloproteinase with Thrombospondin motifs (ADAMTS) and MMP families. 19 secreted endopeptidases belonging to the ADAMTS family are known in humans. ADAMTS are classified into four groups by their major substrates: Aggrecanases or proteoglycanases (1, 4, 5, 8, 9, 15 and 20), pro-collagen N-propeptidases (2, 3 and 14), cartilage oligomeric matrix protein-cleaving enzymes (7 and 12) and von-Willebrand Factor proteinase (13). Six ADAMTS remain orphaned, since their substrates are not yet known (6, 10, 16, 17, 18 and 19) (Kelwick *et al.*, 2015). ADAMTS4 and 5 have been shown to be involved in the progression of OA in human patients (Fosang and Little, 2008). Although both are expressed in murine cartilage, Adamts5 seems to be of more fundamental significance for the maintenance of the AC. After surgical induction by DMM, *Adamts5*$^{-/-}$ mice develop less severe OA signs compared to wildtype controls (Glasson *et al.*, 2005), while *Adamts4*$^{-/-}$ animals show no altered OA progression when challenged with the same surgical approach (Glasson *et al.*, 2004). In general, during the development of OA ADAMTSs with aggrecanase activity, such as ADMTS4 and 5, are thought to break down ECM PGs and expose the collagen scaffold to degradation by other enzymes, for example MMPs (Kelwick *et al.*, 2015).

26 MMPs have been identified in human tissues (Sekhon, 2010), of which the first 13 were originally classified by their major substrates: Collagenases (1, 8, 13), gelatinases (2, 9), stromelysinases (3, 10, 11), a matrilysinase (7) and a metallo-elastanase (12). With the discovery of the first membrane-bound MMP (membrane-type MMP 1 (MT-Mmp1) or Mmp14), which activates MMP2, this classification scheme was discontinued (Parsons *et al.*, 1997). Increased mRNA expression of the collagenase MMP13, which degrades Col2, has been reported in human OA patients (Wieland *et al.*, 2005). Cartilage-specific overexpression of a constitutive active variant of human MMP13 resulted in accelerated OA progression in mice (Neuhold *et al.*, 2001). Accordingly, *Mmp13*$^{-/-}$ mice (Stickens *et al.*, 2004) show decreased cartilage erosion compared to wildtype animals after DMM surgery (Little *et al.*, 2009). In addition to MMP13, MMP3 is also highly expressed in human OA cartilage (Wieland *et al.*, 2005). Since this MMP is able to activate other MMPs, it is possible that it does not directly contribute to matrix decomposition but to the activation of other ECM degrading enzymes (Troeberg and Nagase, 2012). This hypothesis is supported by the finding that both aggrecan and Col2 neo-epitopes are reduced in osteoarthritic cartilage of *Mmp3*$^{-/-}$ mice in an inflammatory OA model (van Meurs *et al.*, 1999a; van Meurs *et al.*, 1999b). Contradictingly, it was reported that loss of Mmp3 accelerates the progression of OA in *Mmp3*$^{-/-}$ mice using a surgical model (Clements *et al.*, 2003). Similarly, *Mmp9*$^{-/-}$ mice develop increased OA after DMM (Glasson *et al.*, 2005) but are protected in an infectious arthritis model (Heilpern *et al.*, 2009). These findings highlight that the roles of the different Mmps during OA progression are versatile and not fully resolved yet.

1.5. Proteoglycans

PGs are composed of core proteins carrying one or more covalently-linked glycosaminoglycan (GAG) side chains. GAGs consist of repetitive disaccharide units consisting of a uronic acid and an amino sugar. Due to hydroxyl, carboxyl and especially sulfate groups GAG chains are negatively charged. HA is the only non-sulfated GAG, it is the main constituent of connective tissues and is composed of glucuronic acid (GlcA) and N-acetylglucosamine (GlcNAc). The sulphated GAGs are divided into four subgroups depending on the composition of their disaccharide units (Figure 5): Keratan sulfate (KS) is typically found in the cornea and consists of galactose (Gal) and GlcNAc. Dermatan sulfate (DS) is named after its presence in

the skin and contains GlcA, which may be epimerised to iduronic acid (IdoA), and N-acetylgalactosamine (GalNAc). Chondroitin sulfate (CS) is the most abundant GAG. It is found in most tissues and is composed of GlcA and GalNAc subunits. Heparan sulfate (HS) is synthesised by almost all animal cells. It contains GlcA and GlcNAc, and the uronic acid can be epimerised to IdoA. In cartilaginous tissue, CS is the most prominent GAG and also KS and HS are found (Bulow and Hobert, 2006) (Horton, 2008).

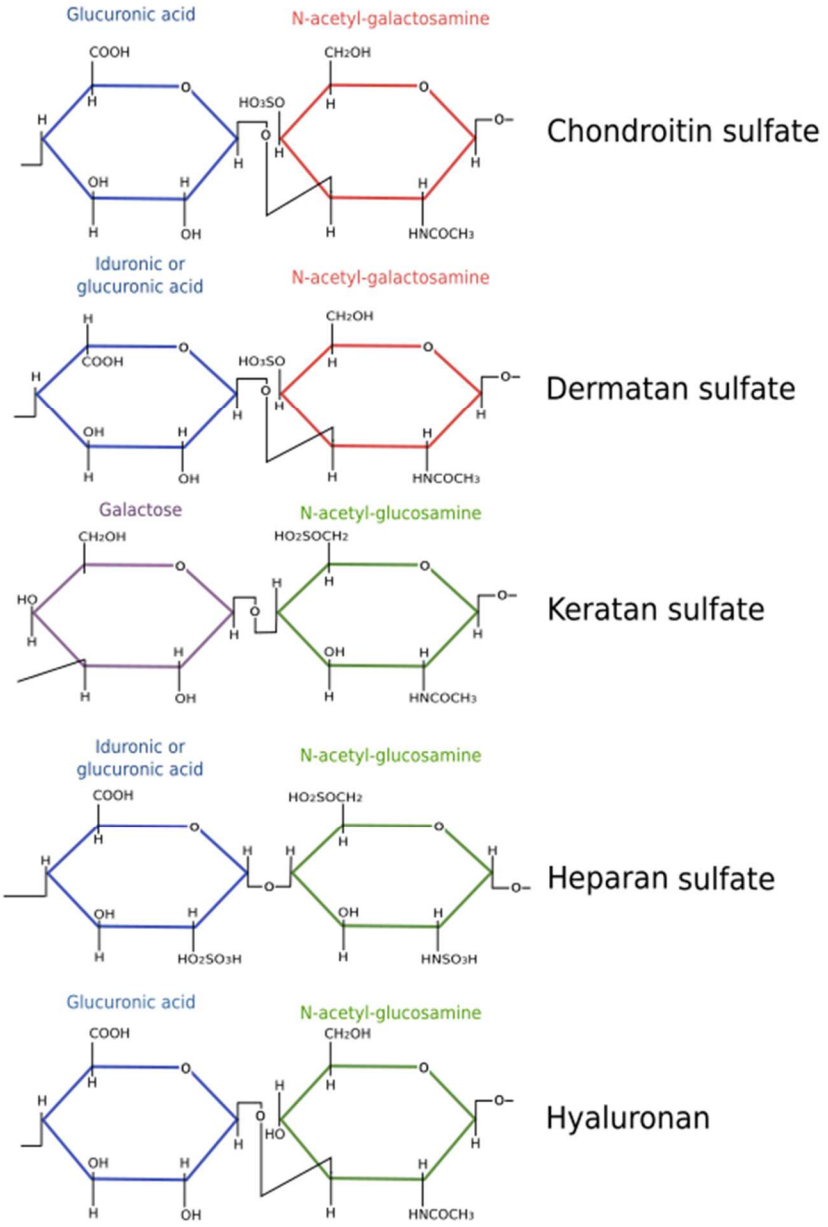

Figure 5: Molecular composition of GAG disaccharide subunits GAG polysaccharides contain disaccharide subunits composed of a uronic acid and an amino sugar. CS consists of GlcA and GalNAc, DS of GlcA or IdoA and GalNAc, KS of Gal and GlcNAc, HS of GlcA or IdoA and GlcNAc and HA of GlcA and GlcNAc. Structural formulas are represented in Haworth projection. Downloaded from Atlas of Plant and Animal Histology, Dep. of Functional Biology and Health Sciences, Faculty of Biology, University of Vigo, Spain; https://mmegias.webs.uvigo.es/02-english/5-celulas/2-componentes_glucidos.php (28.03.2020).

Depending on their core proteins, HSPGs can be found in the extracellular space (e.g. Perlecan) or on the cell membrane, tethered either by a transmembrane domain (Glypicans) or GPI-anchor (Syndecans). HS synthesis starts with the addition of a tetra-saccharide linker, consisting of Xylose-Gal-Gal-GlcA, to a serine residue of the core protein. The first GlcNAc is then added by the Exostosin-Like Glycosyltransferase 3 (Extl3) and alternating units of GlcA and GlcNAc are polymerised by a heterodimeric enzyme complex formed by Exostosin 1 and 2 (Ext1, Ext2). The growing polysaccharide chain can be modified by N-deacetylation and -sulfation of GlcNAc by members of the N-deacetylase/sulfotransferase family (Ndst1-4). This step is thought to be prerequisite for all further modifications, including the epimerisation of GlcA to IdoA by the GlcA-C5-epimerase (Glce), the 2O-sulfation of IdoA (Hs2st1) and the sulfation of GlcNAc in 3O- and 6O-position (Hs3st1-6 and Hs6st1-3). The expression of the HS-modifying enzymes is cell type-dependend, therefore a tissue-specific HS modification pattern is established (Bulow and Hobert, 2006; Esko and Selleck, 2002; Poulain and Yost, 2015) (Fig. 6).

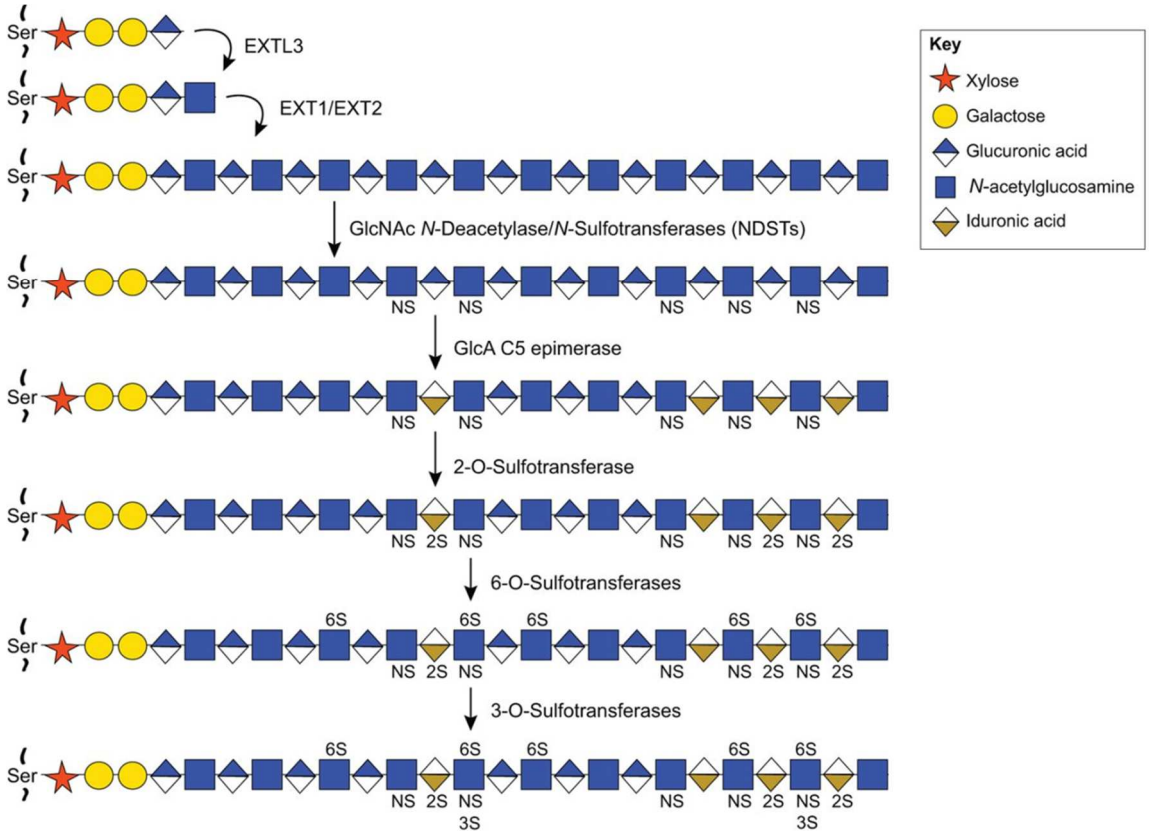

Figure 6: Heparan sulfate biosynthesis The synthesis of HS side chains starts with the addition of a tetrasaccharide linker to a serine residue of the core protein. The first GlcNAc is then added to the linker by Extl3, and the polysaccharide is elongated by the polymerisation of alternating GlcA and GlcNAc units by the Ext1/Ext2 complex. The growing chain can be modified by N-deacetylation and -sulfation of GlcNAc, epimerisation of GlcA to IdoA, 2O-sulfation of IdoA as well as 6O- and 3O-sulfation of GlcNAc. Modified from (Poulain and Yost, 2015).

1.5.1. Interaction of HSPGs with signalling molecules

Not only are HSPGs found everywhere in the vertebrate organism, they can also bind to a large variety of proteins. Binding occurs through electrostatic interactions, with the negatively charged carboxyl and sulfate groups of the HS chain interacting with positively charged amino acids, most often lysine and arginine. Many proteins have distinct HS-binding motifs, such as the Cardin-Weintraub sequence present in members of the Fibroblast Growth Factor (FGF) and Hedgehog (Hh) families. HS-binding may serve various functions: Tethering of signalling molecules to a specific position by HS increases their local concentration, HS can promote diffusion or sequester molecules, aid oligomerisation or act as a co-receptor. Additionally, HS-binding proteins may also be able to bind to other GAGs, such as CS or DS (Xu and Esko, 2014).

The signalling factors directing chondrocyte proliferation and differentiation within the GP are also HS-binding proteins. The interaction of HS with Fgfs has been described in great detail. Many FGF family members, such as Fgf1 and 2, and all Fgf Receptors (FGF-R) bind to HS. The polysaccharides bridge the ligand to its receptor, thus increasing the stability of the Fgf-FgfR interaction ("catch-and-present"). In GP cartilage, HS facilitate the binding of Fgf2 to FgfR1. This interaction depends on the sulfation of IdoA in 2O-position and the N-sulfation of GlcA within the same disaccharide subunit. Under different conditions, HSPGs may sequester Fgf molecules within the matrix withholding them from their receptor (Kirn-Safran *et al.*, 2004; Xu and Esko, 2014). In addition, HSPGs have also been shown to be involved in the directed diffusion of Fgf2 (Duchesne *et al.*, 2012). Similarly, the diffusion of the Bmp-antagonist Noggin is regulated by HSPGs, modulating the formation of Bone Morphogenetic Protein (BMP) signalling gradients. Bmps bind to HS as well, and HS-binding regulates their activity (Kirn-Safran *et al.*, 2004). The morphogen gradient formed by Ihh within the GP is also shaped by HSPGs within the cartilage matrix. In mice carrying a hypomorphic allele of Ext1 (*Ext1*$^{gt/gt}$) the diffusion range of Indian Hedgehog (Ihh) is increased, resulting in an elongated proliferative zone and delayed hypertrophic differentiation (Koziel *et al.*, 2004).

1.5.2. Role of HS in the transient cartilage of the GP

HSPGs are essential for the regulation of developmental processes. *Ext1*$^{-/-}$ as well as *Ext2*$^{-/-}$ embryos do not synthesis HSPGs and fail to undergo gastrulation (Lin *et al.*, 2000; Stickens *et al.*, 2005). Skeletal malformations are often associated with

alteration of the HS level in mouse models. For example, *Ext1*$^{gt/gt}$ embryos display joint fusions and a delay of hypertrophic differentiation, resulting in shortened but broadened skeletal elements (Koziel *et al.*, 2004). Mice with a limb-specific loss of Ext1 activity (*Prx1;Ext1*$^{fl/fl}$) show joint fusions, a delayed condensation of the cartilage anlagen and hypoplastic limbs (Matsumoto *et al.*, 2010). Likewise, inactivation of *Ext1* in chondrocytes by Tamoxifen administration at P5 (*Col2-CreERT;Ext1*$^{fl/fl}$) results in shortened long bones due to disorganisation of the GP and a reduced hypertrophic zone (Sgariglia *et al.*, 2013). Interestingly, even if no Tamoxifen is administered residual Cre activity leads to shortened long bones in *Col2-CreERT;Ext1*$^{fl/fl}$ animals (Matsumoto *et al.*, 2010). Not only the amount of produced HS but also their modification status is important for skeletal development. Ndst1 is the most abundant NDST family member in cartilage and its deletion is embryonically or perinatally lethal (Grobe *et al.*, 2005; Ringvall *et al.*, 2000). In Ndst1-deficient mice, delayed bone mineralisation was observed (Grobe *et al.*, 2005). *Glce*$^{-/-}$ mice showed short stature, excessive bone mineralisation and malformations of limbs and rib cage (Li *et al.*, 2003). Similarly, *Hs2st1*$^{-/-}$ animals display a short stature with increased bone mineralisation (Bullock *et al.*, 1998) and *HS6St1*$^{-/-}$ embryos are of short stature as well (Habuchi *et al.*, 2007). Likewise, *Sulfatase1*$^{-/-}$*;Sulfatase2*$^{-/-}$ (*Sulf1*$^{-/-}$*;Sulf2*$^{-/-}$) compound mutants, in which 6O-sulfations cannot be removed resulting in an oversulfation of this position, display a short stature, likely due to reduce chondrocyte proliferation (Ratzka *et al.*, 2008).

1.5.3. Role of HS in the permanent cartilage of the joint

Joint fusions have been described in mouse embryos carrying a hypomorphic allele of *Ext1* (*Ext1*$^{gt/gt}$) (Koziel *et al.*, 2004). Likewise, loss of Ext1 activity in chondrocytes during joint formation (*Gdf5-Cre;Ext1*$^{fl/fl}$) results in joint malformations (Mundy *et al.*, 2011), indicating a role of the HS composition not only in the GP but also in the development of the AC. A recent analysis of human healthy and osteoarthritic cartilage samples for the expression of 38 HS-associated genes revealed that 45% of the investigated genes were differentially expressed, including *EXT1* and *2*, *NDST1* and *GLCE* (Chanalaris et al., 2019).

Not only cartilage integrity but also its structure is affected by HSPGs. *Col2-rtTA-Cre;Ext1*$^{e2fl/e2fl}$ mice develop osteochondromas, cartilage-capped bony tumours emerging from the sides of the GP, when low doses of Doxycycline are used to induce Cre activity (Jones *et al.*, 2010). This mimics the human skeletal dysplasia

multiple osteochondroma syndrome (MO; OMIM #133700), which is an autosomal-dominant disorder associated with mutations in *EXT1* or *EXT2*. MO is characterised by the formation of osteochondromas and resulting malformations of the skeleton, such as shortened long bones. Similarly, both Tamoxifen-treated and untreated *Col2-CreERT;Ext1$^{fl/fl}$* mice develop osteochondromas (Matsumoto *et al.*, 2010; Sgariglia *et al.*, 2013). Interestingly, in the three mouse models clusters of morphologically distinct, enlarged chondrocytes can be found in the AC.

1.6. Integrins

Integrins are major transmembrane receptors for cell-matrix-adhesions and connect the ECM to the cytoskeleton. Additionally, integrin signals may trigger various intracellular cascades regulating cell shape, migration, cell cycle progression and survival. integrin receptors are heterodimers consisting of non-covalently bound α- and β-subunits. In the mammalian genome, 18 α- and 8 β-subunits are encoded. In general, more β-monomers are present in the cell membrane, thus the availability of α-subunits limits the number of formed heterodimers. The combination of α- and β-subunit specifies the binding affinity of the respective dimer. There are 24 known combinations with overlapping substrate affinities. The amino acid motif RGD is the most well-known integrin binding site, but other motifs are recognised as well. Common binding partners of integrins containing the RGD motif are Fibronectin and Laminin. Another frequent integrin ligand is collagen, which is bound via a triple-helical GFOGER motif (Alday-Parejo *et al.*, 2019; Legate *et al.*, 2009).

1.6.1. Integrin Receptor Structure and Activation

Each heterodimer forms an extracellular ligand-binding head, two extracellular domains, two transmembrane domains and two cytosolic tails. Integrin receptors may assume three different states with low, intermediate or high ligand-binding affinity (Figure 7). In the low-affinity state, the extracellular proportion of the receptor is bent in a V-shape, with the ligand-binding head close to the cell membrane and the two cytosolic tails connected by a salt bridge. Upon activation, the dimer undergoes rapid conformational changes resulting in integrin extension. The head piece is now exposed for ligand binding and the cytoplasmic domains have separated. Integrin activation includes two processes: the extracellular binding of ligands and the intracellular binding of adaptor proteins. Integrin activation results in the binding of Talin to the cytoplasmic tail of the β-subunit, which bridges the integrin receptor to

the cytoskeleton, forming focal complexes (FC). Further proteins are then recruited to the emerging complex, including kinases, such as Focal Adhesion Kinase (FAK) or Sarcoma Proto-Oncogene Non-Receptor Tyrosine Kinase (Src) family members, and adaptor proteins, e.g. Paxillin. The phosphorylation state of the cytoplasmic integrin tails determines the binding affinity to the assembling proteins. Integrins do not exert enzymatic activity themselves, but rely on adaptor proteins for their signalling function. Many of the pathways activated by integrin signals are also addressed by growth factor receptors, such as the mitogen-activated protein kinase/extracellular signal-regulated kinase (MAPK/ERK) pathway (Alday-Parejo *et al.*, 2019; Legate *et al.*, 2009; Wiesner *et al.*, 2006).

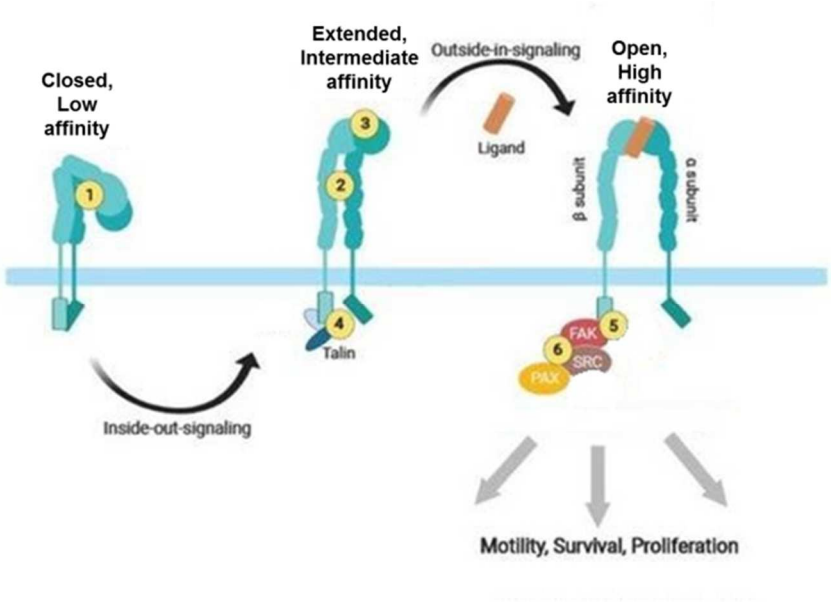

Figure 7: Integrin receptor activation Integrin heterodimers prevail in three different states. In the low affinity state, the extracellular domain is bend towards the cell surface and the ligand-binding head is located close to the membrane (1), while the two cytoplasmic domains are linked to each other. Inside-out signals trigger the extension of the extracellular domains (2), resulting in the exposure of the head domain for extracellular ligands (3). The cytoplasmic tails are now separated and available for binding of adaptor proteins with signalling or structural function, such as Talin (4). Outside-in signalling upon ligand binding triggers the assembly and activation of further intracellular factors (5), including FAK, Src family kinases and Paxillin (6). Modified from (Alday-Parejo *et al.*, 2019).

1.6.2. Integrin Clustering, Cell Adhesion and Cell Migration

Focal adhesions (FA) are integrin-containing complexes connecting the ECM to the cytoskeleton. They are dynamic structures that are constantly remodelled in response to mechanical stimuli, either generated by external strain or cytoskeletal forces. In the low-affinity state, integrins diffuse along the membrane and are not confined to a specific position. For the formation of stable FAs, the clustering of several active integrin receptors in close vicinity is required. The necessary cluster

size is determined by the exerted forces. After initial activation, Talin connects the integrin receptor to stress fibres (SF). These are contractile fibres formed by Actin and non-muscular Myosin Heavy Chain Type II (MHCII). Upon Myosin II-mediated contraction, Talin is stretched revealing a Vinculin binding site. Integrin clustering is then driven by the interaction of Actin, Talin and Vinculin. Through integrin-bound Talin further components are recruited to the nascent FC. FAKs are oligomerised, activated by auto-phosphorylation and able to phosphorylate Srcs, which in turn phosphorylate and activate Paxillin. Paxillin can then bind to Vinculin, stabilising the FC and providing a binding site for Actin-polymerising proteins. Furthermore, FAK recruits further Talin proteins, thereby boosting FA formation. Mature FAs are considerably large complexes of 1-5µm diameter, containing approximately 150 proteins of 80 different types (Legate *et al.*, 2009; Wiesner *et al.*, 2006).

Cell migration requires cycles of membrane protrusion, formation of adhesions, cytoskeletal contraction and disassembly of adhesions. Integrin-mediated FAs play an essential role in this process (Figure 8). The first step of cell migration is polarisation, leading and lagging edge of the cell have to be specified to move in a specific direction. At the leading front of the cell, FCs are formed. Some FCs undergo maturation to FAs while others are not maintained and disassembled, depending on the applied traction. The leading edge develops protrusions towards the direction of movement. The broad, flat membrane protrusion at the leading edge of the cell is called lamellipodium and it is formed by branched actin. To promote branching and thus outward protrusion of the cell membrane, accumulation of Vinculin in FAs is necessary. Vinculin recruits Actin-polymerising complexes formed by Actin related Proteins 2 and 3 (Arp2/3), which connect the FA to the Actin network. Furthermore, Arp2/3 are able to bind to existing filaments and nucleate the branching of newly formed Actin polymers, resulting in membrane protrusion. The orientation of the lamellipodium is controlled by filopodia, which contain bundles of parallel actin filaments and are responsible for mechano-sensing of the adhesion substrate (Innocenti, 2018; Letort *et al.*, 2015; Wiesner *et al.*, 2006).

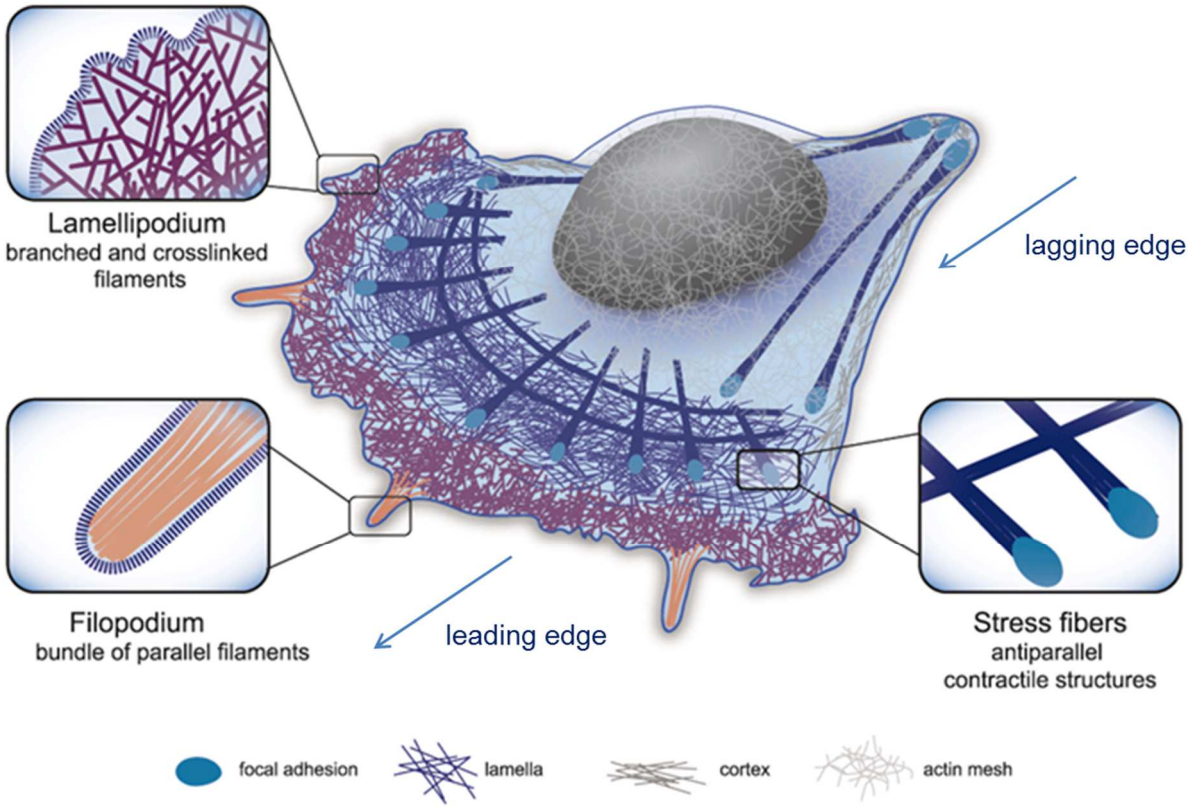

Figure 8: Organisation of the Actin cytoskeleton during cell migration Directed movement requires polarisation of the migrating cell and thus the definition of a leading and a lagging edge. At the leading front, filipodia are formed, thin finger-like membrane protrusions containing bundled actin. Filopodia are rich in cell membrane receptors, are responsible for mechano-sensing of the adhesion substrate and determine the direction of movement. In contrast, the lamellipodium is a broad projection containing a branched Actin network, which pushes the cell membrane forward to the direction of movement. Migration requires the formation of FAs at the leading edge of the cell, the disassembly at the lagging edge and the accumulation of contractile SFs to draw in the lagging edge of the cell. Modified from (Letort et al., 2015).

1.7. Aims

HSPGs control chondrocyte differentiation in the GP, likely by regulating the availability of signalling molecules in the extracellular space or by providing mechanical cues. This suggests that HSPGs are involved in the maintenance of AC as well. This study is based on previous results showing that reduced HS-content or -sulfation in the AC of *Col2-rtTA-Cre;Ext1*$^{e2fl/e2fl}$, *Col2-Cre;Ndst1*$^{fl/fl}$ and *Ndst1*$^{+/-}$ mice protects from the progression of OA. This gives rise to the question, whether other alterations in the HS-modification status also result in a protective effect. To analyse this, the surgical induction of OA by DMM is going to be established and *Glce* and *Hs2st1* mutant mice will be analysed for the progression of OA after DMM surgery an upon ageing. Since heterozygous loss of the two HS-modifying enzymes *Glce* and *Hs2st1* is embryonically lethal, heterozygous mutants are used in this approach.

Furthermore, we and others reported an aberrant cell morphology and ECM composition around HS-deficient cells found in mice with a clonal deletion of *Ext1* in chondrocytes (Severmann *et al.*, 2020; Sgariglia *et al.*, 2013). The quality of the altered ECM around clusters of HS-deficient cells in *Col2-rtTA-Cre;Ext1*$^{e2fl/e2fl}$ animals will be investigated by AFM. To answer the question, how a different matrix composition is sensed by cells, the expression of integrin pathway components in *Col2-rtTA-Cre;Ext1*$^{e2fl/e2fl}$ samples is going to be analysed by immunofluorescence stainings. An *in vitro* model culturing primary cells in presence of the HS-antagonist Surfen will be used to investigate cell adhesion and morphology, intracellular structures and protein content of cells upon the inhibition of HS-protein interactions.

2. Material and Methods

2.1. Material

2.1.1. Mouse strains

Abbreviation	Transgene	Publication
C57BL/6J	purchased from Charles River	
Col2-rtTA-Cre;Ext1$^{e2fl/e2fl}$	Tg(Col2a1-rtTA,tetO-cre)22Pjro;Ext1$^{tm1.1Vcs}$	(Jones *et al.*, 2010)
Glce	*Glce*^{tm1Jpli}	(Li *et al.*, 2003)
Hs2st1$^{fl/fl}$	*Hs2st1*$^{tm1.1Je}$	(Stanford *et al.*, 2010)
Ndst1$^{fl/fl}$	Ndst1^{tm1Grob}	(Grobe *et al.*, 2005)
Prx1-Cre	Tg(Prx1-cre)1Cjt	(Logan *et al.*, 2002)

Ndst1$^{+/-}$ and *Hs2st1$^{+/-}$* mice were generated by crossing *Ndst1$^{+/fl}$* or *Hs2st1$^{+/fl}$* males to *Prx1-Cre^{tg}* females expressing Cre in the germline. Heterozygous mice were kept on a C57BL/6J background.

2.1.2. Cells

Cell line	Publication
CHO pgsD-677	(Lidholt *et al.*, 1992)
CHO-K1	(Puck *et al.*, 1958)

2.1.3. Oligonucleotides

All oligonucleotides were purchased from metabion.

2.1.3.1. Genotyping primers

	Primer 1	Primer 2	Primer 3	Annealing [°C]
Col2-rtTA-Cre	aaagtcgctctgagttgttat	gcgaagagtttgtcctcaacc	ggagcgggagaaatggatatg	60
Ext1$^{e2fl/e2fl}$	gagtccatcctgctctgcat	ttgttgcatgggaaagacaa		62
Glce	agtgttcaaaggataaactac	cgagatcagcagcctctgttcca	actccatgctgctctgac	54

Hs2st1$^{fl/fl}$	gtgcggccgtggggtcc	tgccctaggctcaggcatg		60
Ndst1$^{fl/fl}$	catcctctgaggtgaccgc	ccagggcgtcagggcctcctg	cccagatggcgagactgagg	60

2.1.3.2. qPCR primers

Target	Primer 1	Primer 2
B2M	accgtctactgggatcgaga	tgctatttctttctgcgtgcat
Mmp2	cgcgtaaagtatgggaacgc	ggtaaacaaggcttcatgggg

2.1.4. Antibodies

Primary Antibody	Supplier	Catalogue #
m α FAK	Millipore	05-537
m α Paxillin	BD biosciences	610051
m α pERK	Santa Cruz	Sc136521
m α Src	Cell Signalling	4060
m α YAP	Santa Cruz	sc-101199
r α Mmp2	Chemicon	ab19015
r α β1-Integrin	Millipore	mAB1997
rb α Aggrecan	Millipore	AB1031
rb α ERK	Cell Signalling	4695
rb α pFAK	Invitrogen	44624G
rb α pSmad1/5/9	Cell Signalling	9511
rb α pYAP	Cell Signalling	4911
rb α Smad1/5/9	Invitrogen	PA1-41238

Secondary antibodies were chosen according to the host species of the primary antibody. For Western Blots secondary antibodies labelled with infrared dyes (IRDye, LI-COR) were used, for immunocytochemistry Alexa Fluor (Thermo Scientific) conjugated antibodies were employed. Counterstaining of the actin cytoskeleton was

performed using Phalloidin-AlexaFluor633 (Thermo Scientific). If necessary, signal amplification was performed using biotinylated α rb (BA-1000) or α m (BA-2000) (Vector) and Streptavidin-AlexaFluor (Thermo Scientific) or LI-COR IRDye Streptavidin800CW antibodies.

2.1.5. Consumables

If not indicated otherwise, all cell culture and plastic ware was purchased from Sarstedt.

Product	Description	Supplier
8-well microscopy slides	8-well µ-slides, ibi-treat	ibidi
96-well microscopy plates	96-well Special Optics Flat Clear Bottom Black Polystyrene TC-treated Microplates	Corning
Blotting Paper	580 x 600 mm	Albet LabScience
Cover slides	24x60 mm	Carl Roth
Microtome blades	Type R35	Feather
Object slides	Menzel-Glasses Superfrost plus	Thermo Scientific
PVDF-membrane	Immobilion-FL PVDF-membrane, pore size 0.45µm	Merck Millipore

2.1.6. Purchased chemicals and solutions

Product	Supplier
0.5% Trypsin-EDTA	Thermo Scientific
0.9% Sodium chloride (NaCl)	B Braun
100% Ethanol	Carl Roth
100% Methanol	Fisher Scientifiic
100% Xylene	Carl Roth
30% Acrylamide	AppliChem
95% Ethanol	Carl Roth

Acetic acid	VWR
Agarose	BioBudget
Albumin (BSA) Fraction V	AppliChem
Ammonium peroxide di-sulfate (APS)	AppliChem
Brij-35	VWR
Calcium chloride ($CaCl_2$)	Carl Roth
Carprofen	Bayer
Chondroitinase ABC	Sigma-Aldrich
Citric acid	Carl Roth
Collagenase NB4	Serva
Coomassie Blue R-250	Carl Roth
4′,6-diamidino-2-phenylindole (DAPI)	AppliChem
Di-sodium phosphate (Na_2HPO_4)	Carl Roth
Di-sodium tetra-borate ($Na_2B_4O_7$)	AppliChem
Dithioerythritol (DTT)	AppliChem
DMEM:F12 1:1	Thermo Scientific
DMEM:F12 1:1, w/o phenole red	Thermo Scientific
Deoxyribonucleotide triphosphates (dNTPs)	BioBudget
Dimethylsulfoxid (DMSO) (cell culture grade)	AppliChem
Doxycycline hyclate (≥98% (HPLC))	Sigma-Aldrich
Dulbecco's Phosphate-Buffered Saline (DPBS)	Thermo Scientific
Ethylendiamintetraacetate (EDTA)	AppliChem
Ethidium bromide	Carl Roth
Fast Green FCF	Carl Roth

Fetal calf serum (FCS)	PAN Biotech
Formic acid	Carl Roth
Gelatine	Sigma-Aldrich
Glycerine	Carl Roth
Glycine	AppliChem
Goat serum	Sigma Aldrich
Hyaluronidase from bovine testis	Sigma
Ketamin	Medistar
NP40	Merck Millipore
Orange G	Sigma-Aldrich
Paraffin	Carl Roth
Paraformaldehyde (PFA)	Carl Roth
Potassium chloride (KCl)	Honeywell
Protease Inhibitor Cocktail Set III	Merck Millipore
Proteinase K	Applichem
Retinoic acid	Cayman Chemicals
Safranin O	Merck Millipore
Sodium aceteate (CH_3COONa)	Merck Millipore
Sodium chloride (NaCl)	VWR
Sodium dodecyl sulfate (SDS)	AppliChem
Sodium hydroxide (NaOH)	VWR
Surfen hydrate (≥98% (HPLC))	Sigma Aldrich
Tetra-methylethylendiamin (TEMED)	AppliChem
Tissue-Tek® O.C.T.™ Compound	Sakura

Toluidin Blue	Sigma-Aldrich
Tris	Carl Roth
TrisHCl	AppliChem
Tri-sodium citrate	Carl Roth
Triton X-100	Carl Roth
Tween-20	Carl Roth
Water-free mounting medium, dpx	Sigma Aldrich
Weigert's Solution A and B	Carl Roth
Xylazin	Medistar

2.1.7. Kits and ready-to-use products

Product	Description	Supplier
Blocking solution (WB)	Odyssey blocking buffer (TBS)	LI-COR
Bradford assay	Quick Start Bradford Protein Assay Kit	BioRad
cDNA synthesis	Maxima First Strand cDNA Synthesis Kit for RT-qPCR	Thermo Scientific
DNA Marker	GeneRuler100bp Plus DNA Ladder	Thermo Scientific
gDNA isolation	DirectPCR Lysis Reagent	VIAGEN
Protein marker	PageRuler Prestained Protein Ladder	Thermo Scientific
qPCR reaction	myBudget EvaGreen QPCR-Mix II	BioBudget
RNA isolation	RNeasy Lipid Tissue Mini Kit	QIAGEN
Taq polymerase and buffer	DreamTaq, DreamTaq buffer (10x)	Thermo Scientific
Total protein staining	REVERT staining solution	LI-COR

2.1.8. Composition of solutions and buffers

All buffers and solutions were produced using ddH_2O purified by the Milli-Q Biocel system.

Solution	Components
1% PFA, 4% PFA	20% PFA diluted in 1xPBS
1.5% (w/v) agarose gel	1.5% agarose in TAE, 0.2µg/ml ethidiumbromide
10x electrophoresis buffer	250mM TrisBase, 2.5M glycine, 1% (w/v) SDS, pH 8.3
10x Phosphate Buffered Saline (PBS)	1.37M NaCl, 26.8mM KCl, 100mM Na_2HPO_4, 17 mM KH_2PO_4, pH 7.4
10x Tris Buffered Saline (TBS)	500mM TrisHCl, 1.5M NaCl, pH 7.4
1x Tris Acetatae EDTA buffer (TAE)	40mM TrisBase, 10mM EDTA, pH8.0
20% Paraformaldehyde (PFA)	20% (w/v) PFA, 10mM NaOH
25% Ethylendiaminteteraacetate (EDTA)	25% (w/v) EDTA, pH7.4 with NaOH
4x sample buffer	250mM TrisBase pH 6.8, 40% (v/v) glycerine, 8% (w/v) SDS
6x Orange G loading dye	(30% (v/v) glycerine, 0.2% (w/v) Orange G
Bjerrum Buffer	48mM Tris, 29mM Glycin, 20% (v/v) MeOH
Chondroitinase solution	50mM Tris pH 8.0, 60mM NaAcetat0.02% (w/v) BSA, 50mU/ml Chondroitinase ABC
Citrate Buffer	10mM citrate, pH 6.0 with citric acid
Collection gel (WB)	5% (v/v) acrylamide, 125mM Tris pH 6.8, 1% (w/v) SDS, 1% (w/v) APS, 0.1% TEMED
Collection gel (zymography)	5% (v/v) acrylamide, 125mM Tris pH 6.8, 1% (w/v) SDS, 1% (w/v) APS, 0.1% TEMED
Destaining solution	40% methanol (v/v), 10% (v/v) acetic acid
Developing solution	50mM Tris, 200mM NaCl, 5mM CaCl2, 0.02% (w/v) Brij-35, pH to 7.5
Digestion solution (MEFs)	5% FCS, 0.05% Trypsin-EDTA, 0.3U Collagenase NB4 in DPBS
Fast Green Solution	0.1% (w/v) Fast Green FCF, 1% (v/v) acetic acid
Hyaluronidase solution	1000U/µl hyaluronidase in 1x PBS

Lysis-Buffer	50mM TrisHCl pH7.5, 100mM NaCl, 15mM EDTA pH8.0, 0.1% (v/v) NP40, 1mM DTT, 1:1000 Protease Inhibitor Cocktail
MEF Medium	10% (v/v) FCS in DMEM:F12 1:1
Mowiol/DABCO	6g Glycerin, 2,4g Mowiol 4-88, 6mL ddH_2O.,12mL 0,2M Tris-HCl pH 8.5, 2.5% (w/v) DABCO
PBT/Triton	0.1% (v/v) Triton X-100 in 1xPBS
PBT/Tween	0.05% (v/v) Tween20
Renaturation solution	2.5% Triton X-100
Reversal solution	0.1% (w/v) NaOH, 30% (v/v) MeOH
Safranin O solution	0.1% (w/v) Safranin O
Separation gel (WB)	10% (v/v) acrylamide, 375mM Tris pH 8.8, 1% (w/v) SDS, 1% (w/v) APS, 0.1% (v/v) TEMED
Separation gel (zymography)	8% SDS-PAGE gels supplemented with 0.1% gelatine (10% (v/v) acrylamide, 390mM Tris pH 8.8, 1% (w/v) SDS, 1% (w/v) APS, 0.04% (v/v) TEMED, 0.1% (w/v) gelatine
Staining solution	40% methanol (v/v), 10% (v/v) acetic acid, 0.5% (w/v) Coomassie Blue R-250
TBST	1x TBS with 0.1% Tween-20
Toluidin Blue staining solution	0.1% (w/v) Toluidin Blue, 1% (w/v) $Na_2B_4O_7$
Washing solution	6.7% (v/v) acetic acid, 30% (v/v) MeOH
Weigert's Solution	A:B 1:1, filtered

2.1.9. Equipment

Product	**Type**	**Supplier**
Blotting machine	Novex Semi-Dry Blotter	Invitrogen
Confocal microscope	TCS SP8	Leica
Counting chamber	Neubauer Improved	Marienfeld
Cryostat	HM 560	Microm
Document scanner	Scanjet 8200	HP

Electrophoresis chamber (horizontal)	PerfectBlue Maxi S Plus	Peqlab
Electrophoresis chamber (vertical)	Mini Protean Tetra Cell	BioRad
Embedding station	EG1150 H	Leica
Fluorescence scanner	Odyssey CLx	LI-COR
Gel documentation system	Gel iX20 Imager	INTAS
Incubator, 37°C		Memmert
Incubator, 37°C (cell culture)	HERA Cell 240	Thermo Electron Corporation
Microplate absorbance reader	GENios Pro	Tecan
Microtome	HM340E	Microm
Phase-contrast microscope	Ti Eclipse Epi	Nikon
Reflected light fluorescence microscopes	AxioObserver 7	Zeiss
	TIRF DualCam	Nikon
RT-PCR cycler	Cycler CFX96 Touch Real-Time PCR System	BioRad
Spin Tissue Processor	Microm STP 120	Thermo Scientific
Thermo Cycler	T professional	Biometra
Transmitted light microscope	Axioplan 2	Zeiss
Water purification system	Milli-Q Biocel	Millipore

2.1.10. Software

Product	**Supplier**
CellProfiler 3.0	CellProfiler™
Fiji 2.0.0	(Schindelin *et al.*, 2012)

ImageStudioLite	LI-COR
RStudio 3.6.3	The R Foundation for Statistical Computing

2.2. Methods

2.2.1. Animal experimental methods

2.2.1.1. Mouse husbandry

Up to six mice were kept in individually ventilated cages under specifically pathogen-free conditions with nesting material as environmental enrichment. A 12h light/dark cycle was applied and water and food were provided *ad libidum*.

2.2.1.2. Genotyping

For genotyping of genetically modified mice genomic DNA was isolated form ear biopsies using DirectPCR Lysis Reagent (VIAGEN) supplemented with 0.2mg/ml Proteinase K according to the manufacturers protocol. The polymerase chain reaction (PCR) was prepared (Table 1) and processed (Table 2) according to a standard protocol, with annealing times and temperatures adjusted for the specific primer pairs.

Table 1: Standard PCR reaction mix for genotyping of genetically modified mice

Component	Final concentration
DreamTaq-Buffer	1x
Primer	400µM each
dNTPs	800µM
DreamTaq-Polymerase	20mU
gDNA	4% (v/v)

Table 2: Standard PCR programme for genotyping

	Temperature [°C]	Time [min]	Cycles
Denaturing	95	5	
	95	1	
Annealing	X	XX	30-35x
Extending	72	1	
	72	5	
hold	12		

The resulting PCR products were loaded on an 1.5% (w/v) agarose in 1x TAE gel using an Orange G-containing loading dye and separated by gel electrophoresis at 120V with TAE used as running buffer. To enable size comparison, a DNA marker was used. For visualisation, the agarose gels were supplemented with 0.2µg/ml ethidiumbromide, which was detected with a suitable gel documentation system at 345nm wavelength.

2.2.1.3. DMM surgery

12w old, adult mice were anaesthetised by intraperitoneal injection of 100mg per kg body weight (kgbw) Ketamin and 2mg/kgbw Xylazin in 0.9% NaCl. The medial meniscus of the knee was destabilised by transection of the medial menisco-tibial ligament (Glasson *et al.*, 2007), increasing the mobility of the meniscus and thus enhancing intra-articular friction. As an internal control, a sham surgery was performed on the contralateral hindlimb incising only skin and joint capsule. For analgesia, 5mg/kgbw Carprofen was injected subcutaneously peri-operatively and every 24h for 3 days (3d) post-operatively.

2.2.1.4. Induction of allelic recombination

To induce Cre recombinase activity, 80 mg/kgbw Doxycycline in 0.9% NaCl was injected intraperitoneally into lactating dams at P8. To limit Cre activity to the offspring, *Col2-rtTA;R26R-LacZ;Ext1*$^{e2fl/e2fl}$ males were crossed to *R26R-LacZ;Ext1*$^{e2fl/e2fl}$ females not carrying the Cre transgene. The progeny was sacrifice at 4 weeks (4w) and limbs processed for either immunostaining or AFM analysis.

2.2.2. Histological procedures

2.2.2.1. Immunostaining of tissue sections

Joints *Col2-rtTA-Cre;Ext1*$^{e2fl/e2fl}$ and *Ext1*$^{e2fl/e2fl}$ controls were isolated from 4w old mice. Skin and surrounding connective tissue were removed, the joints washed with 1x PBS and fixed in 4% PFA at 4°C for 48h. The samples were rinsed with 1x PBS and submitted to decalcification in 25% EDTA for 2-3w, until the bony tissue became sufficiently demineralized for sectioning. Afterwards, the joints were washed with 1x PBS and transferred into paraffin using a Spin Tissue Processor running the programme shown in Table 3. For immunohistochemistry, joints were embedded in sagittal orientation and sectioned at 7µM thickness using a microtome and blades suitable for bony tissue.

Table 3: Time schedule for dehydration of tissue samples and embedding into Paraffin

Solution	Time [min]
70% EtOH	90
80% EtOH	90
95% EtOH	90
100% EtOH	90
100% EtOH	90
100% EtOH	60
100% Xylene	30
100% Xylene	30
Paraffin	60
Paraffin	60
Paraffin	60

For staining, slides were deparaffinised by washing with 100% Xylene twice, for 10 minutes (min) 10min and 5min, respectively, and rehydrated with a series of decreasing Ethanol (EtOH) concentrations comprising 99, 95, 70 and 50% EtOH for 3min each.

Using antibodies against β1-Integrin (ItgB1), Paxillin and Src, residual EtOH was removed and the pH neutralised by washing 3 times with tap water for 3min. Then two antigen retrieval procedures were applied: First, slides were boiled in citrate buffer for 3min at 945 Watt and heated another 7min at 105 Watt in a suitable microwave. After cooling to room temperature (RT) for approx. 30-45min, they were washed with 1x PBS for 3min and incubated with 150µl hyaluronidase in a humidified chamber at 37°C for 30min. Afterwards, slides were washed 3 times for 3min with 1xPBS and unspecific binding was blocked 1%BSA in 1x PBS for 30min at RT. Primary antibodies against ItgB1, Paxillin and Src were diluted 1:100 in 1% BSA and incubation was performed at 4°C over night (oN), secondary (1:200) and tertiary antibodies (1:500) were diluted in 1% BSA and added for 40min at RT. Between the different antibodies, slides were washed with 1x PBS three times for 3min. Finally, the samples were washed twice with 1x PBS, permeabilised with PBT/Tween for 10min and incubated for 3min with 500ng/ml DAPI for nuclear staining. Residual DAPI was washed off using 1x PBS three times for 3min, slides were mounted with

Mowiol/DABCO and stored at -20°C. Immunostained sections were imaged using reflected light fluorescence microscopy.

For immunostaining against ERK, the deparaffinised and rehydrated slides were washed once with 1xPBS for 3min and submitted to hyaluronidase digestion. Afterwards, they were washed with 1xPBS and 10% (v/v) goat serum in 1xPBS was applied for blocking. The remaining staining procedure was conducted as described for ItgB1, Paxilin and Src antibodies, with the employed antibodies diluted in 10% goat serum in 1xPBS.

For staining of aggrecan, deparaffinised and rehydrated slides were rinsed with tap water and 10% formic acid was applied for 15min at RT as an antigen retrieval. Afterwards, slides were washed three times with ddH_2O and twice with 1xPBS. A second antigen retrieval with chondroitinase solution was performed for 30min at 37°C. The samples were washed with 1xPBS three times and 1% BSA in 1xPBS was used for blocking for 1h at RT. The primary antibody against aggrecan was diluted 1:150 in the respective blocking solution and samples were incubated oN at 4°C. They were washed three times with 1xPBS before addition of the secondary antibody, which was diluted 1:500. After washing twice with 1xPBS, PBT/Tween was applied to permeabilise the tissue and 500ng/ml DAPI were added for nuclear staining for 3min. Slides were washed three times with 1xPBS and mounted using Mowiol/DABCO.

2.2.2.2. Histological staining of tissue sections

Tissue samples were prepared similarly to IHC, whereas knee joints were embedded and sectioned in frontal direction at 7µm thickness. Slides were deparaffinised by washing with 100% Xylene for 15min and rehydrated using 99, 95 and 70% EtOH for 3min each.

For Toluidine Blue staining, rehydration was followed by washing with ddH_2O and staining with Toludine Blue solution for 2-3min. Residual staining was rinsed off and slides were dehydrated by washing twice with 95 and 99% EtOH. After 15min in 100% xylene, slides were mounted using the water-free mounting medium DPX. Stained slides were imaged using a transmitted light microscope.

For Safranin Weigert staining, slides were stained with Weigert's Solution for 3min and rinsed with tap water to remove excessive staining solution and neutralise the pH, resulting in the characteristic staining of nuclei. Afterwards, an incubation in Fast Green Solution for 5min followed and slides were rinsed with 0.1% acetic acid. Slides

were directly transferred into Safranin O solution for 5min and rinsed twice with 95% and 99% EtOH before incubation in 99% for 2min and in 100% Xylene for 10min. Slides were mounted with DPX and imaged by transmitted light microscopy.

2.2.2.3. Quantification of OA

For the quantification of osteoarthritic joint alterations, the AC was evaluated using the scoring system recommended by the International Osteoarthritis Research Society (OARSI) (Glasson *et al.*, 2010). All samples were examined by two independent scorers. From each joint at least 3 serial sections of approx. 100µm intervals were examined, encompassing the central weight bearing area of the knee which is demarcated by the presence of the cruciate ligaments. The four quadrants of the joint (medial and lateral tibial plateaus as well as medial and lateral femoral condyle) were assessed separately and combined into medial, lateral and total means.

2.2.2.4. Atomic Force Microscopy (AFM) of cartilage tissue

Knee joints from *Col2-rtTA;R26R-LacZ;Ext1*$^{e2fl/e2fl}$ and control littermates were isolated at 4w of age after Cre induction at P8. Tissue samples were embedded in O.C.T. and cooled to -56°C. Frozen samples on dry ice were send to University of Applied Sciences, Munich, where AFM measurements were performed by Lutz Fleischhauer in the lab of Hauke Clausen-Schaumann as published in (Muschter *et al.*, 2020).

In brief, each cartilage zone was assessed on two separate sagittal tissue sections with 1875 force-indentation curves in total distributed on 3 different 9µm² areas. For indentation, a cantilever with a four-sided pyramidal tip geometry and 20 nm tip radius was used. Subsequently, a modified Hertz-Sneddon model was fitted onto the approach curve using the Software Igor Pro (Version 6.3.7.2, WaveMetrics, Portland, USA) and the Young's Modulus was extracted. The resulting values were summarized in histograms.

2.2.3. Cell culture methods

2.2.3.1. Isolation of Murine Embryonic Fibroblasts (MEFs)

Mouse embryos from timed pregnancies (E13.5 – 15.5) were isolated from the uterus and all internal organs were removed. The remaining tissue was homogenised, suspended in 1ml digestion solution per embryo and incubated at 37°C for 15min. 50% of the supernatant (SN) was transferred into a new vial containing 30ml MEF

medium and 1ml of fresh digestion solution per embryo were added to the tissue before a second incubation step at 37°C for 15min. The entire SN was then harvested, pooled with the already harvested medium and centrifuged at 270 x g. Finally, the pelleted cells were resuspended in MEF medium and seeded at a density of 1 embryo per 25cm^2.

2.2.3.2. Adhesion time line

MEFs were covered by 0.05% Trypsin EDTA in DPBS and incubated at 37°C and 5% CO_2. The detached cells were counted in a *Neubauer* counting chamber and seeded into Surfen- or DMSO-containing MEF medium at a density of 5*10^3 cells/well into a 24-well plate. MEFs were then cultured at 37°C and 5% CO_2 for 0.5, 1, 2, 16 and 24 hours (h), using a separate plate for each time point. Subsequently, the adherent MEFs were washed with DPBS, fixed with 4% PFA for 10-15min at RT, covered with 1% PFA and stored at 4°C. For nuclear staining, residual PFA was rinsed off by washing with DPBS twice, cells were incubated covered with 500ng/ml DAPI for 5min at RT, washed again and covered with DPBS. Plates were imaged with a reflected light fluorescence microscope at 200x magnification. From each well, three images were taken and the number of nuclei per frame was quantified using CellProfiler 3.0.

2.2.3.3. Life Cell Imaging

Similar to the adhesion time line described before, cells were detached and counted. Per well 1.5*10^5 cells were seeded into Surfen- or DMSO-containing MEF medium on 8-well µ-slides. For life cell imaging, DMEM:F12 1:1 without phenol red was used. After 15-20min pre-adhesion at 37°C and 5% CO_2, one image per minute was taken at five positions of each well by phase-contrast microscopy. The resulting films were analysed using Fiji 2.0.0.

2.2.3.4. Immunocytochemistry

Cells were detached, counted and seeded into 96-well plates suitable for fluorescence microscopy. For a treatment duration of one hour 5*10^4 and for 24 hours of treatment 2.5*10^4 cells/well were used. Subsequently, the adherent cells were washed with DPBS, fixed with 4%PFA at RT for 10min and stored at 4°C covered with 1%PFA. Before staining, residual PFA was washed of using 1xPBS and cells were permeabilised with PBT/Triton for 15min at RT. After washing twice with 1xPBS, blocking was performed using 2% BSA in ddH_2O for 1h at RT. Primary and secondary antibodies were diluted 1:1000 and 1:500 in blocking solution,

respectively. Additionally, 1:1000 Phalloidin-AlexaFluor633 was added to the solution containing the secondary antibody. Incubation with the primary antibody was conducted at RT for 1h. After washing with 1xPBS, an appropriate secondary antibody was added for 1h at RT. The same volume of 500ng/ml DAPI was then added to each well and left to incubate for 5min at RT. After washing with 1xPBS twice, a post-fixation with 4% PFA followed. Cells were covered with 1% PFA and stored at 4°C. Imaging was performed using a confocal laser microscope (for figures) or reflected light microscope (for evaluation) guided by Nina Schulze and Johannes Koch (Imaging Centre Campus Essen, ICCE).

2.2.4. Proteinbiochemistry

2.2.4.1. Zymography

Femoral head (FH) cartilage of 4w old *Ndst1*$^{+/-}$ and *Ndst1*$^{+/+}$ littermates was isolated in 1xPBS. In a 48-well plate, each FH was incubated in 250µl serum-free medium (DMEM:F12 1:1) at 37°C and 5% CO_2. One FH of each mouse was challenged with 10µM retinoic acid (RA) to induce OA-like cartilage degradation (Little *et al.*, 2003), while the contralateral sample served as a control treated with DMSO only. After three days in culture, SNs were collected.

For zymography, the protein content of the SN samples was determined by a Bradford assay and a microplate absorbance reader. Similar amounts of protein were then applied in each lane. For loading, 1x sample buffer was added to the appropriate volumes of SN. The gel was run in electrophoresis buffer, starting at 50V until all samples had crossed through the collection gel and continued at 120V for protein separation. Afterwards, the gel was rinsed with ddH_2O, incubated in renaturation solution for 15min twice and washed with ddH_2O again. It was transferred into developing solution and incubated at 37°C overnight. The gel was then stained for 1h at RT and destained until clear signals were visible. Gels were imaged using a document scanner and degradation signals were quantified using the ImageStudioLite software.

2.2.4.2. Western Blot

To analyse secreted proteins from FH explant cultures, the protein content of each sample was determined by Bradford assay and equal protein amounts were loaded in each lane after addition of 1x sample buffer without β-Mercaptoethanol. For analysis cell lysates from Surfen- or DMSO-treated MEFs, $2*10^5$ cells were flash-

frozen in liquid nitrogen, resuspended in 100µl lysis buffer and rotated for 30min at 4°C for lysis. After the addition of 1x sample buffer, samples were denatured at 95°C for 5min and 30µl of each sample were loaded per lane.

The horizontal electrophoresis chamber was filled with 1x electrophoresis buffer. The gel was run at 50V for 30min and continued at 100V for 60-90min for size separation. To enable size comparison, a protein marker was applied. After running, gels were fixed in Bjerrum buffer for 10min at RT. PVDF membranes were activated with 100% MeOH, washed three times with purified water (VE) and transferred into Bjerrum buffer. Blotting was performed at 120mA per gel with a maximum voltage of 20V for 100min in a blotting machine suitable for semi-dry blotting. Afterwards, membranes were washed once with VE. Total protein staining (TPS) was performed by adding REVERT staining solution for 2-5min at RT. Subsequently, membranes were washed two times with washing solution and the total protein staining was detected at 680nm wave length using a fluorescence reader. Membranes were de-stained in reversal solution for 5min at RT, washed three times with VE and submitted to blocking for 1h at RT in a TBS-based blocking solution. Primary antibodies were diluted 1:1000 in blocking solution and incubation was performed at RT for 2.5h. Subsequently, membranes were washed with TBST for 10min and appropriate secondary antibodies were added for 45min at RT, diluted 1:50,000 in the respective blocking solution. Membranes were washed three times in TBST for 10min, transferred into TBS and scanned on a fluorescence reader. Signals were then quantified using the software ImageStudioLite.

2.2.5. Molecular methods

2.2.5.1. Quantitative polymerase chain reaction (qPCR)

FH cartilage explants were cultured for 3d in presence or absence of RA. RNA was isolated from the tissue using the RNeasy Lipid Tissue Mini Kit and the synthesis of cDNA was conducted with the Maxima First Strand cDNA Synthesis Kit according to the manufacturers protocol. qPCR reactions were prepared with the EvaGreen qPCR MIX II using the primers listed in table X. The programme shown in table 4 was run on a suitable qPCR cycler.

Table 4: Standard programme for qPCR

Temperature [°C]	Time [min]	Cycles
95	10:00	
95	0:15	
62	0:20	
Plate read		40x
72	0:20	
Melt curve: 60-94.8°C, 0.3°C/0:15 increase		
Plate read		
4		

2.2.6. Statistics

All statistical analyses were performed by Christoph Waterkamp from the Department for Bioinformatics and Computational Biophysics, at the University of Duisburg-Essen. Data-specific generalised linear models were applied for the statistical evaluation of the collected data (listed in Tab. 5). These probability models were implemented in Stan (Carpenter *et al.*, 2017) and interfered using Bayesian statistics. The models were evaluated with posterior predictive checks to match the modelling to the actual data. For this, 4000 iterations (2000 warm-up, 2000 samples) and four chains were used. The modelled effect size is given as a 90% highest density interval (HDI). To facilitate the interpretation of the generated statistical data a p^+ values are displayed. This parameter describes the fraction of the distribution >1. When p+ is ≥0.95 or ≤0.05 this indicates a high probability of the given effect and it can be regarded as stable. p+ has a numerical accuracy of 1/8000 (2000 sample iterations * 4 chains) and includes the values 0 and 1. The output date from Bayesian interference are listed in the annex, chapter 9.1.

Table 5: Probability models applied for Bayesian statistics

Data set		Model	Parameter		PPC
AT		Negative binomial		mu=Experiment, Time, concentration	Acceptable-Good
ICC	SF	Binomial	N: Cell.No	p=Intercept+Condition+treatment+Condition*treatment+experiment	Acceptable
	FA	Binomial	N: Cell.No	p=Intercept+Condition+treatment+Condition*treatment+experiment	Good
	YAP	Binomial	N: Cell.No	p=Intercept+Condition+treatment+Condition*treatment+experiment	Good
LCI	Full	Binomial	N: Cell.No	p=Intercept+Condition+teratment+Condition*treatment+experiment	Good
	Start_End	Binomial	N: Cell.No	p=Intercept+Condition+teratment+Condition*treatment+experiment+Time	Acceptable-Good
Zymmogram		Normal (log-scale)		mu=Genotype+Enzym+Type(pro/active)+type*enzym+gt*enzym	Acceptable-Good
OA	DMM	ordered logistic		eta=genotype+surgery+genotype*surgery	Good
	DMM_establishment	ordered logistic		eta=time+type+id	Good

3. Results

3.1. *In vivo* analyses

Genetically modified mice with reduced HS-levels in a subset of chondrocytes (*Col2-rtTA-Cre;Ext1*$^{e2fl/e2fl}$) and with undersulfated HS (*Col2-Cre;Ndst1*$^{fl/fl}$ and *Ndst1*$^{+/-}$) show decreased OA development after surgical induction. This raises the questions which molecular mechanisms are causing the observed effect and whether other alterations of the HS modification pattern result in a similar protection.

1.1.1. Reduced activity of Mmp2 in *Ndst1*$^{+/-}$ samples

Increased proteolysis of cartilage matrix mediated by enzymes of the ADAMTS and MMP families is a prominent feature of OA pathogenesis (Wieland *et al.*, 2005). Accordingly, a decreased protease activity poses a possible mechanism underlying the protective effect seen in HS mutants. Decreased amounts of neo-epitopes resulting from the degradation of aggrecan by both ADAMTS and MMP proteases were detected in culture medium and tissue extracts from *Ndst1*$^{+/-}$ mice compared to *Ndst1*$^{+/+}$ controls. This raises the question, if the degradation of other substrates by MMPs is decreased as well. Preliminary results indicated that the gelatinase activity of MMPs was reduced in the culture medium of *Ndst1*$^{+/-}$ cartilage samples.

In preliminary experiments using culture medium containing FCS, a degradation band was found at around 65kDa, which might either be derived by proMmp2 activity (68kDa) or from the serum-containing medium. To investigate this, FH cartilage was isolated from 4w old C57Bl/6 wild type mice and incubated in presence or absence of FCS. Media were collected after 3d and analysed by gelatine zymography.

In samples from FH explants cultured in medium with FCS two signals were detected at ~65kDa and ~55kDa, while the serum-containing medium showed only the larger degradation band. In culture medium from FH incubated under serum-free conditions the lower signal was detected but not the larger one. Size comparison to recombinant Mmp2 showed, that the ~55kDa band corresponded to active Mmp2 (58kDa). Recombinant proMmp2 (72kDa) ran slightly higher than the ~65kDa signal detected in FCS-containing samples (Fig. 9, A).

The results show that degradation signals generated by proMmp2 were masked by proteases contained in the FCS in prior experiments using serum-containing media. Comparison to rMmp2 confirmed that the ~55kDa signal analysed before was indeed caused by Mmp2. To substantiate this, FH from 4w old C57Bl/6 mice were isolated

and cultured under serum-free conditions in presence or absence of RA. The culture media were then analysed by Western Blot. In both samples two bands were detected, confirming the presence of proMmp2 and active Mmp2 in the medium of FH explant cultures. Taken together, these results show that proteolysis by active Mmp2 is reduced in cartilage samples from mice with reduced HS sulfation (Fig. 9, B).

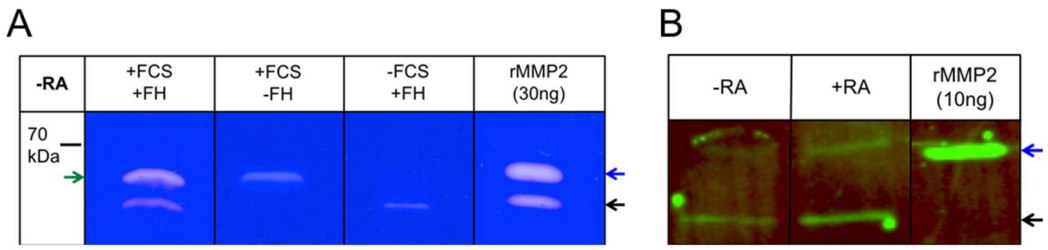

Figure 9: FH-specific degradation signal is likely caused by Mmp2 (A) Analysis of medium from FH cultured in presence of FCS, FCS-containing medium, and FH culture medium from serum-free conditions. In samples with both HF cartilage and FCS two degradation signals are detected. The larger one originates from the serum (green arrow), while the smaller one is FH-specific. Comparison to recombinant Mmp2 protein identifies the smaller signal at ~55kDa as active Mmp2. Experiments conducted by KP under the supervision of ACS. (B) Analysis of samples from serum-free conditions by Western Blot demonstrates the presence of proMmp2 (blue arrow) and active Mmp2 (black arrow) in FH culture medium. Modified from (Severmann *et al.*, 2020).

To confirm these results, FH cartilage explants of 4w of *Ndst1*$^{+/-}$ mice and *Ndst1*$^{+/+}$ littermates were isolated and cultured under serum-free conditions. One FH of each individual was treated with 10µM RA to mimic osteoarthritic conditions, while the other was treated with an equimolar amount of DMSO as a solvent control. After 3d in culture, the culture media were collected and the protein content quantified by Bradford assay. Similar amounts of protein from each sample were then loaded for gelatine zymography. Two proteases were detected at ~65kDa and ~55kDa. Given the sizes of the degradation bands and the MMP family members with gelatinase activities these bands likely represent proMmp2 (72kDa) and active Mmp2 (58kDa). Additionally, two degradation signals were detected around 100kDa, which likely correspond to proMmp9 (92kDa) and active Mmp9 (82kDa) (Fig. 10, A, B).

Quantification of the band intensities from untreated *Ndst1*$^{+/+}$ samples showed moderate gelatine degradation by proMmp2 (mean signal intensity 9903), active Mmp2 (14633) and proMmp9 (17100) while digestion by active Mmp9 was barely measurable (Fig. 10, A, C). After addition of RA, proMmp2 activity was reduced (5040), while the signals generated by active Mmp2 (24733) and proMmp9 (24480)

were increased. Degradation by active Mmp9 was also elevated and detectable (8657) (Fig. 10, B, D). When culture medium from untreated *Ndst1*$^{+/-}$ samples was applied, moderate signal intensities were quantified for proMmp2, active Mmp2 and proMmp9 (9837, 19567 and 19547, respectively). For active Mmp9, no clear degradation bands were detectable (Fig. 10, A, C). In the culture medium from RA-treated *Ndst1*$^{+/-}$ samples, proMmp2 mediated gelatine digestion decreased to a mean signal intensity of 3478. Likewise, degradation signals from active Mmp2 and proMmp9 were lower than in the untreated *Ndst1*$^{+/-}$ samples (8790 and 12007, respectively). In contrast to the results in absence of RA, digestion by active Mmp9 was measurable but showed a relatively low signal intensity (1363) (Fig. 10, B, D). Compared to *Ndst1*$^{+/+}$ controls, samples from heterozygous *Ndst1*$^{+/-}$ mutants showed similar activities of proMmp2 (change factor, 1.02, p^+=0.8276), active Mmp2 (change factor 1.02, p^+=0.8276) and proMmp9 (change factor 1.02, p^+=0.8416) under RA-free conditions. After the addition of RA, the activity of proMmp2 was decreased compared to untreated conditions in samples from both *Ndst1*$^{+/+}$ and *Ndst1*$^{+/-}$ mice, but stayed similar between the two genotypes In contrast, degradation by active Mmp2 and proMmp9 was increased in *Ndst1*$^{+/+}$ but decreased in *Ndst1*$^{+/-}$ samples compared to RA-free conditions, resulting in lower signal intensities in the heterozygous mutants relative to the wild type controls (ratio 0.36 and 0.49, change factors 0.88 and 0.90, p^+= 0.1691 and 0.0348, respectively). Likewise, the activity of active Mmp9 was reduced in culture medium from *Ndst1*$^{+/-}$ compared to *Ndst1*$^{+/+}$ mice (ratio 0.16, change factor 0.88, p^+=0.0378).

These results show that there are no striking differences in protease activities between the two genotypes under physiological conditions. When OA-like alterations are induced by the addition of RA, Mmp activity is upregulated in *Ndst1*$^{+/+}$ samples but downregulated in *Ndst1*$^{+/-}$, resulting in decreased proteolytic digestion in heterozygous mutants compared to controls. The reduced proteolytic activity of active Mmp2 observed in *Ndst1*$^{+/-}$ mutants was statistically stable (median change factor 0.77, 90% HDI 0.60 – 0.96) when the data obtained for Mmp2 were pooled with the results from preliminary experiments, (Severmann *et al.*, 2020).

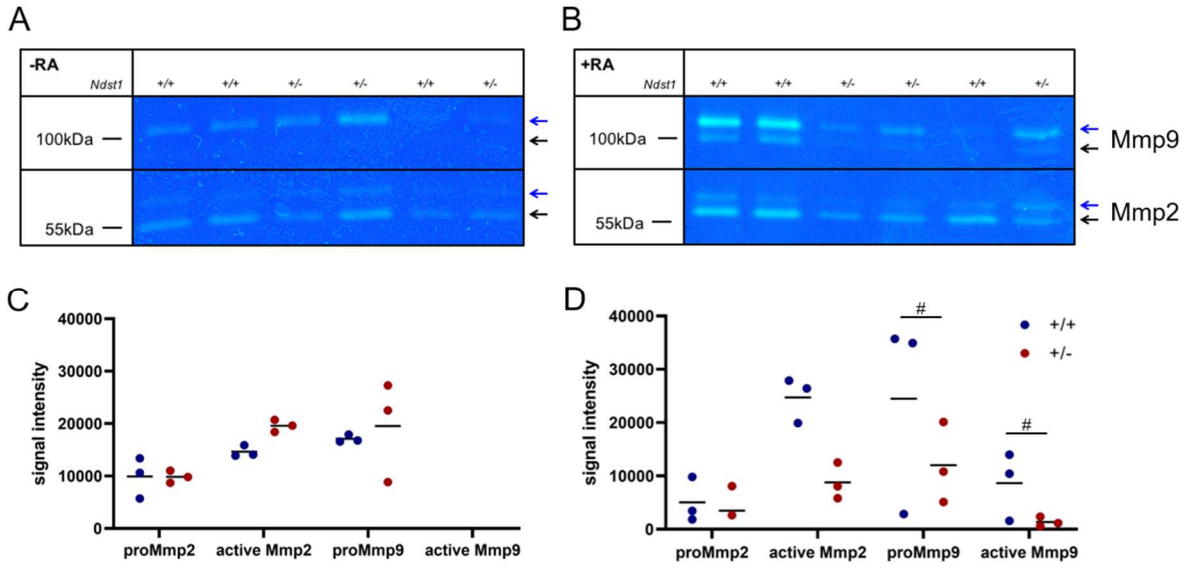

Figure 10: Reduced gelatinase activity in *Ndst1*$^{+/-}$ samples (A, B) Serum-free culture medium from *Ndst1*$^{+/-}$ and *Ndst1*$^{+/+}$ FH explants were analysed by gelatine zymography after 3d in culture in presence or absence of RA. (C, D) Band intensities of degradation signals likely originating from proMmp2 and active Mmp2 (~55kDa), proMmp9 and active Mmp9 (~100kDa) were quantified (blue arrow: pro-enzyme, black arrow: active form). No differences between the genotypes were detected under RA-free conditions, while decreased activities of active Mmp2, proMmp9 and active Mmp9 were detected in *Ndst1*$^{+/-}$ samples upon RA-treatment. Data points represent individual mice of the same litter. Black lines indicate means. Modified from (Severmann et al., 2020).

A reduced degradation of cartilage matrix by Mmp2 may be explained by a reduced gene expression of *Mmp2*. To analysed this, FH explants from 4w old *Ndst1*$^{+/-}$ and *Ndst1*$^{+/+}$ mice were incubated in presence or absence of RA. After 3d in culture, the relative levels of *Mmp2* mRNA were quantified by qPCR. No differences in the expression levels of *Mmp2* were detected between the two genotypes in presence or absence of RA (Fig. 11).

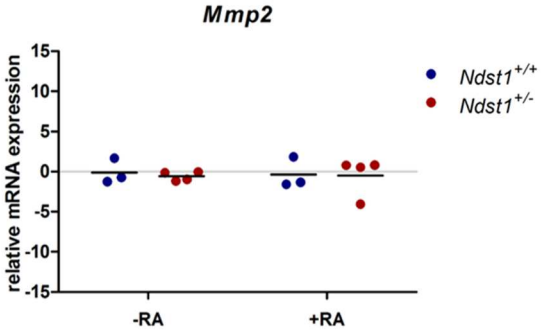

Figure 11: Mmp2 is not differentially expressed in *Ndst1*$^{+/-}$mice RNA was isolated from FH cartilage of *Ndst1*$^{+/+}$ and *Ndst1*$^{+/-}$ animals after 3d in culture in presence or absence of RA. Under both conditions no differences between the two genotypes. Data points represent ΔCT values relative to B2M, each sample containing pooled RNA from littermates with the same genotype (n≥3 litters). Experiments conducted by YK under the supervision of ACS. Modified from (Severmann *et al.*, 2020).

These data indicate that the regulation of Mmp2 takes place on protein rather than on expression level. This may include reduced proteolytic activation, increased inhibition of enzyme activity or elevated internalisation and degradation of Mmp2.

1.1.2. *Glce*$^{+/-}$ and *Hs2st1*$^{+/-}$ mice do not show accelerated progression of OA

A previous study from our group showed that *Col2-rtTA-Cre;Ext1*$^{e2fl/e2fl}$, *Col2-Cre;Ndst1*$^{fl/fl}$ and *Ndst1*$^{+/-}$ are protected against the development of OA., leading to the question if genetically modified mice with other alterations of the HS modification pattern show a similarly reduced progression of OA. Heterozygous *Glce* and *Hs2st1* mice and their wild type littermates were aged, their knee joints collected at different time points and assessed for signs of OA according to the guidelines recommended by the International Osteoarthritis Research Society (OARSI). The four quadrants of the joint (medial tibial plateau, medial femoral condyle, lateral femoral plateau and lateral femoral condyle) were scored separately, analysing three or more sectioning planes within the weight bearing area. Mean values for the two medial or lateral quadrants or for the whole joint are shown.

At 6 months (m) of age, *Glce*$^{+/+}$ animals displayed barely any osteoarthritic alterations, with mean OA scores of 0.16, 0.32 and 0.24 in the medial and lateral proportion or the complete joint, respectively. Similarly, no signs of OA were detected in heterozygous *Glce*$^{+/-}$ mutants (mean scores: medial 0.08, lateral 0.24, total 0.11) (Fig. 12, A). After 18m, in *Glce*$^{+/+}$ animals weak OA scores of 0.25, 0.71 and 0.48 were detected in medial and lateral compartment and the complete knee, respectively. Similarly, heterozygous *Glce*$^{+/-}$ mice showed only weak signs of OA (medial 0.07, lateral 0.58, total 0.33) (Fig. 12, B). At the same age, *Hs2st1*$^{+/+}$ controls (medial 0.63, lateral 0.85, total 0.74) and *Hs2st1*$^{+/-}$ mutants (medial 0.57, lateral 1.1, total 0.84) displayed low OA scores as well (Fig. 12, C).

These data show that the progression of OA is not accelerated in the two HS mutants. Since only weak spontaneous OA was developed at both 6m and 18m of age, a possible protective effect cannot be evaluated by ageing of the two mouse strains. Due to the low sample numbers and large variations between individual mice, the data could not be modelled sufficiently and not statistical evaluation was performed.

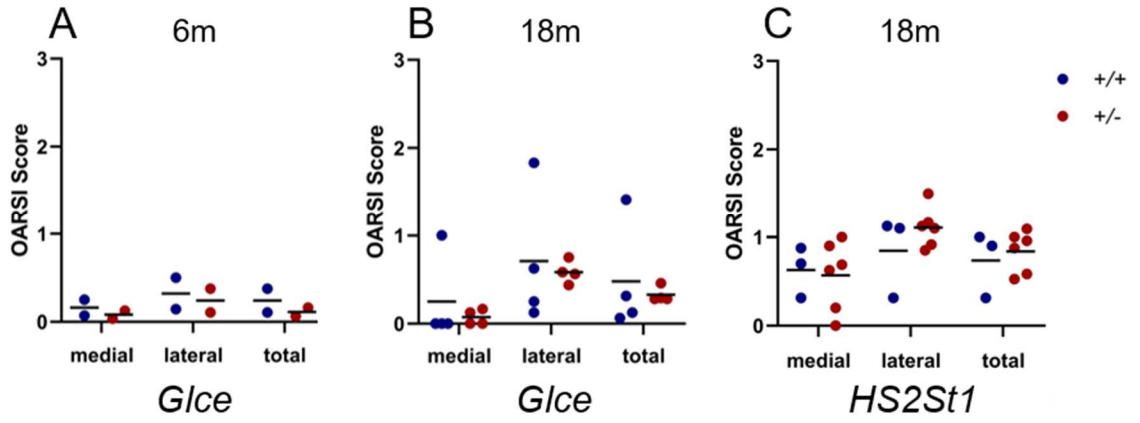

Figure 12: *Glce* and *Hs2st1* mice develop only mild signs of OA upon ageing Heterozygous *Glce*$^{+/-}$ and *Hs2st1*$^{+/-}$ animals as well as their wild type littermates were aged to analyse spontaneous OA development. *Glce* mice were analysed at (A) 6m as well as (B) 18m of age and *Hs2st1* animals (C) at 18m. Data points represent mean values of individuals, black lines indicate group means. *Glce*, 6m: 2 mice of each genotype from 1 litter; *Glce*, 18m: 4 mice of each genotype from 2 litters; *Hs2st1*, 18m: ≥3 mice of each genotype from 2 litters.

Since ageing did not result in sufficient osteoarthritic changes to analyse a potential protective effect, OA was surgically induced to generate more pronounced signs of OA. The DMM technique was established, which was also used by other members of the ExCarBon research consortium. First, DMM was performed on 12w old C57Bl/6 wild type mice and the degree of cartilage erosion was analysed after Toluidine Blue staining at different post-operative time points using the OARSI scoring system (Fig. 13, A). After 2w, first signs of OA were detected, such as minor loss of PGs visualised by Toluidine Blue staining, and scores greater than 0 could be observed in the medial compartment of the operated knees. For the complete joints, a total mean of 0.34 was determined, with OA scores ranging between 0.06 and 0.56 for individual mice. Compared to 2w after surgery, a similar degree of OA was seen after 4w (p^+=0.8376), as demonstrated by loss of PG staining, with a total mean of 0.36 and individual values between 0.12-0.71. Interestingly, the scores in the lateral compartment were increased compared to the earlier analysis timepoint and were now more similar to those found on the medial side of the joints. At 8w post-operation, the analysed animals displayed mild signs of OA, such as fibrillations of the superficial cartilage zone. A mean OA score of 0.83 in total was detected, with individual values between 0.31 and 1.17. Compared to 2w and 4w after OA induction, the OA scores were increased (p^+=1 and p^+=1, respectively). After 12w, the total mean score had further increased compared to 2, 4 and 8w after DMM (p^+=1, p^+=1,

p^+=0.994, respectively) to a mean of 1.06, though the analysed mice still displayed relatively mild OA. Scores ranged between 0.38 and 1.55 and included more pronounced signs of OA in some individuals, such as fissures reaching into the middle zone of the AC. Regarding the two compartments of the knee joint, fewer signs of OA were observed laterally (2w: medial 0.48, lateral: 0.20) 2w after surgery, while at 4w and 8w rather similar mean scores were found in the medial and lateral compartments (4w: medial 0.42, lateral 0.29; 8w: medial 0.75, lateral 0.90). Interestingly, at 12w the degree of OA found in the lateral compartment was markedly higher compared to the medial side (12w: medial 0.71, lateral 1.41) (Fig. 13, B). Although the surgical procedure was performed on the medial compartment of the knee, the integrity of the whole joint seemed to be affected by it.

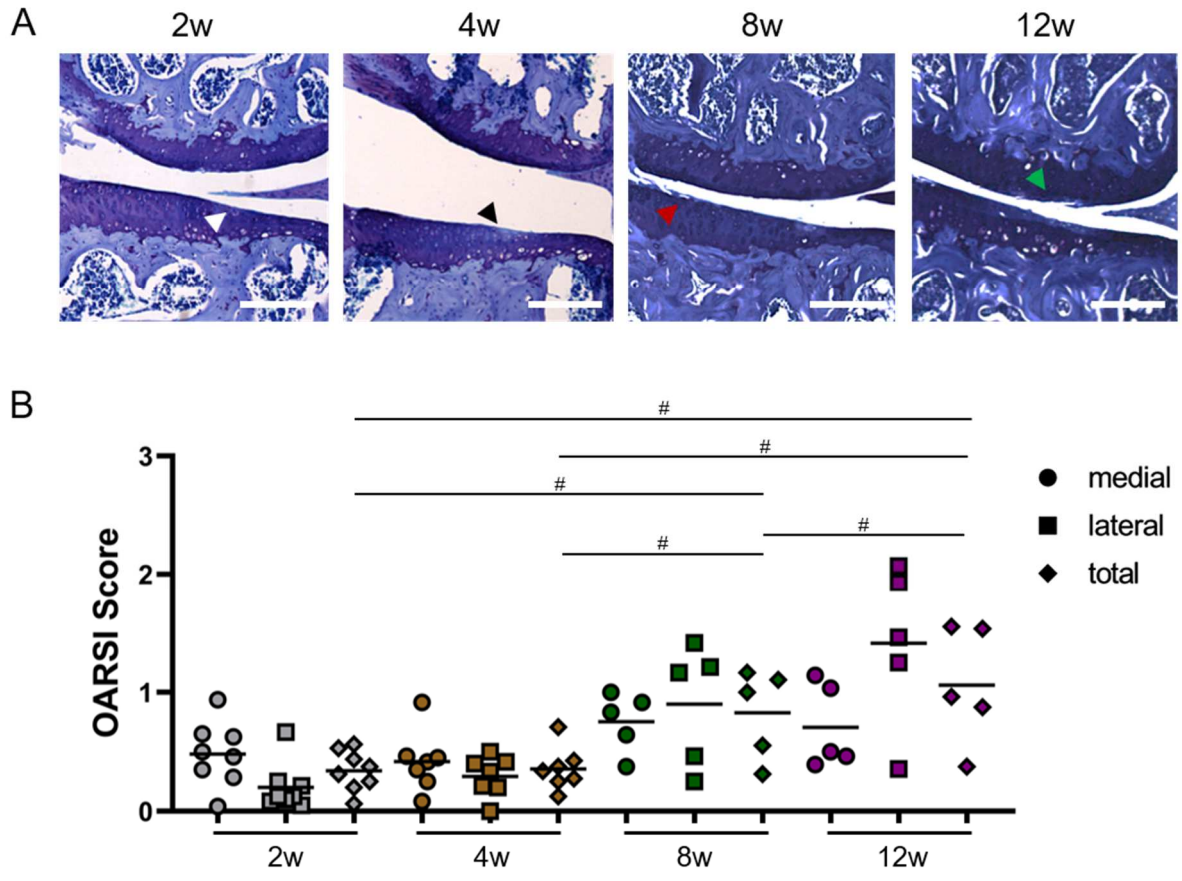

Figure 13: DMM surgery induces mild signs of OA 12w old C57Bl/6 mice were operated and their knee joints analysed for signs of OA at 2, 4, 8 and 12 post-surgery (A) Toluidine Blue staining of frontal sections through DMM operated knee joints showing the medial joint compartment. White arrow: minor loss of PG staining, black arrow: major loss of PG staining, red arrow: fibrillation of superficial cartilage zone, green arrow: fissure into middle zone. Scale bar: 200µm. (B) Quantification of OA signs in medial and lateral compartment as well as total knee joint. Data point represent mean values of individual mice, black lines indicate group means. n≥5, # $p^+ \leq 0.05$ or $p^+ \geq 0.95$.

Taken together, these data show that mild OA was induced by DMM surgery. For all further experiments, the post-operative time point with the highest OA scores was chosen and analyses were performed 12w after surgery. Heterozygous *Glce* and *Hs2st1* mice as well as their wild type littermates were operated at 12w of age. On the right hind limb DMM was performed while a sham surgery was conducted on the contralateral leg, serving as an internal control for iatrogenic effects. In both mouse strains osteoarthritic changes were induced by the DMM procedure, such as minor or major loss of PGs, fibrillations of the superficial cartilage zone, or fissures in the AC (Fig. 14, A).

Sham operated *Glce*$^{+/+}$ mice did not show any signs of OA, resulting in mean scores of 0.05, 0.23 and 0.14 for medial, lateral and total knee joints, respectively. In contrast, DMM surgery induced mild OA (medial 0.90, lateral 1.36, total 1.13), including moderate scores between 2 and 3 in some individuals. Similarly, no osteoarthritic alterations were found in joints of *Glce*$^{+/-}$ animals after Sham surgery, with means of 0.08, 0.11 and 0.09 within the medial and lateral compartment and the complete knee. After DMM, mild signs of OA were detected in the heterozygous mutants (medial 1.28, lateral 0.61, total 0.95). Compared to *Glce*$^{+/+}$ controls, scores were increased in the medial joint compartment (ratio 1.42), but decreased on the lateral side (ratio 0.45), resulting in a total ratio of 0.84 between heterozygous mutants and wild type mice, which was not statistically stable (p^+=0.3023). In *Hs2st1*$^{+/+}$ animals, sham surgery did not induce any signs of OA (medial 0.05, lateral 0.09, total 0.07). In contrast, mild OA was detected after DMM, with mean scores of 0.81, 0.74 and 0.77 in the medial and lateral compartments and the complete knee joints. Likewise, sham surgery did not result in osteoarthritic alterations in *Hs2st1*$^{+/-}$ mutants (medial 0.02, lateral 0.14, total 0.08). By DMM mild OA scores were obtained, with means of 1.02, 1.07 and 1.05 for medial, lateral and total joints (Fig. 14, B). Both genotypes developed mild signs of OA after induction by DMM. Compared to *Hs2st1*$^{+/+}$ animals, the scores of *Hs2st1*$^{+/-}$ mice were elevated with ratios of 1.26, 1.45 and 1.36 for medial and lateral compartment and total joints. Still, due to the large variation observed between individual animals this effect is not statistically stable (p^+=0.2845).

Nevertheless, no severe signs of OA were detected in any of the mice, showing that neither *Glce*$^{+/-}$ nor *Hs2st1*$^{+/-}$ display a markedly increased susceptibility to OA.

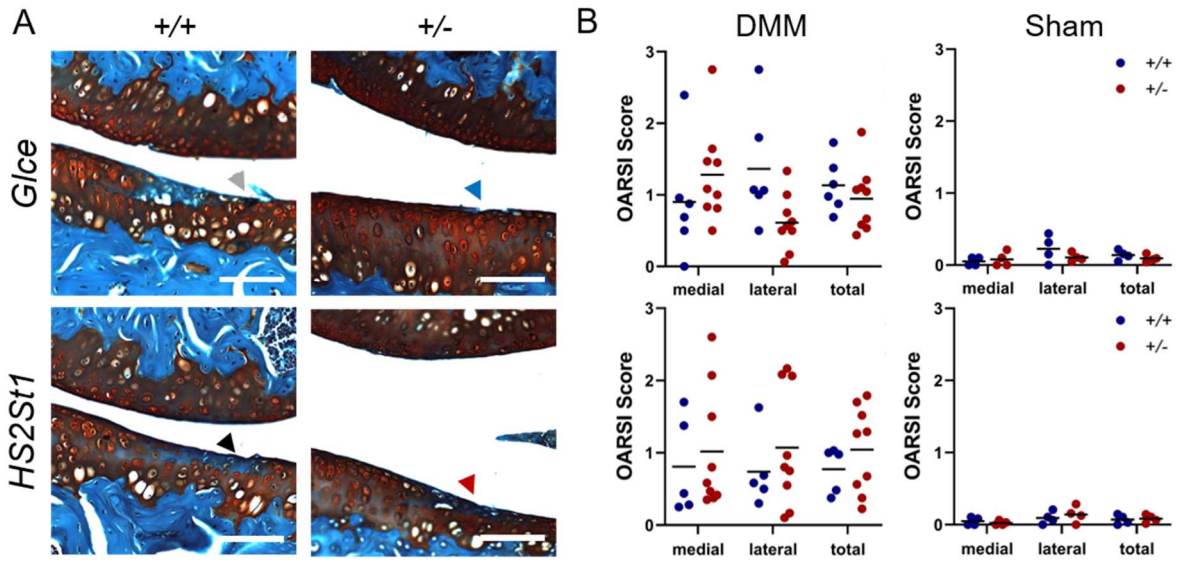

Figure 14: DMM surgery of *Glce* and *Hs2st1* mice (A) Safranin Weigert staining of frontal sections from mice operated by DMM, showing various signs of OA. Grey arrow: fissure in AC, blue arrow: fibrillation of superficial cartilage layer, black arrow: major loss of PG staining, red arrow: minor loss of PG staining. Scale bars: 100µm. (B) Quantification of OA. Data points represent mean values of individual mice, black lines indicate group means. n= 9 *Glce*$^{+/+}$, 12 *Glce*$^{+/-}$; 5 *Hs2st1*$^{+/+}$, 12 *Hs2st1*$^{+/-}$.

1.1.3. Clusters of HS-deficient cells produce severely altered cartilage matrix

Mice with a clonal loss of HS-synthesis in chondrocytes (*Col2-CreERT;Ext1*$^{fl/fl}$) display clusters of enlarged, morphologically distinct cells in the AC. Around those clusters, an altered matrix composition with increased PG content has been reported (Sgariglia *et al.*, 2013). To examine the altered matrix found around HS-deficient clusters, a mouse model with a clonal loss of function of *Ext1* in a subset of chondrocytes (*Col2-rtTA-Cre;Ext1*$^{e2fl/e2fl}$) was analysed. Joints were isolated from 4w old mice after Cre induction at P8 and the presence of clusters of enlarged cells in the AC of *Col2-rtTA-Cre;Ext1*$^{e2fl/e2fl}$ mice (Fig. 15, A) and an increased aggrecan content around those clusters (Fig. 15, B) were confirmed.

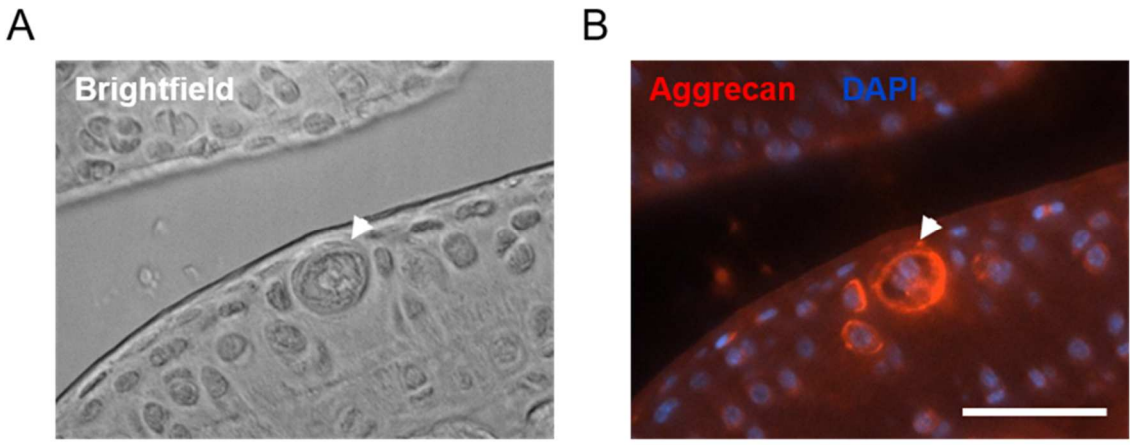

Figure 15: Increased aggrecan content around clusters of HS-deficient chondrocytes Limbs from *Col2-rtTA-Cre;Ext1*$^{e2fl/e2fl}$ mice were isolated at 4w of age after Cre induction at P8. (A) Brightfield image showing the presence of clusters of enlarged cells in the AC. (B) Immunostaining demonstrates an increased aggrecan content in the matrix surrounding those clusters. Scale bar: 50µM (modified from Severmann, 2020).

The ECM around HS-deficient cells displays a severely altered composition, raising the question how this changes the mechanical properties of this matrix. To investigate this, cryo samples of 4w old *Col2-rtTA-Cre;Ext1*$^{e2fl/e2fl}$ mice and analysed by AFM in collaboration with the lab of Hauke Clausen-Schaumann at the University of Applied Sciences in Munich. By AFM, the Young's Modulus is determined as a parameter for matrix stiffness: Lower values are associated with more elastic properties while higher values are found in stiffer materials.

AFM measurements were conducted in the superficial, middle and deep zone of the AC and bimodal distributions of individual measurement values were obtained. Within the superficial zone of *Ext1*$^{e2fl/e2fl}$ mice, peak values of 79.69 and 160.26kPa were detected. In the middle zone, the value of the lower peak was increased to 108.77kPa, while the higher peak was rather similar to that of the superficial zone (166.71kPa). Both peaks were shifted to a higher Young's Modulus in the deep zone of *Ext1*$^{e2fl/e2fl}$ samples, with peak values of 130.31 and 238.31kPa. AFM analysis of the wild type-like cartilage of *Col2-rtTA-Cre;Ext1*$^{e2fl/e2fl}$ mutants showed peak values of 133.19 and 186.49kPa in the superficial cartilage layer. In the middle zone, both peaks were shifted to higher values of 183.84 and 287.83kPa. Within the deep zone, a rather similar value compared to the middle zone was found for the lower peak (179.98kPa) while the higher one was increased to 372.85kPa (Fig. 16). In general, the detected Young's Moduli increased with the depth of the cartilage zone in both genotypes. Compared to *Ext1*$^{e2fl/e2fl}$ controls, the values detected for the lower peak

were elevated in *Col2-rtTA-Cre;Ext1*$^{e2fl/e2fl}$ mice by increase factors of 1.67, 1.,69 and 1.38 in superficial, middle and deep zone, respectively. Likewise, the detected values for the higher peak of the bimodal distribution were increased by 1.16, 1.73 and 1.56 in the three cartilage zones of the mutant samples. This enhanced pressure resistance of the AC might be one the mechanisms contributing to the decreased development of OA seen in *Col2-rtTA-Cre;Ext1*$^{e2fl/e2fl}$ mice. Surprisingly, the altered ECM found around clusters of HS-deficient cells was outside of the measurement range, showing that the mechanical properties of the mutant matrix are massively altered, though exact values could not be obtained.

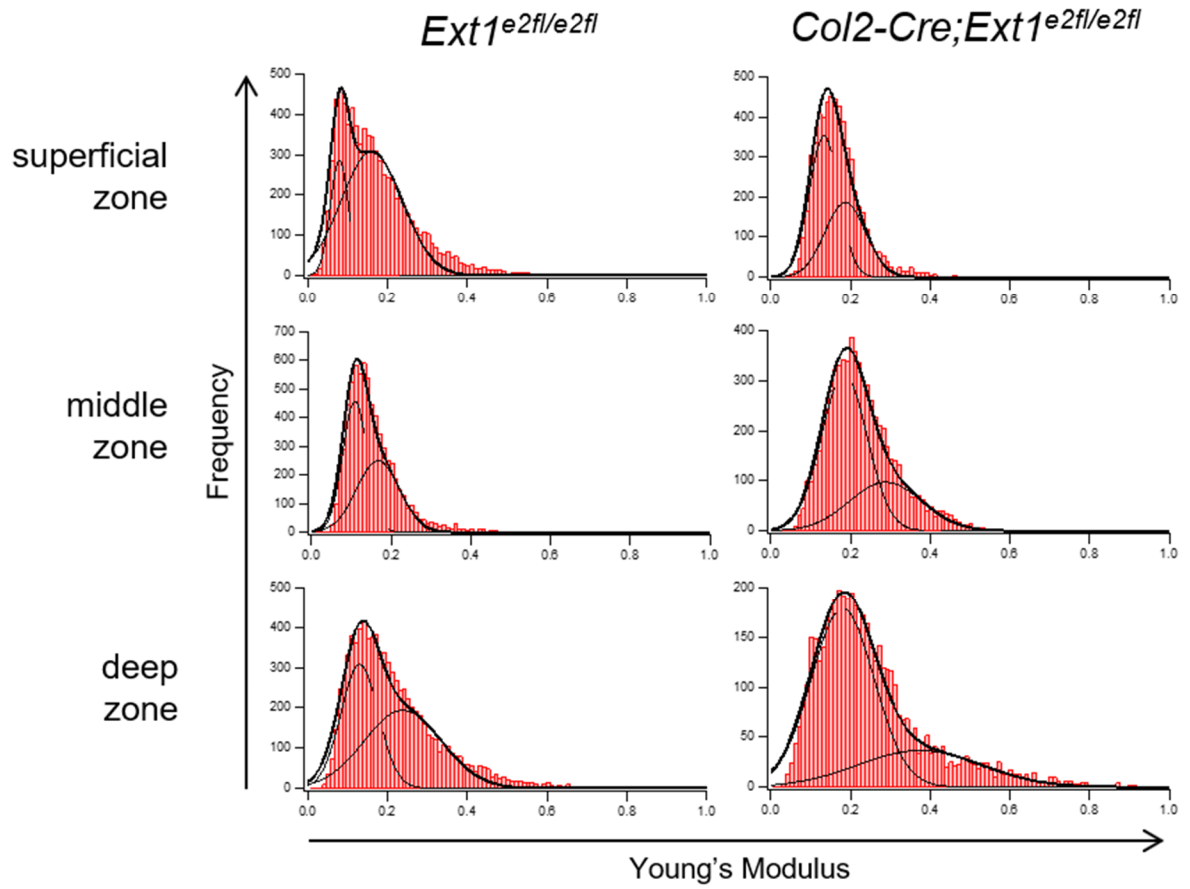

Figure 16: Increased Young's Modulus of wild type-like cartilage matrix in *Col2-rtTA-Cre;Ext1*$^{e2fl/e2fl}$ mice Superficial, middle and deep zone of the AC of *Col2-rtTA-Cre;Ext1*$^{e2fl/e2fl}$ mice and *Ext1*$^{e2fl/e2fl}$ control animals were assessed by AFM. Distributions of individual readings and peak values of the Young's Modulus are displayed. 3 individual mice of each genotype were analysed, collected from 2 litters. AFM measurements were performed by Lutz Fleischhauer at CANTER (Centre for Applied Tissue Engineering and Regenerative Medicine), University of Applied Sciences, within the ExCarBon network.

To overcome this limitation, mice with a hypomorphic allele of *Ext1* were analysed. In *Ext1*$^{gt/gt}$ animals HS synthesis is reduced throughout the tissue leading to a

decreased HS-level of 20% (Koziel *et al.*, 2004). Since homozygous presence of the genetrap allele is embryonically lethal, AC tissue cannot be investigated at postnatal stages. Therefore, limbs of *Ext1*$^{gt/gt}$ mutants and *Ext1*$^{+/+}$ littermates were isolated at E15.0 and the cartilage of the GP was analysed by AFM. In the proliferating zone, two types of ECM can be distinguished: The territorial matrix directly surrounding the cells and the interterritorial matrix between columns of proliferating chondrocytes.

In the *Ext1*$^{+/+}$ control embryo, the bimodal distribution of measurement values showed two peaks at 7.64 and 13.13kPa in the interterritorial matrix. The territorial matrix displayed a lower stiffness with peaks at 2.58 and 4.78kPa. Within the interterritorial matrix of the *Ext1*$^{gt/gt}$ embryo the distribution of individual measurements showed peaks at 1.62 and 2.31kPa, while in the territorial matrix peaks were detected at higher values of 2.49 and 5.12kPa (Fig. 17). Taken together, the Young's Moduli measured in the wild type tissue were higher in the interterritorial matrix than in the territorial area. On contrast, the HS-deficient ECM displayed higher values in the territorial than in the interterritorial matrix. Compared to the *Ext1*$^{+/+}$ control, both peaks detected in the territorial area of *Ext1*$^{gt/gt}$ sample were similar with change factors of 0.97 and 1.07. In the interterritorial matrix, both peak values were decreased in the mutant (change factors of 0.21 and 0.17).

This preliminary result (n=1) shows that HS-deficiency leads to a reduced matrix stiffness.

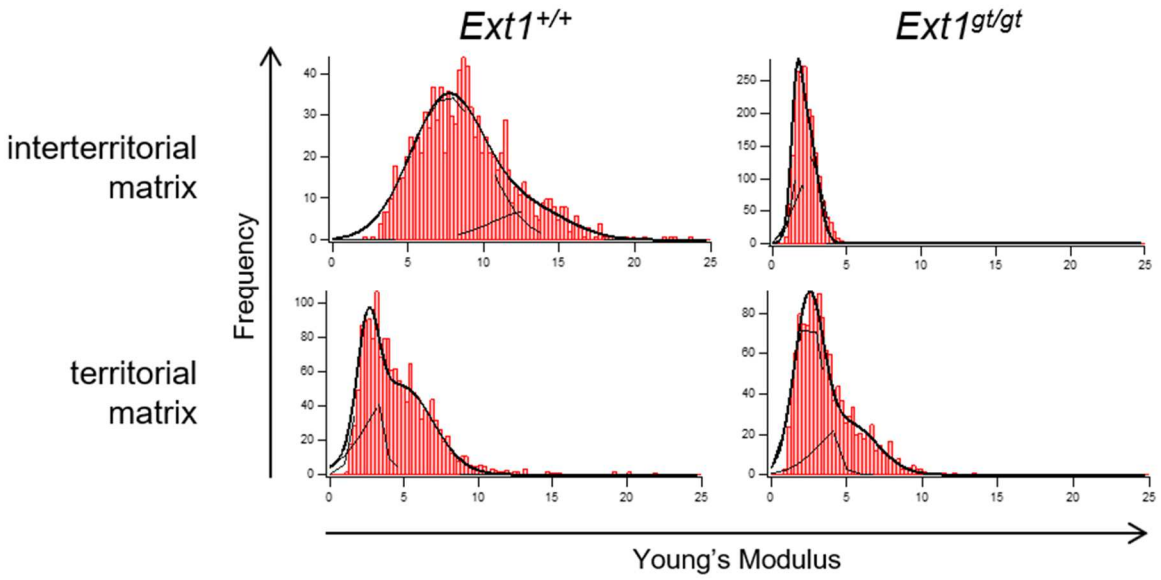

Figure 17: Decreased Young's Modulus in embryonic cartilage of Ext1gt/gt mutants The stiffness of interterritorial and territorial matrix was assessed in *Ext1*$^{gt/gt}$ and *Ext1*$^{gt/+}$ samples by AFM. Distribution curves of individual measurements and peak values are displayed. One embryo of each genotype from the same litter was analysed. AFM measurements were conducted by Lutz Fleischhauer.

1.1.4. Integrin pathway components are upregulated in HS-deficient cells

As stated before, the clusters of HS-deficient chondrocytes found in the AC of *Col2-rtTA-Cre;Ext1*$^{e2fl/e2fl}$ mice produce matrix of aberrant composition and severely altered mechanical properties. This raises the question, how the lack of HS within the ECM is sensed by the cells. Integrin dimers are major receptors for cell matrix adhesion, anchoring cells within their surrounding matrix and conveying signals into the cells. Previously, an upregulation of the integrin pathway components FAK, pFAK, pERK and MHCII in HS-deficient chondrocytes of *Col2-rtTA-Cre;Ext1*$^{e2fl/e2fl}$ mice was demonstrated by immunohistochemistry (Jochmann, 2016, PhD thesis).

These results were confirmed by immunostaining against additional integrin pathway components. Paraffin sections of 4w old *Col2-rtTA-Cre;Ext1*$^{e2fl/e2fl}$ mice were analysed for the presence of ItgB1, Src and ERK. Within the HS-deficient clusters, a strong signal for β1-Integrin was detected, though the protein also seemed to be expressed at high levels in a few chondrocytes within the superficial zone. In contrast, Src kinase and ERK were distinctly upregulated in the clustered, mutant cells compared to the surrounding wild type-like matrix (Fig. 18).

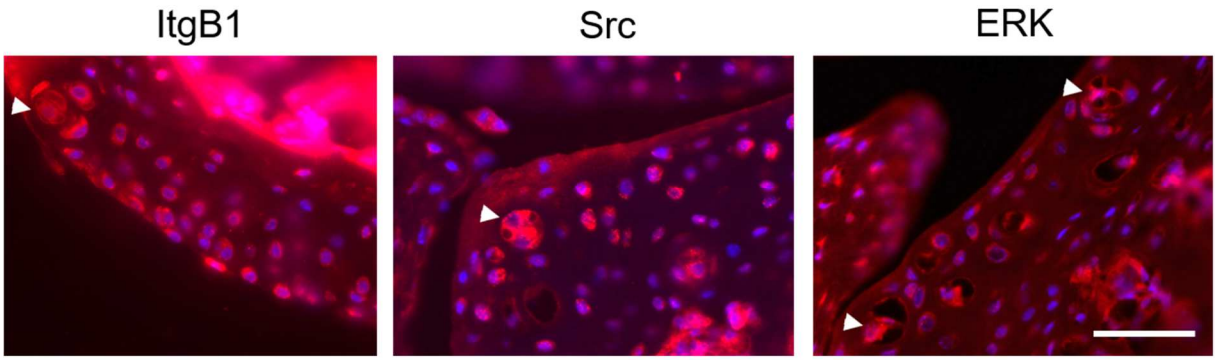

Figure 18: Increased amounts of integrin pathway components Src and ERK in HS-deficient clusters Sagittal paraffin section of 4w old *Col2-rtTA-Cre;Ext1*$^{e2fl/e2fl}$ mice were submitted to immunostaining against ItgB1, Src and ERK. Staining intensities around HS-deficient clusters (white arrow) were documented by fluorescence microscopy While increased staining for ItgB1 was not only found in HS-deficient cells but also in chondrocytes of the superficial zone, Src and ERK signals were only upregulated in clusters. Scale bar: 50µM.

Taken together, these results demonstrate that many components of the integrin pathway are upregulated in response to a loss of HS synthesis.

3.2. *In vitro* analyses

To study the effect of an impaired HS-protein interaction on cellular processes *in vitro*, MEFs were treated with bis-2-methyl-4-amino-quinolyl-6-carbamide (Surfen). Surfen is a small molecule antagonist that interacts electrostatically with GAG chains,

masking the negative charges of their sulfate groups (Schukz *et al.*, 2008). Immunohistochemistry revealed increased expression of integrin pathway components in HS-deficient cells *in vivo*. This raises the question if cell-matrix-adhesion is altered upon disturbed integrin function, since integrins are major components of FA.

3.2.1. HS-antagonist Surfen delays cell adhesion

To analyse cell-matrix interactions, MEFs were chosen as a model. These are primary cells of murine origin and more closely resemble *in vivo* conditions than immortalised cell lines. Additionally, MEFs are large cells with easily recognisable adhesion, spreading and polarisation behaviour. To investigate the consequences of HS inhibition on cell adhesion, a time course experiment was conducted adding different Surfen concentrations to adhering cells. MEFs were seeded into 24-well plates in a density of 5000 cells/well and cultured for 0.5, 1, 2, 16 and 24h in the presence of 10, 5 or 2.5µM Surfen. In the different samples and the solvent control equimolar amounts of DMSO were applied. After fixing and nuclear staining, three images were taken from each well and the number of adherent cells in each image was quantified using the software CellProfiler. The mean number of imaged cells per image is displayed for each well.

In the controls the number of adherent cells increased markedly over time. After 0.5h an average of 91 adherent cells per image were detected. The number of adherent MEFs increased to an average of 164 after 1h and to 265 after 2h. After an overnight incubation of 16h, the mean number of attached cells reached 475 and stayed relatively constant at 24h with 495 cells on average (Fig. 19, A).

Compared to the control, the relative number of adherent cells was decreased in the Surfen-treated samples in a dose-dependent manner. At 0.5h, the numbers of adherent cells were reduced to 24% ($p^+ \approx 0$), 43% ($p^+ = 0.0003$) and 50% ($p^+ = 0.0234$) in the three Surfen concentrations of 10, 5 and 2.5µM compared to the DMSO control. After 1h, cell counts were decreased to 32% ($p^+ = 0$), 47% ($p^+ = 0$) and 49% ($p^+ = 0$) for 10, 5 and 2.5µM Surfen compared to the control. Later, cell numbers in Surfen-treated samples were still decreased compared to the solvent control, but the differences were less pronounced. At 2h, relative cell counts had increased to 62% ($p^+ = 0$), 88% ($p^+ = 0.0215$) and 88% ($p^+ = 0.0355$) for 10µM, 5µM and 2.5µM Surfen, respectively. At 16h, the numbers of adherent cells were mildly reduced 78% ($p^+ = 0.0064$) and 84% ($p^+ = 0.0309$) in presence of 10 and 2.5µM Surfen ($p^+ \leq 0.05$),

while the proportion of adherent cells for 5µM Surfen was similar to the control (94%, p^+=0.2275). After 24h adhesion, reduced cell adhesion was detected for 10µM (68%; p^+=0) and 5µM Surfen (89%; p^+=0.0431) but not in presence of 2.5µM Surfen (93%; p^+=0.3864) (Fig. 19, B). The changes observed between the different Surfen concentrations were statistically stable after 0.5h adhesion ($p^+ \leq 0.05$). A stable difference between the concentrations 5µM and 2.5µM was not observable at later time points. In addition, no difference between 2.5 and 10µM Surfen was found at 16h of adhesion.

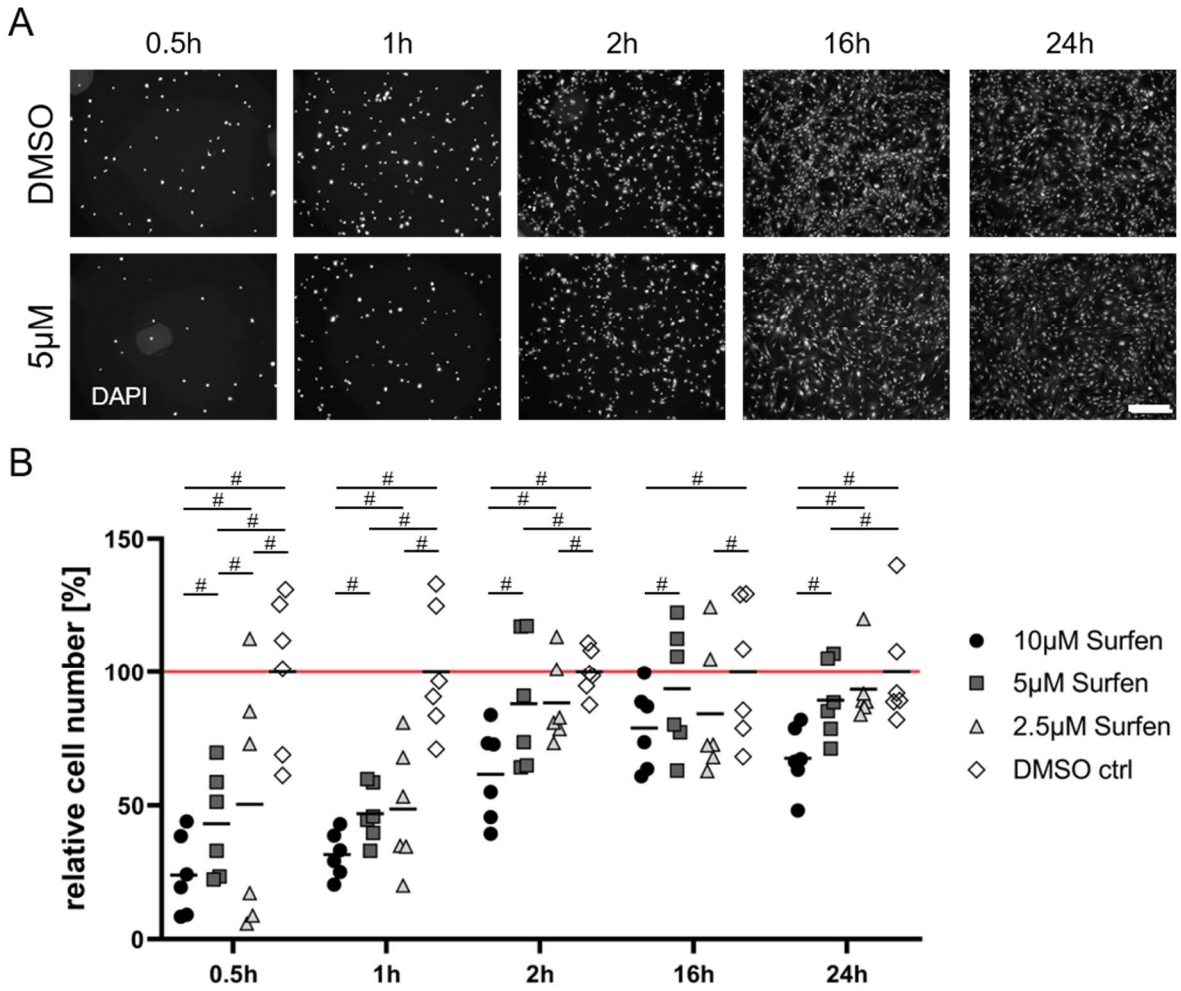

Figure 19: Reduced adhesion of MEFs in presence of Surfen (A) Nuclear Staining of MEFs after different time periods reveals decreased numbers of adherent cells upon Surfen-treatment compared to DMSO controls. 5µM Surfen is shown as an example. Scale bar: 500µM. (B) Cell counts of samples treated with different Surfen concentrations relative to DMSO control. Two biological replicates with three technical replicates each are shown. Data points represent individual samples. Black lines indicate means, # $p^+ \leq 0.05$ or $p^+ \geq 0.95$.

These data indicate that the initial cell adhesion process is impaired in the presence of Surfen. This leads to the question, which subcellular structures are affected by the inhibited HS function and how the cells are able to overcome this limitation. To investigate this, a concentration of 5µM Surfen was used for all further experiments.

3.2.2. Surfen-treated MEFs form filopodia-like protrusions

To gain insight into the behaviour of Surfen treated MEFs during the early adhesion process, life cell imaging was performed. Cells were incubated with 5µM Surfen or an equimolar amount of the solvent DMSO. MEFs were seeded into 8-well slides at a density of $1.5*10^5$ cells per well and cultured for 20min for pre-adhesion before transfer to a phase contrast microscope. Images were taken once per min for 1h, capturing the time period determined to be critical in the previous experiment. Surfen-treated MEFs appeared to have irregularly shaped cell seams with highly dynamic membrane protrusions. Accordingly, the morphology of single cells was assessed and the formation of membrane protrusions analysed. The percentage of cells forming a clean cell seam or lamellipodium-like structure, finger-shaped, filopodia-like protrusions or branched pseudopodia-like protrusions was documented for each video (Fig. 20, A).

In the first frame of the videos an average of 71% of the DMSO-treated MEFs had formed lamellipodium-like structures or displayed areas with a clean cell seam. At the same time point, 30% of the cells formed pseudopodia-like and 14% filopodia-like protrusions. The proportion of MEFs displaying one or both of the two protrusions was 37%. When treated with Surfen, a mean of 57% of cells per video showed a clean cell seam or a lamellipodium-like structure. 33% of the MEFs formed pseudopodia-like and 24% filopodia-like protrusions in presence of Surfen and an average of 40% of the cells had one or both of the two protrusions. Compared to the solvent control, fewer cells were able to form a clean cell border in the Surfen-treated samples, with a change factor of 0.74 ($p^+=0$). The proportions of cells with pseudopodia-like protrusions were similar (change factor 0.95, $p^+=0.2600$), as well as the percentages of cells with either one or both protrusions (change factor 1.03, $p^+=0.6521$). Interestingly, in the presence of Surfen an increased proportion of cells forming filopodia-like structures was detected (change factor 1.42, $p^+=0.9989$) (Fig. 20, B, Start).

The indicated features were assessed again in the last frame of each video. Upon treatment with DMSO, the mean proportion of untreated cells forming a clean cell

seam or a lamellipodium-like structure was decreased to 56% while the relative number of cells with pseudopodia-like protrusions was elevated to 54% compared to the beginning of the imaging sequence. The percentage of MEFs with filopodia-like structures was increased at this time point, as well as the fraction displaying any kind of protrusion (24% and 69%, respectively). When Surfen was present, the number of cells forming a clean border or a lamellipodium at the end of the video remained similar to the first frame (50%). In contrast, higher percentages of MEFs forming pseudopodia-like or filopodia-like structures were detected (45% and 70%, respectively) and the number of cells with any or both protrusions was increased to 70%. Compared to the DMSO control, at the end of the videos fewer Surfen-treated cells displayed lamellipodium-like structures (change factor of 0.81, $p^+=0$). or

The proportions of MEFs forming pseudopodia-like and one or both protrusion were similar (change factors 0.96 and 1.02, $p^+=0.2600$ and 0.6521, respectively), while the percentage of cells with filopodia was clearly increased in the Surfen-treated samples (change factor 1.34, $p^+=0.9989$) (Fig. 20, B, End).

This raised the question, whether the number of filopodia per cell was also altered. At the first frames of the videos MEFs that produced filopodia-like structures showed an average of 4.4 protrusions per cell in the presence of DMSO. The number of such structures remained similar at the end of the videos with a mean of 4.7. In the Surfen-treated samples 4.7 filopodia-like protrusions were detected per cell on average in the first frame of the videos. By the end of the imaging sequence, the number of filopodia-like structures per cell was 5.5. Comparing DMSO- and Surfen-treated samples, similar numbers of filopodia-like structures per cell were detected at the start of the videos (change factor 1.07) and at the end of the imaging period (increase factor 1.17) (Fig. 20, C). Due to a large variation between individual cells the data could not be modelled sufficiently and no statistical evaluation was performed concerning the number of filopodia per cell.

For cell migration, the specification of a leading edge and the formation of a lamellipodium at this position are required. Therefore, an aberrant morphology of the cell seam might have an effect on cell mobility. To analyse this, the number of cells migrating or polarising was documented for each video. Among the DMSO-treated MEFs, 7.3% of the cells migrated during the imaging period and 28.9% became polarised. During the analysis of the full videos, cells starting to detach from the surface were detected, making up 7.1% of the MEFs in presence of DMSO. When

Surfen was added, 2.9% of the cells migrated and 18.7% polarised during the time course of the imaging while 11.6% of the Surfen-treated MEFs started to detach from the plate. In relation to the DMSO control, the proportions of migratory (change factors 0.34, p^+=0.0014) and polarised cells (change factor 0.67, p^+=0.0055) were decreased in the presence of Surfen and. In contrast, the percentage of cells detaching showed a tendency to be increased in the Surfen-treated samples (change factor 1.53), although this was not a stable effect (p^+=0.9138) (Fig. 20, A, D).

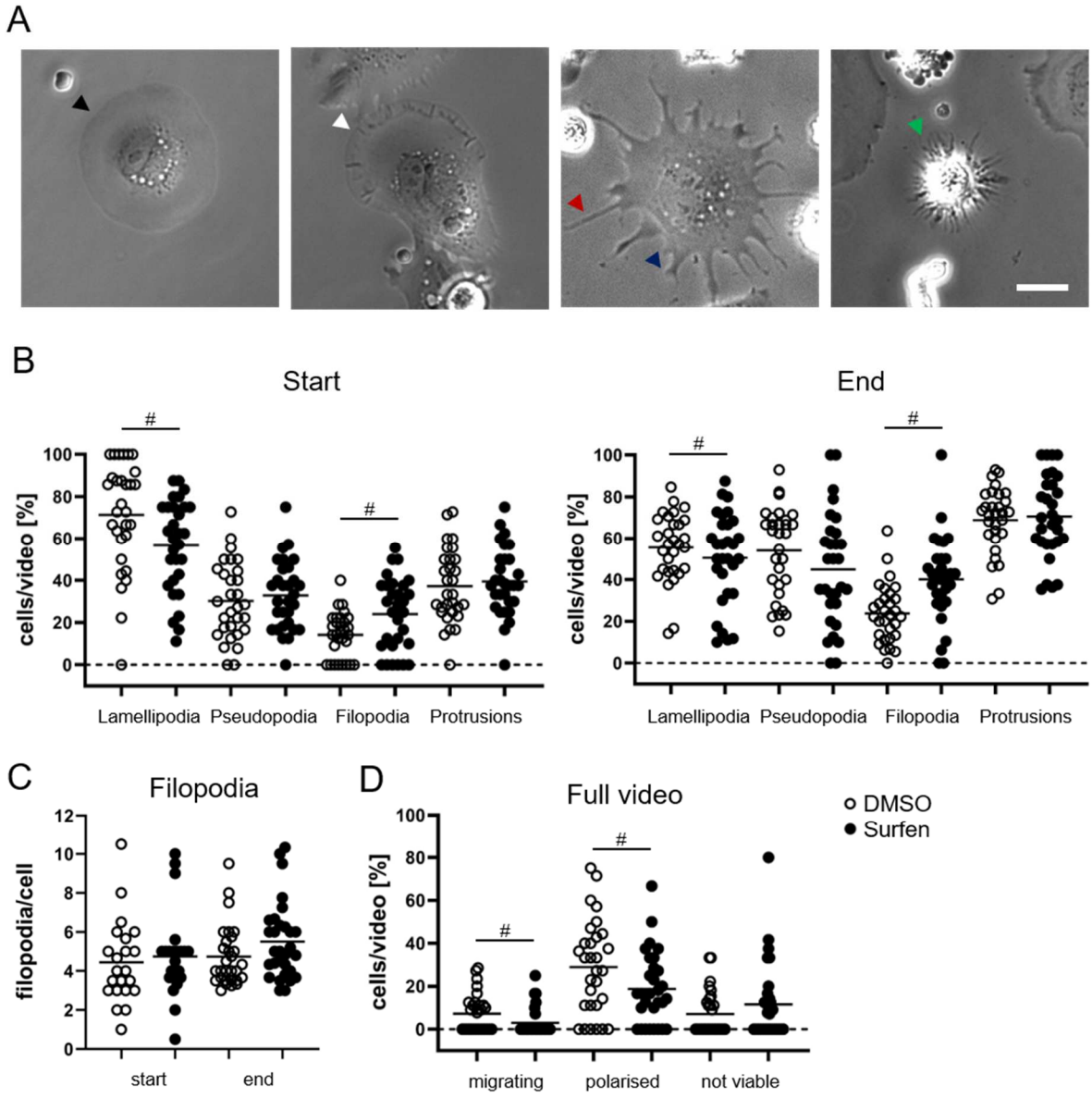

Figure 20: Increased formation of membrane protrusions and reduced cell polarisation in Surfen-treated MEFs (A) Exemplary depiction of cell seam morphologies imaged under phase contrast conditions. Black arrow: clean cell seam, white arrow: lamellipodium-like structure, red arrow: filopodia-like protrusion, blue arrow: pseudopodia-like protrusion, green arrow: detaching, non-viable cell. Scale bar: 20µM. (B) Assessment of first (Start) and last (End) video frame. The proportions of cells displaying the indicated features are shown, each data point representing an individual video. Three biological replicates with two technical replicates each are displayed. Black lines indicate means, # $p^+ \leq 0.05$ or $p^+ \geq 0.95$.

Taken together, upon HS-inhibition MEFs showed an impaired adhesion to the plate and more often detached from the surface, and fewer cells were able to migrate or polarise. Additionally, a higher proportion of MEFs formed filopodia-like structures under treatment with Surfen. It has been described that filopodia contain high amounts of integrins and are responsible for mechano-sensing of the substrate during cell migration (Innocenti, 2018). In the context of the upregulation of integrin pathway components observed in HS-deficient cells *in vivo*, this underlines an effect of the loss of HS on integrin function.

3.2.3. During cell adhesion, the formation of FA and SF is impaired by inhibition of HS function

Integrin receptors are integral components of FAs, which anchor cells to their surrounding substrate and connect the ECM to the cytoskeleton. An impaired integrin function may alter the formation of FA or result in changes of cytoskeletal structures. To analyse the formation of FA, MEFs were incubated in medium containing 5µM Surfen or an equimolar amount of DMSO as a solvent control. For an adhesion time of 1h, which was previously determined to be a critical time point, $5*10^4$ cells were seeded in each well of a 96-well plate. For 24h of culture time, $2.5*10^4$ cells per well were used. Within this time frame, MEFs were able to compensate limited cell-matrix adhesion in the presence of Surfen in the experiments already described. Additionally, MEFs were pre-adhered for 24h and subsequently treated with Surfen or DMSO for 1h to investigate effects unrelated to the impaired adhesion process. FA were detected by immunostaining as clusters of Paxillin at the cell seam or in membrane protrusions (Fig. 21, B). From every condition 10 images were taken and the relative proportion of cells forming FA was quantified in each picture.

After 1h of adhesion, FA were detected in an average of 64% of the control MEFs. The proportion of cells with FA decreased to a mean of 34% after 24h adhesion. When DMSO-containing medium was added after 24h incubation, 40% of the MEFs displayed FA. When MEFs adhered for 1h in the presence of Surfen, an average of 36% of the cells formed FA. This proportion was further reduced to 25% after 24h adhesion. When Surfen was added to already adhered MEFs, an increased fraction of cells displayed FA (57%). Compared to DMSO-treated controls, a reduced percentage of MEFs formed FA after 1h adhesion in presence of Surfen (change factor 0.50, $p^+=0$). After 24h adhesion, the proportion of cells with FA adhesions

recovered and was similar to the control (change factor 0.84, p^+=0.2228). In contrast, subsequent addition of Surfen to MEFs that had already adhered induced a higher percentage of cells forming FA (change factor 1.56, p^+=0.9993) (Fig. 21, A).

This demonstrates that HS function is required for the formation of FA. Additionally, an excessive formation of FA was induced by the addition of Surfen to already adhered MEFs which mirrors the upregulation of integrin pathway components seen in HS-deficient cells *in vivo*.

FA are connected to contractile SFs of the actin cytoskeleton, thus the structure of the cytoskeleton is likely altered in absence of FA. To analyse the formation of SFs intracellular actin was detected using fluorescence-labelled Phalloidin (Fig. 21, D). After 1h adhesion in the presence of DMSO, an average of 58% of the MEFs displayed SFs. This proportion increased to 83% after 24h of adhesion. When DMSO was added at 24h for 1h, SF were detected in 72% of the cells. Seeding of MEFs into Surfen-containing medium resulted in an average of 20% of cells with SF after 1h. At 24h, the proportion of MEFs forming SF had increased to 73%. Addition of Surfen to already adhered cells resulted in the formation of SF in 88% of the treated MEFs. In contrast to DMSO controls a reduced fraction of cells contained SF in Surfen-treated samples after 1h of adhesion (change factor 0.41, p^+=0). After 24h adhesion time, Surfen-treated samples recovered and showed a more similar percentage of cells with SF (change factor 0.93, p^+=0.20). As seen before during the analysis of FA, addition of Surfen to adherent MEFs induced the formation of SF in a higher proportion of cells (change factor 1.22, p^+=0.9998) (Fig. 21, C).

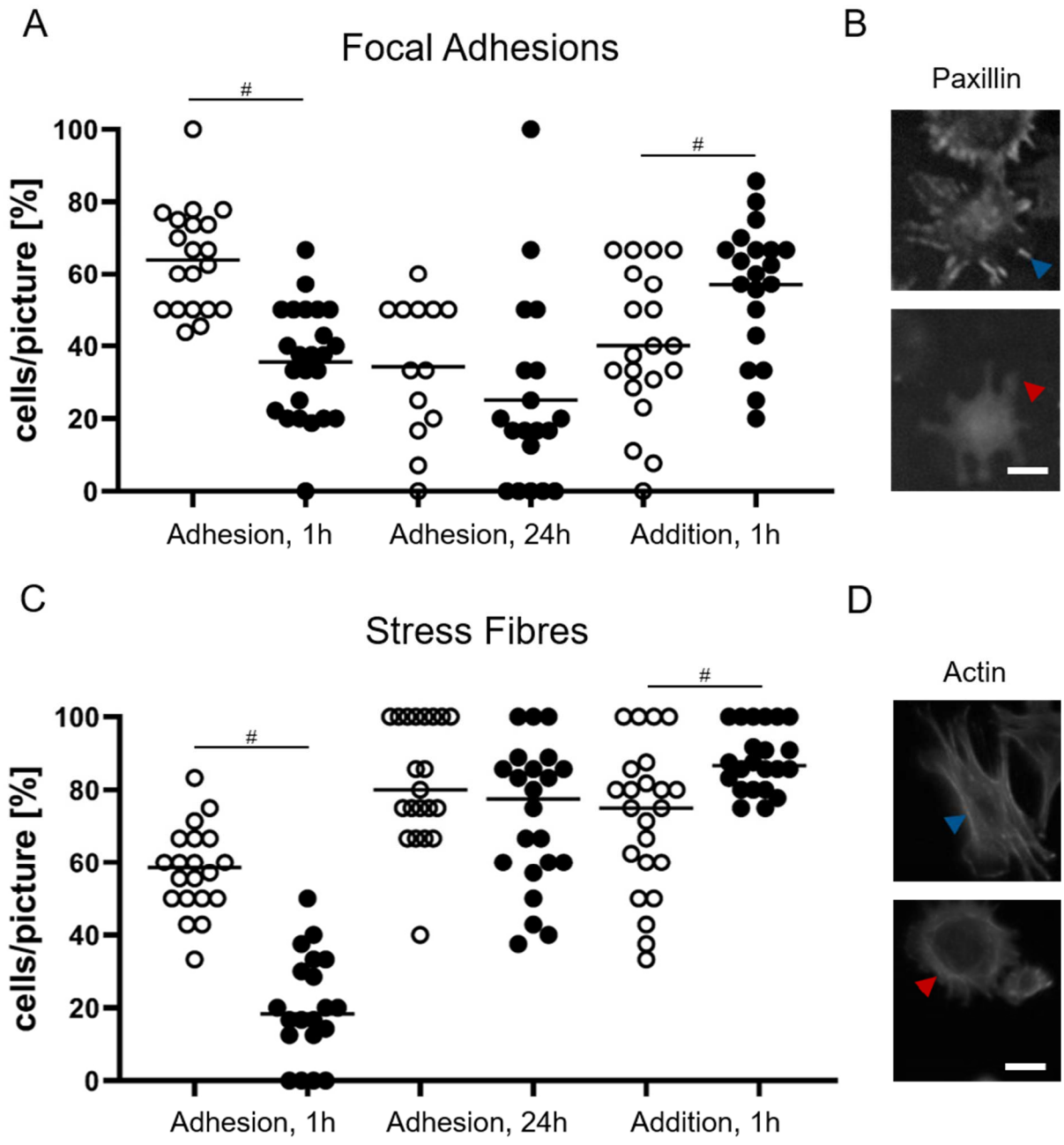

Figure 21: Reduced proportion of cells forming FAs and SFs under Surfen-treatment MEFs were seeded into DMSO- or Surfen containing medium and cultured for 1h or 24, or pre-adhered for 24h and subsequently treated with either DMSO or Surfen. (A, C) The relative proportion of cells displaying the indicated features was assessed after the different treatment regimes. Two biological replicates were evaluated, each data point representing an individual picture. White dots: DMSO control, black dots: 5µM Surfen. Black lines indicate means, # $p+\leq 0.05$ or $p+\geq 0.95$. (B) For the detection of FA, immunostaining against Paxillin was performed. Clustered signals indicate FA (blue arrow), which are absent in a subset of cells (red arrow). (D) Intracellular actin was visualised using Phalloidin to detect presence (blue arrow) or absence (red arrow) of SFs. (B, D) Scale bars: 20µM.

In line with the decreased cell adhesion and migration described above, these results demonstrate that the formation of FA and SF is impaired in the presence of the HS-antagonist Surfen. Interestingly, the proportion of cells forming FA and SF increased

when Surfen was added subsequently to adherent cells, emphasising a role of HS in integrin-mediated cell signalling.

Fluorescence staining for Paxillin showed that the formation of FA was affected by a loss of HS function. Therefore, the phosphorylation and activation status the FA component FAK was investigated by Western Blot (Fig. 22, A). Since the proportion of cells with FA was decreased after 1h adhesion in presence of Surfen, but increased when Surfen was added after 24h for 1h, these conditions were chosen for the analysis. MEFs were treated with 5µM Surfen or an equimolar ratio of DMSO as a solvent control. For each sample the signal intensity was quantified using ImageStudioLite and normalised against the total protein content of the sample visualised by total protein staining (TPS).

In general, higher amounts of FAK were found during initial cell adhesion compared to already adhered cells. The relative levels of pFAK were similar between both conditions, resulting in an increased pFAK/FAK ratio in adhered MEFs. Compared to DMSO controls, no differences were detected after treatment with Surfen under the two conditions (Fig. 22, B). Due to the low number of samples analysed in this experiment, the data set could not be modelled sufficiently and no statistical information was generated.

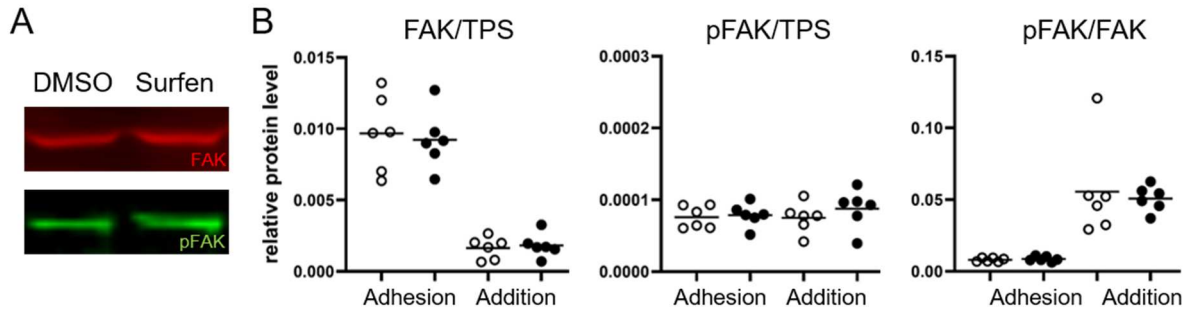

Figure 22: FAK and pFAK levels are unaltered in presence of Surfen MEFs were seeded into DMSO- or Surfen-containing medium and incubated for 1h (Adhesion) or medium containing the two agents was added to already adhere cells for 1h (Addition). (A) FAK and pFAK were detected in cell lysates by Western Blot. (B) The relative amount of FAK is higher during the adhesion process compared to adhered cells, while the relative amount of pFAK is similar between the two conditions resulting in a reduced pFAK/FAK ratio during adhesion. No differences were detected between DMSO- and Surfen-treated samples. Relative protein levels of FAK and pFAK were normalised over TPS. Three biological replicates including two technical replicates each were assessed, each data point represents an individual sample. White dots: DMSO control, black dots: 5µM Surfen. Black lines indicate means.

To analyse whether this effect is specific to treatment with Surfen or also occurs when HS-synthesis is lost endogenously, mutant Chinese Hamster Ovary (CHO)

cells were analysed that lack N-acetylglucosaminyltransferase and glucuronyltransferase activities (CHO pgsD-677) and consequently do not produce HS (Lidholt *et al.*, 1992). As a control, wildtype CHO cells with functional HS synthesis were used (CHO-K1) (Puck *et al.*, 1958). The cells were seeded at a density of $5*10^4$ cells per well of a 96-well plate, left to adhere for 1h and subsequently stained for Paxillin to detect FA. Surprisingly, only very few CHO cells were able to spread on the plate surface. Out of 2496 wildtype and 4312 HS-deficient cells, which had adhered to the cell culture ware, only 65 and 69 cells (2.6% and 1.6%), respectively, displayed a flattened, spread morphology. Among these, a small proportion had formed FA which were present in 6% of the wildtype and in 3% of the mutant CHO cells (data not shown). Though only few cells could be analysed, this hints at a reduction of FA formation upon endogenous loss of HS synthesis, indicating that reduced formation of FA is not an artificial effect of exogenous HS inhibition.

3.2.4. YAP is translocated to the cytoplasm in Surfen treated MEFs

Besides integrin-mediated signals, other pathways sense the composition of the ECM. It has been reported that Yes-Associated Protein (YAP) is involved in mechano-sensing of the adhesion substrate in chondrocytes (Zhong *et al.*, 2013) and fibroblasts (Liu *et al.*, 2015). The effect on HS-inhibition on YAP localisation was analysed by immunofluorescence staining against YAP using the same conditions as described above (Fig. 23, B). Ten images were taken from each sample and the percentage of cells with predominantly nuclear staining was quantified for each image.

In the controls, an average of 65% of the MEFs displayed a nuclear localisation of YAP after 1h adhesion and 64% after 24h. When DMSO was added to already adhered MEFs for 1h, 71% of the cells showed a nuclear YAP signal. In contrast, only 53% of the Surfen-treated MEFs had a predominantly nuclear localisation of YAP after 1h adhesion. This number further decreased to 33% after 24h. Upon addition of Surfen, 69% of the cells displayed a nuclear signal for YAP. The proportions of cells with nuclear YAP localisation were similar between the three conditions in DMSO treated MEFs. In contrast, adhesion in presence of Surfen reduced the average proportion of MEFs with nuclear YAP by change factors of 0.81 (p^+=0.0158) and 0.56 (p^+=0) after 1h and 24h adhesion, respectively. When Surfen was added to cells that had already adhered, no difference was found compared to

DMSO MEFs (change factor 0.93, p+=0.1251). This shows that the observed shift of YAP to the cytoplasm specifically occurs when HS function is inhibited by Surfen during the adhesion process (Fig. 23, A).

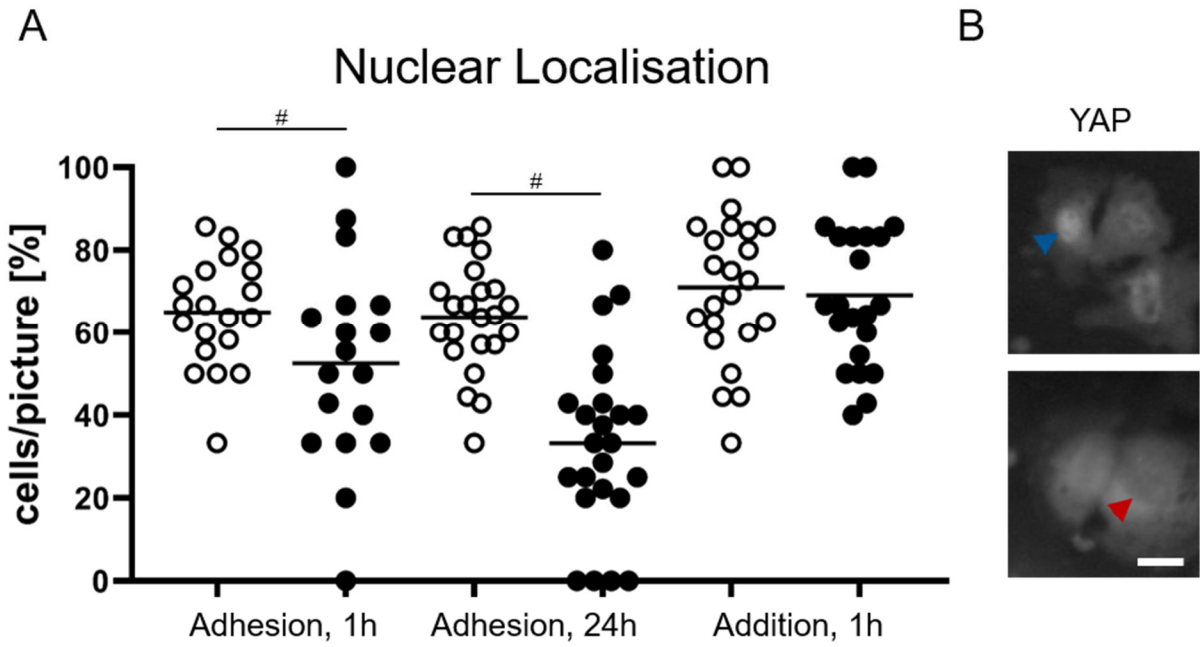

Figure 23: Localisation of YAP is shifted to cytoplasm in Surfen-treated MEFs Cells were seeded into DMSO- or Surfen-containing medium and cultured for 1h or 24h, or DMSO and Surfen were added after 24h adhesion for a duration of 1h. (A) The relative fraction of cells displaying a prominent nuclear YAP signal was quantified. Two biological replicates were assessed, each data point representing an individual image. White dots: DMSO control, black dots: 5µM Surfen. Black lines indicate means, # $p^{+} \leq 0.05$ or $p^{+} \geq 0.95$. (B) Cells with predominantly nuclear (blue arrow) or cytosolic (red arrow) signals were detected by immunostaining against YAP. Scale bar: 20µM.

It has been described that the nuclear function of YAP is deactivated by sequestration of phosphorylated YAP in the cytoplasm (Hansen *et al.*, 2015). Therefore, the phosphorylation status of YAP was analysed by Western Blot (Fig. 24, A). The same conditions as described for the investigation of FAK phosphorylation were used.

Increased phosphorylation of YAP was detected during the initial adhesion process compared to already adhered cells. Between Surfen- and DMSO-treated samples no differences were observe in both conditions (Fig. 24, B), showing that the translocation of YAP to the cytoplasm observed after 1h adhesion in the presence of Surfen is regulated by a mechanism other than YAP phosphorylation. As stated for the analysis of FAK, that data obtained by Western Blot experiments could not be modelled sufficiently and no statistical evaluation was performed.

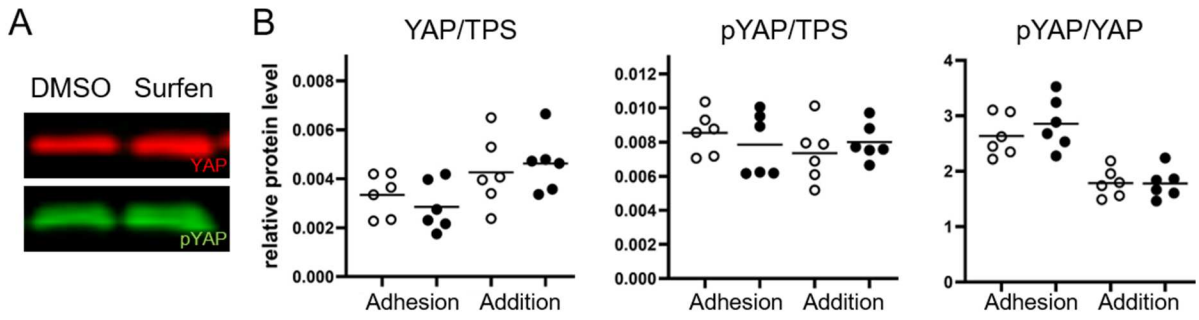

Figure 24: YAP and pYAP levels are not affected by HS-antagonism MEFS were seeded and adhered in the presence of DMSO or Surfen for 1h (Adhesion) or medium containing either DMSO or Surfen was added to already adhered cells for 1h (Addition). (A) YAP and pYAP were detected by Western Blot. (B) The relative amount of YAP was slightly decreased during the adhesion process, while pYAP levels remained similar between the two conditions resulting in an increased pYAP/YAP ratio after 1h adhesion. No differences between DMSO- and Surfen-treated samples were detected. Three biological replicates comprising two technical replicates each were analysed. Data point represent individual samples. White dots: DMSO control, black dots: 5µM Surfen. Black lines indicate means.

4. Discussion

OA is the most prevalent degenerative joint disease worldwide (WHO). To investigate its pathogenesis, it is crucial to the understand underlying mechanisms regulating cartilage integrity and maintenance. HSPGs control various processes in cartilaginous tissue, including cell-cell-signalling between chondrocytes and mechanical properties of cartilage matrix (Xu and Esko, 2014). This raises the question, how an altered HSPG content or composition impacts cartilage integrity and how chondrocytes sense the quality of surrounding HSPGs.

4.1. Reduced Mmp2 activity in *Ndst1*$^{+/-}$ samples

A shifted balance between matrix synthesis and degradation is widely regarded as a hallmark of OA development (Wieland *et al.*, 2005). Mice with decreased HS content in the AC (*Col2-rtTA-Cre;Ext1*$^{e2fl/e2fl}$) as well as animals with chondrocyte-specific and ubiquitously reduced HS sulfation (*Col2-Cre;Ndst1*$^{fl/fl}$ and *Ndst1*$^{+/-}$) are protected from OA progression. The altered properties of the AC observed in the *Ndst1*$^{+/-}$ mice are at least partly caused by a reduced matrix degradation, since aggrecan neo-epitopes generated by enzymes of the ADAMTS and MMP families were shown to be decreased in the culture medium of *Ndst1*$^{+/-}$ cartilage explants. Additionally, the gelatinase activity of a ~55kDa protease was reduced (Jochmann, 2016, PhD thesis). In the study presented here, this protease was shown to be secreted by the cartilage explants and identified as Mmp2.

A reduced level of Mmp2 proteins in the ECM might explain its decreased proteolytic activity, but no difference in *Mmp2* expression could be detected between *Ndst1*$^{+/-}$ animals and *Ndst1*$^{+/+}$ controls. Additionally, the activity of Mmp9 was also reduced in *Ndst1*$^{+/-}$ samples, pointing to a superordinate mechanism controlling the activity of multiple proteases. Since MMPs are synthesised as pro-enzymes and catalytically activated by the removal of the pro-peptide (Sekhon, 2010), this could include the proteolytic activation of Mmp2 by other enzymes, such as Mmp14 (Sato *et al.*, 1994). Furthermore, Mmp activity in the extracellular space is regulated by the non-covalent binding of tissue inhibitors of metalloproteinases (TIMP1-4) (Sekhon, 2010). It was already shown in the prior study that TIMPs are not differentially expressed in *Ndst1*$^{+/-}$ mutants. However, the amount of TIMPs in the extracellular space is also controlled by their uptake and degradation. It was demonstrated, that the LRP-1-mediated internalisation of TIMP3 is controlled by GAGs (Troeberg *et al.*, 2014).

Addition of heparin, HS and CS to human bone marrow stem cells inhibited TIMP3 endocytosis and increased extracellular TIMP3 concentrations, *in vitro*. Although the binding affinity of TIMP3 to N-desulfated HS was reduced, TIMP3 internalisation might be reduced in *Ndst1*$^{+/-}$ cartilage. Our group has recently shown that reduced HS levels (*Ext1*$^{gt/gt}$) or reduced 2O-sulfation (*Hs2st1*$^{-/-}$) are associated with an increased CS content of the ECM (Bachvarova *et al.*, 2020). If the same effect is found in *Ndst1* mutants, elevated extracellular levels of CS might inhibit the uptake of TIMP3 via Low Density Lipoprotein Receptor-related Protein 1 (LRP1) in the cartilage of those mice. Additionally, LRP1 was shown to be involved in the internalisation of Mmp2 (Yang *et al.*, 2001). An increased internalisation of Mmp2 from the extracellular space could explain the decreased protease activity detected in *Ndst1*$^{+/-}$ samples.

The reduced activity of Mmp2 found in samples from heterozygous *Ndst1* mutants may be one of the underlying causes resulting in the decreased development of OA seen in those mice. Together with the data from Katja Jochmanns work, the results presented in chapter 1.1 were published in *Osteoarthritis and Cartilage* (Severmann *et al.*, 2020).

4.2. OA progression in *Glce* and *Hs2st1* mice

As stated before, genetically modified *Col2-rtTA-Cre;Ext1*$^{e2fl/e2fl}$, *Col2-Cre;Ndst1*$^{fl/fl}$ and *Ndst1*$^{+/-}$ mice showed a delayed progression of OA. It has already been reported that HSPGs play a role in the progression of OA. The expression of the HS-carrying core protein Syndecan 4 (Sdc4) is increased in samples from human OA patients and in murine OA cartilage and loss of Sdc4 in *Sdc4*$^{-/-}$ mice has a protective effect after surgical induction by DMM (Echtermeyer *et al.*, 2009). Likewise, mice expressing a Perlecan variant lacking the HS-carrying exon 3 (*Hspg2*$^{\Delta 3-/\Delta 3-}$) develop less severe signs of OA after DMM surgery (Shu *et al.*, 2016). When Perlecan is expressed only in the AC but not in other joint tissues, the formation of osteophytes is reduced after surgical induction of OA by transection of the medial collateral ligament and removal of the medial meniscus (Kaneko *et al.*, 2013). These findings indicate a role of HS also in non-cartilaginous joint tissues. In contrast, *Sulfatase1*$^{-/-}$*;Sulfatase2*$^{-/-}$ (*Sulf1*$^{-/-}$*;Sulf2*$^{-/-}$) compound mice, displaying oversulfated HS chains, develop more severe OA upon ageing and surgical induction (Otsuki *et al.*, 2010) and intra-articular injection of Sulf1 resulted in reduced signs of OA after DMM surgery (Otsuki *et al.*,

2017). Taken together, the findings point to a protective effect of reduced HS-levels. Contradictingly, *Sulf1* and *Sulf2* were reported to be overexpressed in human OA cartilage and in aged wildtype mice (Otsuki *et al.*, 2008). In human OA samples *HS6ST2* expression was reported to be downregulated (Wang *et al.*, 2011), but *HS6ST1* was found to be upregulated (Chanalaris *et al.*, 2019). Nevertheless, these conflicting findings highlight the importance of tightly regulated HS synthesis and modification within the AC.

This leads to the question, how other alterations of the HS modification pattern impact the development of OA. To answer this, *Glce*$^{+/-}$ and *Hs2st1*$^{+/-}$ animals were analysed for the progression of OA. Heterozygous mutants and wild type animals of both strains developed weak signs of OA during ageing and mild differences in OA progression between the genotypes were hard to assess. Therefore, a surgical procedure for the induction of OA was applied. DMM is an established model leading mild to moderate signs of OA 4w after surgery and moderate to severe scores after 8w in 129/SvEv mice (Glasson *et al.*, 2007). Since the *Glce*$^{+/-}$ and *Hs2st1*$^{+/-}$ mice were generated on a C57Bl/6 genetic background, the DMM technique was established using C57Bl/6 wild type animals. In contrast to the original publication, weak signs of OA were detected 2 and 4w after surgery and mild signs of OA after 8 and 12w. Still, the results may not be directly comparable between the different mouse strains.

In the DMM-operated *Glce* and *Hs2st1* animals, mild signs OA were detected 12w after surgery, similar to the C57Bl/6 mice used for the establishment of the operation. Previously, OA was induced in *Col2-rtTA-Cre;Ext1*$^{e2fl/e2fl}$, *Col2-Cre;Ndst1*$^{fl/fl}$ and *Ndst1*$^{+/-}$ mice using the ACLT technique, which resulted in moderate to severe scores. Small but statistically clear differences were observed between HS mutants and their wildtype littermates. Such subtle alterations may be masked by the low OA scores induced by DMM surgery and it remains unclear whether *Glce*$^{+/-}$ or *HS2St*$^{+/-}$ are protected from OA development. Nevertheless, the onset of OA was not accelerated since no severe OA was detected in the heterozygous mutants.

The low OA scores obtained after DMM may be caused by the use of female mice for the experiments, since it has been shown, that OA scores developed by female 129/SvEv mice are reduced to 20% compared to males 2w and 4w after DMM surgery (Ma *et al.*, 2007). Still, when HS-mutants were analysed by ACLT no unusually low OA scores were detected in female mice after surgery (Jochmann,

2016, PhD thesis). In a recent study published by Muschter *et al.* mice were operated using the same DMM protocol and male mice displayed OA scores between 2 and 4 12w after surgery (Muschter *et al.*, 2020). These data are similar to our results, although maximum scores were quantified instead of means. This indicates that the values observed in male mice are not strikingly higher than the ones detected in female animals. Additionally, a small number of males was analysed 12w after DMM surgery within the scope of the study presented here. In these preliminary experiments, no obvious differences were observed between male and female individuals (data not shown).

Interestingly, although the destabilisation of the meniscus was performed in the lateral compartment of the knee joint, 12w after surgery higher scores were found on the lateral side of the analysed joints of C57Bl/6 mice. Additionally, individual animals among the operated *Glce* and *Hs2st1* mice also showed increased signs of OA in the lateral compartment. It has been shown, that in contrast to other mouse strains C57Bl/6 animals are prone to develop OA in the lateral compartment of the knee joint upon ageing (Lapveteläinen *et al.*, 1995; Stoop *et al.*, 1999; van der Kraan *et al.*, 2001). Both *Glce* and *Hs2st1* mice were kept on a C57Bl/6 background, which explains the presence of this strain-specific characteristic in all three mouse lines.

Taken together, OA progression was not accelerated in $Glce^{+/-}$ or $Hs2st1^{+/-}$ mice. Still, a possible protective effect of altered epimerisation of GlA to IdoA or 2O-sulfation of IdoA could not be assessed upon ageing or after surgical induction of OA by DMM.

To answer this question, a harsher OA-inducing surgery technique has to be applied, such as ACTL, or a combination of DMM and forced exercise. Additionally, mouse models with cartilage-specific modifications, such as loss of 2O-sulfation in chondrocytes (*Col2-CreERT;*$Hs2st1^{fl/fl}$), might show more pronounced differences to wild type animals compared to heterozygous mutants. If a protective effect is found in any of the mouse mutants, the activity of matrix-degrading enzymes should be analysed to investigate if the same molecular mechanisms occur in different HS-mutants.

4.3. Altered matrix properties around clusters of HS-deficient cells

The appearance of clusters of enlarged, morphologically distinct cells surrounded by excessive matrix deposition in the AC of mice with a clonal deletion of HS-synthesis in chondrocytes was previously described by others (Sgariglia *et al.*, 2013) and also demonstrated by our group (Jochmann, 2016, PhD thesis). The same phenotype was observed during the study presented here: Immunostaining detected clusters of enlarged chondrocytes in the AC of *Col2-rtTA-Cre;Ext1*$^{e2fl/e2fl}$ mice and an increased aggrecan content around the clusters.

The mechanical properties of the altered matrix were analysed by AFM and a bimodal distribution of individual measurement values was detected in the cartilage samples. The two observed peaks are widely accepted to originate from the more tensile collagen network and the rather elastic gel created by PGs (Loparic *et al.*, 2010). The stiffness of the matrix has been reported to increase with the depth of the AC (Muschter *et al.*, 2020) which was reflected by samples from *Ext1*$^{e2fl/e2fl}$ control mice and also by the wild type-like AC of *Col2-rtTA-Cre;Ext1*$^{e2fl/e2fl}$ animals. In the mutants, a mildly increased stiffness was detected in all three cartilage zones of the wild type-like matrix surrounding the clusters. This might result in a slightly enhanced stability of the AC of *Col2-rtTA-Cre;Ext1*$^{e2fl/e2fl}$ mice, contributing to the protective effect observed in this mouse strain. Contradictingly, an increased matrix stiffness has been associated with accelerated OA development in mice lacking the ECM components Matrillin1-4 (Li *et al.*, 2020), the PG Decorin (Gronau *et al.*, 2017) or carrying a hypomorphic allele of *Acan* (Alberton *et al.*, 2019).

In contrast to the wild type-like matrix, the ECM found around clusters of HS-deficient cells was outside of the measurement range during AFM analysis, demonstrating vastly altered mechanical properties of the aberrantly composed ECM. To overcome this limitation, mice with a hypomorphic allele of *Ext1* showing a residual HS content of 20% (Koziel *et al.*, 2004) were analysed in a preliminary experiment. Since homozygous presence of the genetrap allele is embryonically lethal, matrix stiffness of *Ext1*$^{gt/gt}$ and *Ext1*$^{+/+}$ embryos was assessed in GP cartilage at E15.0. Territorial matrix, directly surrounding the cells, and interterritorial matrix between columns of fast proliferating chondrocytes are distinguished in the proliferating zone of the GP. It has been reported that the matrix of the interterritorial area is stiffer compared to the

territorial area under physiological conditions (Prein *et al.*, 2016). This characteristic was observed in the *Ext1*$^{+/+}$, but not in the *Ext1*$^{gt/gt}$ sample. The stiffness of the mutant territorial matrix was similar to the control, but the interterritorial matrix was markedly softer. This is in line with a previous publication of our group showing a disorganised appearance of the proliferating zone lacking clearly distinguishable chondrocyte columns and longitudinal septa of interterritorial matrix (Koziel *et al.*, 2004). Interestingly, a similar phenotype is found in mice with a chondrocyte-specific deletion of ItgB1 (*Col2-Cre;β1*$^{fl/fl}$) (Aszodi *et al.*, 2003). In these mice, the proliferating chondrocytes failed to form and longitudinal septa, supporting an interaction of HS and integrin receptors during the formation of chondrocyte columns.

Though the stiffness of the wild type-like matrix is slightly enhanced in *Col2-rtTA-Cre;Ext1*$^{e2fl/e2fl}$ mice, the ECM around clustered HS-deficient cells seems to be markedly softer. This may be due to the increased PG content detected in the HS-deficient matrix and might result in an overall enhanced compressive capacity of the AC and thus in a reduced susceptibility for OA.

4.4. Adhesion and polarisation defects upon inhibition of HS function

Integrins are major receptors for cell-matrix interactions. Increased levels of the integrin pathway components pFAK, FAK, pERK and MHCII were detected in clusters of HS-deficient cells found in *Col2-rtTA-Cre;Ext1*$^{e2fl/e2fl}$ animals (Jochmann, 2016, PhD thesis). An upregulation of integrin pathway components in the clusters was verified by additional immunostainings. Strong signals for ItgB1 were found in the clusters, although ItgB1 was also highly expressed in other cells. In contrast, Src kinase and ERK levels were clearly increased in the *Ext1*-deficient chondrocytes. Taken together, these results show an activation of the integrin pathway upon loss of HS. To investigate the impact of an inhibited HS function on integrin-mediated cell-matrix adhesion, an *in vitro* model using the HS antagonist Surfen was employed.

In the presence of Surfen, cell adhesion was decreased at early time points (0.5, 1h) but recovered after longer treatment periods (2, 16, 24h). This is in line with results obtained from the treatment of primary bovine aortic endothelial cells with heparinase, which show a reduced cell adhesion on fibronectin-coated surfaces after 30min incubation time (Moon *et al.*, 2005).

Time lapse recordings of the critical time period around 1h of adhesion showed that a lower proportion of the Surfen-treated MEFs formed a clean cell seam or lamellipodium while more cells displayed thin, filopodia-like protrusions. Filopodia are abundantly equipped with cell adhesion molecules and contain integrins in un-ligated, but activated form. When cells adhere under physiological conditions, initial adhesion complexes are formed within filopodia. Later, filopodia with stable adhesion sites are converted to lamellipodia-like protrusions (Mattila and Lappalainen, 2008). The orientation of cell movement is then controlled by filopodia protruding from the lamellipodium and sensing the matrix composition in the direction of movement (Innocenti, 2018; Letort *et al.*, 2015). The effect observed in Surfen-treated MEFs indicates that the conversion of initially formed filopodia to a lamellipodium structure is disturbed upon loss of HS function. These findings are in line with *in vivo* observations from *ext2* and *extl3* zebrafish mutants. Cells of the developing lateral line display an extensive formation of filopodia in embryos with disrupted HS synthesis (Galanternik *et al.*, 2015). Together with the decreased cell adhesion and polarisation capacity observed in Surfen-treated MEFs this indicates that loss of HS function leads to an impaired formation of initial adhesion complexes and hence a reduced remodelling of the cell seam to lamellipodium-like structures and persisting filopodia.

This is substantiated by the investigation of the formation of adhesion complexes. FAs were detected in Surfen-treated MEFs by immunostaining against Paxillin and the formation of SFs was investigated using a fluorescence-labelled Phalloidin. After 1h of adhesion, a lower proportion of cells had formed FA and SF in the presence of Surfen compared to the solvent control. Likewise, endothelial cells treated with heparinase which how reduced numbers of SFs and decreased FA sizes after 30min adhesion (Moon *et al.*, 2005). Similar defects in cell adhesion have also been reported in primary chondrocytes isolated from *Col2-Cre;β1$^{fl/fl}$* mice (Aszodi *et al.*, 2003). It has been shown that clustered Sdc4 units are components of FAs and that Sdc4 colocalises with β1-integrin (Oh and Couchman, 2004; Sarrazin *et al.*, 2011). Reduced formation of SF and FA has been reported in fibroblast lacking Sdc4 (Gopal *et al.*, 2010). Accordingly, overexpression of Sdc4 in CHO cells results in increased formation of FAs and SFs as well as reduced mobility (Longley *et al.*, 1999). Taken together, HS function seems to be critical for the integrin-mediated formation of FA.

The reduced formation of FA and SF detected upon HS inhibition is regulated independently of FAK activation. Analysis of protein extracts from Surfen-treated cells did not shown altered protein level of FAK or pFAK or a shifted pFAK/FAK ratio. After 24h adhesion, the treated MEFs had recovered and similar proportions of cells displaying FA and SF were seen in the two groups, suggesting the cells are able to compensate for the initially deprived adhesion. Interestingly, when Surfen was applied to already adhered cells the number of cells forming FA and SF was increased. This might be due to an upregulation of FA components upon reduced integrin binding. Alternatively, or in parallel, other matrix-sensing signalling pathways may be addressed by a loss of HS binding.

4.5. Altered adhesion behaviour in CHO *psgD-677* cells

In the study presented here, elevated formation of filopodia-like protrusions, decreased cell polarisation and reduced formation of FA as well as SFs were demonstrated in Surfen-treated MEFs. Similar results were previously reported by Moon *et al.* for epithelial cells after heparinase digestion (Moon *et al.*, 2005). Still, the two described experimental strategies are external treatments that may result in artificial phenotypes. Thus, CHO psgD-677 cells displaying and endogenous loss of HS-synthesis were analysed for an altered cell morphology after 1h of adhesion. Apparently, both CHO-K1 controls and CHO psgD-677 mutants do not adhere well to the culture ware used in the prior experiments and only very few cells were able to spread. Still, the number of cells forming FA seemed to be reduced by a factor of 0.5 in the HS-mutant cell line (CHO-K1: 6%, CHO psgD-677: 3%).

In a different project conducted in our group (by Velina Bachvarova, Essen, and Julius Sefkow-Werner, Grenoble) CHO cells were seeded onto RGD-presenting platforms and cultured for 75min. The CHO cells were able to adhere to the plate surface under these conditions and their morphology was analysed. This preliminary experiment showed an increased formation of membrane protrusions in the HS-mutants compared to control cells (CHO-K1: 13%, CHO pgsD-677: 77%) and a reduced polarisation capacity of the HS-deficient cells (CHO-K1: 78%, CHO pgsD-677: 18%).

The preliminary data have to be verified but strongly indicate that the defects seen in Surfen-treated cells are not artificial effects evoked by an exogenous HS-antagonism.

4.6. Cytoplasmic YAP localisation in presence of Surfen

The increased levels of integrin pathway components seen in HS-deficient clusters of *Col2-rtTA-Cre;Ext1*$^{e2fl/e2fl}$ mice might be the result of an upregulating integrin pathway components upon reduced integrin binding. Alternatively, or in parallel to that, other signalling pathways may be involved. YAP is a well-known mechano-sensing factor regulating cell proliferation, survival and differentiation. It is shuttling between the cytoplasm and nucleus, where it interacts with transcription factors and controls gene expression. The Hippo signalling pathway is known to respond to extracellular cues, such as mechanical stress, through YAP phosphorylation by Large Tumour Suppressor kinase 1 (LATS1). Phosphorylated YAP is sequestered in the cytoplasm by binding of 14-3-3 or degraded (Hansen *et al.*, 2015). In general, YAP is accumulated in the cytoplasm upon inactivating inputs including soft substrates and contact inhibition (Dupont, 2016). In the study presented here, YAP was shown to be translocated to the cytoplasm when MEFs adhered in presence of Surfen. No difference in YAP localisation was detected when Surfen was added to already adhered cells, indicating that the described effect is adhesion specific. A similar translocation of YAP to the cytoplasm was reported for primary rat chondrocytes, where YAP was primarily localised to the nucleus when the cells were seeded onto a hard substrate and shifted to the cytoplasm on a soft surface (Zhong *et al.*, 2013). This could indicate that cells perceive the plate surface as soft upon HS inhibition regardless of the actual substrate properties. In addition to extracellular cues, the localisation of YAP is controlled by intracellular tension generated by the actin cytoskeleton (Seo and Kim, 2018). Based on this, the shift of YAP to the cytoplasm in Surfen-treated MEFs may be due to the lack of contractile SF observed in these cells. Disruption of the formation of acto-myosin fibres by Cytochalasin D results in the retention of YAP in the cytoplasm. However, this effect is phosphorylation-dependent and mediated through LATS1/2 (Wada *et al.*, 2011; Zhao *et al.*, 2012). Although the localisation of YAP was shifted to the cytoplasm in Surfen-treated MEFs, the phosphorylation status of YAP was not altered in protein extracts. A phosphorylation-independent sequestration of YAP in the cytoplasm has been shown for proteins of the Angiomotin (AMOT) family (Zhao *et al.*, 2011). AMOTs promote the formation of SF in endothelial cells (Ernkvist *et al.*, 2006). In absence of SF

unbound AMOT proteins might associated with YAP causing its retention in the cytoplasm.

4.7. Outlook

Col2-rtTA-Cre;Ext1$^{e2fl/e2fl}$ animals display clusters of morphologically distinct, HS-deficient chondrocytes in the AC which are surrounded by ECM with altered composition (Jochmann, 2016, PhD thesis) The analysis of this matrix by AFM revealed vastly different mechanical properties, although an exact Young's Modulus could not be determined. A preliminary analysis of *Ext1*$^{gt/gt}$ tissue containing decreased HS level indicated that HS-deficient matrix is markedly softer than wild type tissue. This needs to be verified and a strategy to determine the Young's Modulus of the aberrant matrix found around HS-deficient clusters in *Col2-rtTA-Cre;Ext1*$^{e2fl/e2fl}$ mice has to be established. To investigate the influence of reduced HS sulfation on the mechanical properties of cartilage tissue, AC of *Col2-Cre;Ndst1*$^{fl/fl}$ and *Ndst1*$^{+/-}$ mutants, which are also protected from OA progression, should be analysed by AFM.

The altered ECM composition around clusters of HS deficient cells leads to the question how a lack of HS is sensed and transmitted. An upregulation of integrin pathway components within the clustered cells was confirmed and an *in vitro* model used to investigate the effects of inhibited HS-function. Treatment with the HS-antagonist Surfen during the adhesion process resulted in decreased cell adhesion, reduced formation of lamellipodium-like structures, increased generation of filopodia-like protrusions and reduced formation of FA and SF. In contrast, the formation of FA and SF was increased when Surfen was added to already adherend cells.

Taken together, these data indicate an upregulation of integrin pathway components upon reduced integrin binding due to HS inhibition. Besides integrins other signalling pathways participate in mechano-sensing of the adhesion substrate. A translocation of YAP to the cytoplasm was found in Surfen- treated cells. This shift is regulated independent of YAP phosphorylation, since the analysis of its phosphorylation status by Western Blot did not detect differences between treated cells and controls. Besides canonical Hippo signalling, other mechanisms regulate YAP localisation independent of its phosphorylation status, such as binding by AMOT, protein tyrosine phosphatase 14 or α-catenin (Hansen *et al.*, 2015). The binding partners involved in

the sequestration of YAP within the cytoplasm of Surfen-treated cells will be investigated by Co-Immunoprecipitation in future experiments.

Taken together, the presented results show an important role of HS function for cartilage integrity. Still, it remains unclear how the HS-content of the ECM is sensed by chondrocytes. Within the study presented here, a major role for integrin receptors and integrin dependent adhesion in this process were demonstrated and mechano-sensing via YAP was shown to be involved as well. In future projects, the exact intracellular signalling events and their downstream effects have to be revealed.

5. Summary

A previous study demonstrated that *Col2-rtTA-Cre;Ext1*$^{e2fl/e2fl}$, *Col2-Cre;Ndst1*$^{fl/fl}$ and *Ndst1*$^{+/-}$ mice are protected from OA development. In samples from *Ndst1*$^{+/-}$ animals, decreased amounts of ADAMTS- and MMP-specific aggrecan neo-epitopes and a reduced gelatinase activity were detected. In the study presented here, a decreased gelatinase activity was confirmed and attributed to Mmp2. Since *Mmp2* expression was unaltered, protease activity is regulated on protein rather than on expression level. Additionally, preliminary results showed that Mmp9 activity is similarly decreased. Attenuated cartilage degradation due to decreased protease activity is likely one of the mechanisms underlying the protective effect seen in these mice. The attenuated development observed in *Col2-rtTA-Cre;Ext1*$^{e2fl/e2fl}$, *Col2-Cre;Ndst1*$^{fl/fl}$ and *Ndst1*$^{+/-}$ mice raises the question if other mouse strains with altered HS modification patterns are also protected from OA and whether the same molecular mechanisms are involved. To answer this, *Glce*$^{+/-}$ and *Hs2st1*$^{+/-}$ mice as well as their wild type littermates were aged and analysed for signs of OA at 6m and 18m. At both stages no spontaneous development of OA could be detected. Surgical induction of OA by DMM showed that OA progression is not accelerated in *Glce*$^{+/-}$ and *Hs2st1*$^{+/-}$ mice. Still, due to the low OA scores induced by DMM a possible protective effect remains unclear.

In addition to a protection from OA progression *Col2-rtTA-Cre;Ext1*$^{e2fl/e2fl}$ animals display clusters of enlarged, morphologically distinct HS-deficient cells in the AC. These cells are surrounded by an excessive amount of matrix of aberrant composition, including an increased aggrecan content. Investigation of the mechanical properties of the ECM of *Col2-rtTA-Cre;Ext1*$^{e2fl/e2fl}$ mice by AFM showed that the wild type-like matrix outside the clusters was slightly stiffer compared to the AC of *Ext1*$^{e2fl/e2fl}$ mice. The ECM directly surrounding the clusters displayed a massively altered quality and was outside of the measurement range. To overcome this limitation, a mouse mutant with a hypomorphic allele of Ext1 was investigated. The GP cartilage of the *Ext1*$^{gt/gt}$ mutant was softer compared to the *Ext1*$^{+/+}$ control. The altered compressive properties of the AC may thus be another underlying cause resulting in the protective effect against OA seen in *Col2-rtTA-Cre;Ext1*$^{e2fl/e2fl}$ animals. This leads to the question how chondrocytes sense the PG content of their surrounding matrix and how the cells react to an altered composition.

Preliminary results indicated an upregulation of the integrin pathway components FAK, pFAK, pERK and MHCII in HS-deficient cells of *Col2-rtTA-Cre;Ext1*$^{e2fl/e2fl}$ mice. This was confirmed by immunostaining against additional integrin pathway components. ItgB1, ERK and Src, were highly expressed in the clusters of mutant chondrocytes as well. To analyse the effect of an inhibited HS function on cellular processes, primary murine embryonic fibroblasts (MEFs) were treated with the HS-antagonist Surfen. This showed delayed adhesion of MEFs upon loss of HS function at early time points (0.5, 1, 2h) while the cells were able to overcome this limitation later (16h, 24h). Life cell imaging of the early adhesion process showed the formation of thin, filopodia-like membrane protrusions in an increased fraction of cells in the Surfen-treated samples. Additionally, cell migration and polarisation were reduced and the proportion of cells detaching from the plate surface increased in the presence of Surfen. The adaptor protein Paxillin and the Actin cytoskeleton were visualised. After 1h of adhesion, the proportions of MEFs forming FA and SF were reduced in presence of Surfen. The cells recovered after 24h. Together the findings point to a compensatory mechanism rescuing cell adhesion in absence of HS function. This is backed up by the finding that addition of Surfen to already adhered MEFs increases the proportion of cells forming FA and SF. These effects were not regulated by FAK, since protein level and phosphorylation status of FAK were unaltered between Surfen-treated samples and controls.

Matrix composition is also monitored by other pathways besides integrin signalling. The Hippo pathway is known for mechano-sensing of substrates and is mediated through YAP. In Surfen-treated MEFs, a shift of YAP to the cytoplasm was detected after 1h and 24h of adhesion. Its localisation was not affected by the subsequent addition of Surfen to already adhered cells, showing that the translocation of YAP to the cytoplasm is adhesion dependent. Since the phosphorylation of YAP was unaltered, the shift of YAP to the cytoplasm was regulated by a phosphorylation independent mechanism.

6. Zusammenfassung

In einer früheren Studie wurde gezeigt, dass *Col2-rtTA-Cre;Ext1*$^{e2fl/e2fl}$, *Col2-Cre;Ndst1*$^{fl/fl}$ und *Ndst1*$^{+/-}$ Mäuse vor der Entwicklung von Osteoarthrose (OA) geschützt sind. In Proben von *Ndst1*$^{+/-}$ Tieren wurden verringerte Mengen von ADAMTS und MMP spezifischen Aggrecan Neo-Epitopen sowie eine reduzierte Gelatinase-Aktivität festgestellt. Bei dem hier beschriebenen Projekt konnte eine herabgesetzte Gelatinase-Aktivität bestätigt und der Protease Mmp2 zugeordnet werden. Da die Expression von Mmp2 unverändert war, kann davon ausgegangen werden, dass die Aktivität der Protease auf Protein-Ebene reguliert wird. Zusätzlich zeigten vorläufige Ergebnisse außerdem eine erniedrigte Aktivität von Mmp9. Eine herabgesetzte Degradation des artikulären Knorpels durch eine geringere Protease-Aktivität ist daher wahrscheinlich einer der zugrundeliegenden Mechanismen, die den Schutz der Mausmutanten hervorrufen.

Die eingeschränkte Entwicklung von OA in *Col2-rtTA-Cre;Ext1*$^{e2fl/e2fl}$, *Col2-Cre;Ndst1*$^{fl/fl}$ und *Ndst1*$^{+/-}$ Mäusen führte zu der Frage, ob andere Mausstämme mit veränderten Sulfatierungsmustern von Heparansulfaten (HS) ebenfalls vor OA geschützt sind und welche molekularen Mechanismen daran beteiligt sein könnten. Um diese Fragestellung zu beantworten wurden *Glce*$^{+/-}$ und *Hs2st1*$^{+/-}$ Mäuse sowie ihre Wildtyp-Geschwistertiere gealtert und im Alter von 6 Monaten und 18 Monaten auf das Auftreten von OA hin untersucht. In beiden Altersstufen konnte keine spontane Entwicklung von OA festgestellt werden. Die chirurgische Induktion von OA durch die Destabilisierung des medialen Meniskus zeigte, dass die Entwicklung von OA in *Glce*$^{+/-}$ und *Hs2st1*$^{+/-}$ Mäusen nicht beschleunigt ist. Durch die niedrigen OA Werte, die durch die Operation ausgelöst wurden, konnte ein protektiver Mechanismus jedoch nicht nachgewiesen werden.

Zusätzlich zum Schutz vor OA zeigen *Col2-rtTA-Cre;Ext1*$^{e2fl/e2fl}$ Tiere das Auftreten von gruppierten vergrößerten und morphologisch abgrenzbaren HS-defizienten Zellen im artikulären Knorpel. Diese Zellen sind umgeben von einer abweichend zusammengesetzten extrazellulären Matrix (ECM), die einen erhöhten Aggrecan Anteil enthält. Die Untersuchung der mechanischen Eigenschaften der Knorpelmatrix von *Col2-rtTA-Cre;Ext1*$^{e2fl/e2fl}$ Tieren durch *Atomic Force Microscopy* (AFM) zeigte, dass die Wildtyp-ähnliche Matrix der HS-synthetisierenden Zellen etwas fester war als bei *Ext1*$^{e2fl/e2fl}$ Mäusen. Die ECM der HS-defizienten Gruppen hatte jedoch eine

stark veränderte Qualität außerhalb des Messbereichs. Um diese Einschränkung zu umgehen wurde eine Mausmutante mit einem hypomorphen *Ext1*- Allel analysiert. Der Wachstumsknorpel der *Ext1*$^{gt/gt}$ Mutante war im Vergleich zur *Ext1*$^{+/+}$ Kontrolle weicher. Die veränderte Kompressionsfähigkeit des artikulären Knorpels könnte ein weiterer Mechanismus sein, der dem Schutz von *Col2-rtTA-Cre;Ext1*$^{e2fl/e2fl}$ Tieren vor OA zugrunde liegt.

Dies führt zu der Frage, wie die Chondrozyten ihre umgebende ECM wahrnehmen und wie sie auf Änderungen der Matrixkomposition reagieren. Vorläufige Ergebnisse wiesen darauf hin, dass FAK, pFAK, pERK and MHCII, Faktoren aus dem Integrin-Signalweg, in den HS-defizienten Zellen hochreguliert waren. Dies konnte durch Immunodetektion von weiteren Integrin-Signalweg Proteinen bestätigt werden. β1-Integrin, ERK und Src waren in den Gruppen mutanter Chondrozyten ebenfalls hoch exprimiert.

Um analysieren zu können, wie sich der Verlust der HS-Funktion auf zellbiologische Prozesse auswirkt, wurden primäre murine Fibroblasten (MEFs) mit dem HS-Antagonisten Surfen behandelt. Dies zeigte eine verlangsamte Zelladhäsion zu frühen Zeitpunkten (0,5h, 1h, 2h), welche jedoch zu späteren Zeitpunkten (16h, 24h) von den Zellen ausgeglichen wurde. *Life Cell Imaging* Aufnahmen der frühen Adhäsionsphase zeigte in Anwesenheit von Surfen die Ausbildung dünner, Filopodien-artiger Membranfortsätze bei einem erhöhten Anteil von Zellen. Zusätzlich waren Migration und Polarisation der behandelten Zellen eingeschränkt und ein erhöhter Anteil von Zellen löste sich vom Untergrund ab. Die Visualisierung des Adaptor-Proteins Paxillin und des Aktin-Zytoskeletts zeigten nach 1h außerdem einen verringerten Anteil von Zellen, die Fokaladhäsionen (FA) oder Stressfasern (SF) gebildet hatten. Diese Veränderung konnte von den Zellen innerhalb von 24h ausgeglichen werden. Zusammengenommen weisen diese Ergebnisse darauf hin, dass die durch den Verlust der HS-Funktion eingeschränkte Zelladhäsion durch einen kompensatorischen Mechanismus wiederhergestellt wird. Dies wird dadurch untermauert, dass das Hinzufügen von Surfen zu bereits adhärierten Zellen den Anteil von Zellen, die FA und SF ausbilden, ansteigen lässt. Dieser Effekt wird nicht durch *Focal Adhesion Kinase* (FAK) vermittelt, da Proteinmenge und Phosphorylierungsstatus in den behandelten Zellen unverändert waren.

Die Zusammensetzung der ECM wird zusätzlich zu Integrin-abhängigen Prozessen auch durch andere Signalwege überwacht. Der Hippo-Signalweg ist für die Mechano-

Rezeption von Adhäsionssubstraten bekannt und wird durch das intrazelluläre Protein YAP vermittelt. In mit Surfen behandelten MEFs wurde nach 1h sowie nach 24h eine in das Zytoplasma verlagerte Lokalisation von YAP festgestellt. Die Lokalisation des Proteins wurde jedoch nicht durch eine nachträgliche Zugabe von Surfen zu bereits adhärierten Zellen beeinflusst. Dies zeigt, dass die Translokation von YAP ins Zytoplasma abhängig vom Adhäsionsprozess geschah. Da der Phosphorylierungsstatus von YAP in den behandelten Zellen unverändert war, wurde die Verlegung von YAP ins Zytoplasma durch einen Phosphorylierungs-unabhängigen Mechanismus kontrolliert.

7. References

Akiyama, H., Chaboissier, M. C., Martin, J. F., Schedl, A. and de Crombrugghe, B. (2002). "The transcription factor Sox9 has essential roles in successive steps of the chondrocyte differentiation pathway and is required for expression of Sox5 and Sox6." *Genes Dev* 16(21).

Alberton, P., Dugonitsch, H. C., Hartmann, B.*, et al.* (2019). "Aggrecan Hypomorphism Compromises Articular Cartilage Biomechanical Properties and Is Associated with Increased Incidence of Spontaneous Osteoarthritis." *Int J Mol Sci* 20(5).

Alday-Parejo, B., Stupp, R. and Ruegg, C. (2019). "Are Integrins Still Practicable Targets for Anti-Cancer Therapy?" *Cancers (Basel)* 11(7).

Aszodi, A., Hunziker, E. B., Brakebusch, C. and Fassler, R. (2003). "Beta1 integrins regulate chondrocyte rotation, G1 progression, and cytokinesis." *Genes Dev* 17(19).

Bachvarova, V., Dierker, T., Esko, J.*, et al.* (2020). "Chondrocytes respond to an altered heparan sulfate composition with distinct changes of heparan sulfate structure and increased levels of chondroitin sulfate." *Matrix Biol*.

Bi, W., Deng, J. M., Zhang, Z., Behringer, R. and de Crombrugghe, B. (1999). "Sox9 is required for cartilage formation." *Nature Genetics* 22.

Bullock, S. L., Fletcher, J. M., Beddington, R. S. P. and Wilson, V. A. (1998). "Renal agenesis in mice homozygous for a gene trap mutation in the gene encoding heparan sulfate 2-sulfotransferase." *Genes and Development* 12.

Bulow, H. E. and Hobert, O. (2006). "The molecular diversity of glycosaminoglycans shapes animal development." *Annu Rev Cell Dev Biol* 22.

Carpenter, B., Gelman, A., Hoffman, M. D.*, et al.* (2017). "Stan: A Probabilistic Programming Language." *Journal of Statistical Software* 76(1).

Chanalaris, A., Clarke, H., Guimond, S. E.*, et al.* (2019). "Heparan Sulfate Proteoglycan Synthesis Is Dysregulated in Human Osteoarthritic Cartilage." *Am J Pathol* 189(3).

Clarke, B. (2008). "Normal bone anatomy and physiology." *Clin J Am Soc Nephrol* 3 Suppl 3.

Clements, K. M., Price, J. S., Chambers, M. G.*, et al.* (2003). "Gene deletion of either interleukin-1beta, interleukin-1beta-converting enzyme, inducible nitric oxide synthase, or stromelysin 1 accelerates the development of knee osteoarthritis in mice after surgical transection of the medial collateral ligament and partial medial meniscectomy." *Arthritis Rheum* 48(12).

Decker, R. S., Koyama, E. and Pacifici, M. (2014). "Genesis and morphogenesis of limb synovial joints and articular cartilage." *Matrix Biol* 39.

Decker, R. S., Koyama, E. and Pacifici, M. (2015). "Articular Cartilage: Structural and Developmental Intricacies and Questions." *Curr Osteoporos Rep* 13(6).

Duchesne, L., Octeau, V., Bearon, R. N.*, et al.* (2012). "Transport of fibroblast growth factor 2 in the pericellular matrix is controlled by the spatial distribution of its binding sites in heparan sulfate." *PLoS Biol* 10(7).

Dupont, S. (2016). "Role of YAP/TAZ in cell-matrix adhesion-mediated signalling and mechanotransduction." *Exp Cell Res* 343(1).

Echtermeyer, F., Bertrand, J., Dreier, R.*, et al.* (2009). "Syndecan-4 regulates ADAMTS-5 activation and cartilage breakdown in osteoarthritis." *Nat Med* 15(9).

Ernkvist, M., Aase, K., Ukomadu, C.*, et al.* (2006). "p130-angiomotin associates to actin and controls endothelial cell shape." *FEBS J* 273(9).

Esko, J. D. and Selleck, S. B. (2002). "Order out of chaos: assembly of ligand binding sites in heparan sulfate." *Annu Rev Biochem* 71.

Fang, H. and Beier, F. (2014). "Mouse models of osteoarthritis: modelling risk factors and assessing outcomes." *Nat Rev Rheumatol* 10(7).

Fosang, A. J. and Little, C. B. (2008). "Drug insight: aggrecanases as therapeutic targets for osteoarthritis." *Nat Clin Pract Rheumatol* 4(8).

Fox, A. J. S., Bedi, A. and Rodeo, S. A. (2009). "The basic science of articular cartilage: structure, composition, and function." *Sports Health* 1(6).

Galanternik, M. V., Kramer, K. L. and Piotrowski, T. (2015). "Heparan Sulfate Proteoglycans Regulate Fgf Signaling and Cell Polarity during Collective Cell Migration." *Cell Rep* 10(3).

Glasson, S. S., Askew, R., Sheppard, B.*, et al.* (2004). "Characterization of and osteoarthritis susceptibility in ADAMTS-4-knockout mice." *Arthritis Rheum* 50(8).

Glasson, S. S., Blanchet, T. and Morris, E. A. (2005). "Less severe OA is observed in IL-1beta KO mice and more severe OA is observed in MMP-9 and MK2 KO mice in a surgical model of OA." *Annual Meeting of the Orthopaedic Research Society* 51.

Glasson, S. S., Blanchet, T. J. and Morris, E. A. (2007). "The surgical destabilization of the medial meniscus (DMM) model of osteoarthritis in the 129/SvEv mouse." *Osteoarthritis Cartilage* 15(9).

Glasson, S. S., Chambers, M. G., Van Den Berg, W. B. and Little, C. B. (2010). "The OARSI histopathology initiative - recommendations for histological assessments of osteoarthritis in the mouse." *Osteoarthritis Cartilage* 18 Suppl 3.

Gopal, S., Bober, A., Whiteford, J. R.*, et al.* (2010). "Heparan sulfate chain valency controls syndecan-4 function in cell adhesion." *J Biol Chem* 285(19).

Grobe, K., Inatani, M., Pallerla, S. R.*, et al.* (2005). "Cerebral hypoplasia and craniofacial defects in mice lacking heparan sulfate Ndst1 gene function." *Development* 132(16).

Gronau, T., Kruger, K., Prein, C.*, et al.* (2017). "Forced exercise-induced osteoarthritis is attenuated in mice lacking the small leucine-rich proteoglycan decorin." *Ann Rheum Dis* 76(2).

Habuchi, H., Nagai, N., Sugaya, N.*, et al.* (2007). "Mice deficient in heparan sulfate 6-O-sulfotransferase-1 exhibit defective heparan sulfate biosynthesis, abnormal placentation, and late embryonic lethality." *J Biol Chem* 282(21).

Hansen, C. G., Moroishi, T. and Guan, K. L. (2015). "YAP and TAZ: a nexus for Hippo signaling and beyond." *Trends Cell Biol* 25(9).

Heilpern, A. J., Wertheim, W., He, J.*, et al.* (2009). "Matrix metalloproteinase 9 plays a key role in lyme arthritis but not in dissemination of Borrelia burgdorferi." *Infect Immun* 77(7).

Hunziker, E. B., Staeubli, H.-U. and Jakob, R. P. (1992). "Surgical Anatomy of the Knee Joint." *The knee and the cruciate ligaments. Hrsg. Springer Verlag*.

Innocenti, M. (2018). "New insights into the formation and the function of lamellipodia and ruffles in mesenchymal cell migration." *Cell Adh Migr* 12(5).

Jochmann, K. (2016, PhD thesis). "Heparansulfate als Regulatoren der Knorpelhomöostase." *PhD thesis*.

Jones, K. B., Piombo, V., Searby, C.*, et al.* (2010). "A mouse model of osteochondromagenesis from clonal inactivation of Ext1 in chondrocytes." *Proc Natl Acad Sci U S A* 107(5).

Kaneko, H., Ishijima, M., Futami, I.*, et al.* (2013). "Synovial perlecan is required for osteophyte formation in knee osteoarthritis." *Matrix Biol* 32(3-4).

Kelwick, R., Desanlis, I., Wheeler, G. N. and Edwards, D. R. (2015). "The ADAMTS (A Disintegrin and Metalloproteinase with Thrombospondin motifs) family." *Genome Biol* 16.

Kirn-Safran, C. B., Gomes, R. R., Brown, A. J. and Carson, D. D. (2004). "Heparan sulfate proteoglycans: coordinators of multiple signaling pathways during chondrogenesis." *Birth Defects Res C Embryo Today* 72(1).

Kozhemyakina, E., Lassar, A. B. and Zelzer, E. (2015). "A pathway to bone: signaling molecules and transcription factors involved in chondrocyte development and maturation." *Development* 142(5).

Koziel, L., Kunath, M., Kelly, O. G. and Vortkamp, A. (2004). "Ext1-dependent heparan sulfate regulates the range of Ihh signaling during endochondral ossification." *Dev Cell* 6(6).

Lapveteläinen, T., Nevalainen, T., Parkkinen, J. J.*, et al.* (1995). "Lifelong moderate running training increases the incidence and severity of osteoarthritis in the knee joint of C57BL mice." *The Anatomical Record* 242.

Legate, K. R., Wickstrom, S. A. and Fassler, R. (2009). "Genetic and cell biological analysis of integrin outside-in signaling." *Genes Dev* 23(4).

Letort, G., Ennomani, H., Gressin, L., Thery, M. and Blanchoin, L. (2015). "Dynamic reorganization of the actin cytoskeleton." *F1000Res* 4.

Li, J. P., Gong, F., Hagner-McWhirter, A.*, et al.* (2003). "Targeted disruption of a murine glucuronyl C5-epimerase gene results in heparan sulfate lacking L-iduronic acid and in neonatal lethality." *J Biol Chem* 278(31).

Li, P., Fleischhauer, L., Nicolae, C.*, et al.* (2020). "Mice Lacking the Matrilin Family of Extracellular Matrix Proteins Develop Mild Skeletal Abnormalities and Are Susceptible to Age-Associated Osteoarthritis." *Int J Mol Sci* 21(2).

Lidholt, K., Weinke, J. L., Kiser, C. S.*, et al.* (1992). "A single mutation affects both N-acetylglucosaminyltransferase and glucuronosyltransferase activities in a Chinese hamster ovary cell mutant defective in heparan sulfate biosynthesis." *Proc Natl Acad Sci U S A* 89.

Lin, X., Wei, G., Shi, Z.*, et al.* (2000). "Disruption of gastrulation and heparan sulfate biosynthesis in EXT1-deficient mice." *Dev Biol* 224(2).

Little, C. B., Barai, A., Burkhardt, D.*, et al.* (2009). "Matrix metalloproteinase 13-deficient mice are resistant to osteoarthritic cartilage erosion but not chondrocyte hypertrophy or osteophyte development." *Arthritis Rheum* 60(12).

Little, C. B., Meeker, C. T. and Fosang, A. J. (2003). "Degenerative mechanisms in mouse articular cartilage: use of in vitro models to analyse proteolysis and loss of Aggrecan and Link protein." *Annual Meeting of the Orthopaedic Research Society* 49.

Liu, F., Lagares, D., Choi, K. M.*, et al.* (2015). "Mechanosignaling through YAP and TAZ drives fibroblast activation and fibrosis." *Am J Physiol Lung Cell Mol Physiol* 308(4).

Loeser, R. F., Goldring, S. R., Scanzello, C. R. and Goldring, M. B. (2012). "Osteoarthritis: a disease of the joint as an organ." *Arthritis Rheum* 64(6).

Logan, M., Martin, J. F., Nagy, A.*, et al.* (2002). "Expression of Cre Recombinase in the developing mouse limb bud driven by a Prxl enhancer." *Genesis* 33(2).

Longley, R. L., Woods, A., Fleetwood, A.*, et al.* (1999). "Control of morphology, cytoskeleton and migration by syndecan-4." *J Cell Sci* 112.

Loparic, M., Wirz, D., Daniels, A. U.*, et al.* (2010). "Micro- and nanomechanical analysis of articular cartilage by indentation-type atomic force microscopy: validation with a gel-microfiber composite." *Biophys J* 98(11).

Ma, H. L., Blanchet, T. J., Peluso, D.*, et al.* (2007). "Osteoarthritis severity is sex dependent in a surgical mouse model." *Osteoarthritis Cartilage* 15(6).

Matsumoto, K., Irie, F., Mackem, S. and Yamaguchi, Y. (2010). "A mouse model of chondrocyte-specific somatic mutation reveals a role for Ext1 loss of heterozygosity in multiple hereditary exostoses." *Proc Natl Acad Sci U S A* 107(24).

Mattila, P. K. and Lappalainen, P. (2008). "Filopodia: molecular architecture and cellular functions." *Nat Rev Mol Cell Biol* 9(6).

Moon, J. J., Matsumoto, M., Patel, S.*, et al.* (2005). "Role of cell surface heparan sulfate proteoglycans in endothelial cell migration and mechanotransduction." *J Cell Physiol* 203(1).

Mundy, C., Yasuda, T., Kinumatsu, T.*, et al.* (2011). "Synovial joint formation requires local Ext1 expression and heparan sulfate production in developing mouse embryo limbs and spine." *Dev Biol* 351(1).

Muschter, D., Fleischhauer, L., Taheri, S.*, et al.* (2020). "Sensory neuropeptides are required for bone and cartilage homeostasis in a murine destabilization-induced osteoarthritis model." *Bone* 133.

Neuhold, L. A., Killar, L., Zhao, W.*, et al.* (2001). "Postnatal expression in hyaline cartilage of constitutively active human collagenase-3 (MMP-13) induces osteoarthritis in mice." *J Clin Invest* 107(1).

Oh, E.-S. and Couchman, J. R. (2004). "Syndecans-2 and -4 - Close Cousins, but not Identical Twins." *Mol Cells* 12(2).

Ortega, N., Behonick, D. J. and Werb, Z. (2004). "Matrix remodeling during endochondral ossification." *Trends Cell Biol* 14(2).

Otsuki, S., Hanson, S. R., Miyaki, S.*, et al.* (2010). "Extracellular sulfatases support cartilage homeostasis by regulating BMP and FGF signaling pathways." *Proc Natl Acad Sci U S A* 107(22).

Otsuki, S., Murakami, T., Okamoto, Y.*, et al.* (2017). "Suppression of cartilage degeneration by intra-articular injection of heparan sulfate 6-O endosulfatase in a mouse osteoarthritis model." *Histol Histopathol* 32(7).

Otsuki, S., Taniguchi, N., Grogan, S. P.*, et al.* (2008). "Expression of novel extracellular sulfatases Sulf-1 and Sulf-2 in normal and osteoarthritic articular cartilage." *Arthritis Res Ther* 10(3).

Parsons, S. L., Watson, S. A., Brown, P. D., Collins, H. M. and Steele, R. J. C. (1997). "Matrix Metalloproteinases." *British Journal of Surgery* 84.

Piombo, V. (2017). "Small animal models to understand pathogenesis of osteoarthritis and use of stem cell in cartilage regeneration." *Cell Biochem Funct* 35(1).

Poulain, F. E. and Yost, H. J. (2015). "Heparan sulfate proteoglycans: a sugar code for vertebrate development?" *Development* 142(20).

Prein, C., Warmbold, N., Farkas, Z.*, et al.* (2016). "Structural and mechanical properties of the proliferative zone of the developing murine growth plate cartilage assessed by atomic force microscopy." *Matrix Biol* 50.

Puck, T. T., Cieciura, S. J. and Robinson, A. (1958). "Genetics of somatic mammalian cells, III - Long-term cultivation of euploid cells from human and animal subjects."

Ratzka, A., Kalus, I., Moser, M.*, et al.* (2008). "Redundant function of the heparan sulfate 6-O-endosulfatases Sulf1 and Sulf2 during skeletal development." *Dev Dyn* 237(2).

Ringvall, M., Ledin, J., Holmborn, K.*, et al.* (2000). "Defective heparan sulfate biosynthesis and neonatal lethality in mice lacking N-deacetylase/N-sulfotransferase-1." *J Biol Chem* 275(34).

Sarrazin, S., Lamanna, W. C. and Esko, J. D. (2011). "Heparan sulfate proteoglycans." *Cold Spring Harb Perspect Biol* 3(7).

Sato, H., Takino, T., Okada, Y.*, et al.* (1994). "A matrix metalloproteinase expressed on the surface of invasive tumour cells." *Nature* 370.

Schindelin, J., Arganda-Carreras, I., Frise, E.*, et al.* (2012). "Fiji: an open-source platform for biological-image analysis." *Nat Methods* 9(7).

Schukz, M., Fuster, M. M., Brown, J. R.*, et al.* (2008). "Surfen, a small molecule antagonistof heparan sulfate." *Proc Natl Acad Sci U S A* 105(35).

Sekhon, B. S. (2010). "Matrix metalloproteinases - an overview." *Research and Reports in Biology*.

Seo, J. and Kim, J. (2018). "Regulation of Hippo signaling by actin remodeling." *BMB Rep* 51(3).

Severmann, A. C., Jochmann, K., Feller, K.*, et al.* (2020). "An altered heparan sulfate structure in the articular cartilage protects against osteoarthritis." *Osteoarthritis Cartilage* 28(7).

Severmann, A. C. and Vortkamp, A. (2015). "[Hypertrophic chondrocytes: Programmed cell death or stem cell reservoir?]." *Z Rheumatol* 74(10).

Sgariglia, F., Candela, M. E., Huegel, J.*, et al.* (2013). "Epiphyseal abnormalities, trabecular bone loss and articular chondrocyte hypertrophy develop in the long bones of postnatal Ext1-deficient mice." *Bone* 57(1).

Shu, C. C., Jackson, M. T., Smith, M. M.*, et al.* (2016). "Ablation of Perlecan Domain 1 Heparan Sulfate Reduces Progressive Cartilage Degradation, Synovitis, and Osteophyte Size in a Preclinical Model of Posttraumatic Osteoarthritis." *Arthritis Rheumatol* 68(4).

Stanford, K. I., Wang, L., Castagnola, J.*, et al.* (2010). "Heparan sulfate 2-O-sulfotransferase is required for triglyceride-rich lipoprotein clearance." *J Biol Chem* 285(1).

Stevens-Lapsley, J. E. and Kohrt, W. M. (2010). "Osteoarthritis in Women - Effects of Estrogen, Obesity and Physical Activity." *Women's Health* 6(4).

Stickens, D., Behonick, D. J., Ortega, N.*, et al.* (2004). "Altered endochondral bone development in matrix metalloproteinase 13-deficient mice." *Development* 131(23).

Stickens, D., Zak, B. M., Rougier, N., Esko, J. D. and Werb, Z. (2005). "Mice deficient in Ext2 lack heparan sulfate and develop exostoses." *Development* 132(22).

Stoop, R., van der Kraan, P. M., Buma, P.*, et al.* (1999). "Type II collagen degradation in spontaneous osteoarthritis in C57BL6 and BALBc mice." *Arthritis and Rheumatism* 45(11).

Thysen, S., Luyten, F. P. and Lories, R. J. (2015). "Targets, models and challenges in osteoarthritis research." *Dis Model Mech* 8(1).

Troeberg, L., Lazenbatt, C., Anower, E. K. M. F.*, et al.* (2014). "Sulfated glycosaminoglycans control the extracellular trafficking and the activity of the metalloprotease inhibitor TIMP-3." *Chem Biol* 21(10).

Troeberg, L. and Nagase, H. (2012). "Proteases involved in cartilage matrix degradation in osteoarthritis." *Biochim Biophys Acta* 1824(1).

van der Kraan, P. M., Stoop, R., Meijers, T. H., Poole, A. R. and van den Berg, W. B. (2001). "Expression of type X collagen in young and old C57Bl/6 and Balb/c mice. Relation with articular cartilage degeneration." *Osteoarthritis Cartilage* 9(2).

van Meurs, J., van Lent, P., Stoop, R.*, et al.* (1999a). "Cleavage of aggrecan at the Asn341–Phe342 site coincides with the initiation of collagen damage in murine antigen-induced arthritis - A pivotal role for stromelysin 1 in matrix metalloproteinase activity." *Arthritis and Rheumatism* 42(10).

van Meurs, J., van Lent, P. L. E. M., Holthuysen, A.*, et al.* (1999b). "Kinetics of aggrecanase- and metalloproteinase-induced neoepitopes in various stages of cartilage destruction in murine arthritis." *Arthritis and Rheumatism* 42(6).

Wada, K., Itoga, K., Okano, T., Yonemura, S. and Sasaki, H. (2011). "Hippo pathway regulation by cell morphology and stress fibers." *Development* 138(18).

Wang, W., Zhong, B., Sun, J.*, et al.* (2011). "Down-regulated HS6ST2 in osteoarthritis and Kashin-Beck disease inhibits cell viability and influences expression of the genes relevant to aggrecan metabolism of human chondrocytes." *Rheumatology (Oxford)* 50(12).

Wieland, H. A., Michaelis, M., Kirschbaum, B. J. and Rudolphi, K. A. (2005). "Osteoarthritis - an untreatable disease?" *Nat Rev Drug Discov* 4(4).

Wiesner, S., Lange, A. and Fassler, R. (2006). "Local call: from integrins to actin assembly." *Trends Cell Biol* 16(7).

Wuelling, M. and Vortkamp, A. (2011). "Chondrocyte proliferation and differentiation." *Cartilage and Bone Development and its Disorders* 21.

Xu, D. and Esko, J. D. (2014). "Demystifying heparan sulfate-protein interactions." *Annu Rev Biochem* 83.

Yang, Z., Strickland, D. K. and Bornstein, P. (2001). "Extracellular matrix metalloproteinase 2 levels are regulated by the low density lipoprotein-related scavenger receptor and thrombospondin 2." *J Biol Chem* 276(11).

Zhao, B., Li, L., Lu, Q.*, et al.* (2011). "Angiomotin is a novel Hippo pathway component that inhibits YAP oncoprotein." *Genes Dev* 25(1).

Zhao, B., Li, L., Wang, L.*, et al.* (2012). "Cell detachment activates the Hippo pathway via cytoskeleton reorganization to induce anoikis." *Genes Dev* 26(1).

Zhong, W., Li, Y., Li, L.*, et al.* (2013). "YAP-mediated regulation of the chondrogenic phenotype in response to matrix elasticity." *J Mol Histol* 44(5).

8. List of Publications

8.1. Papers

Severmann, A.C., Jochmann, K., Feller, K., Bachvarova, V., Piombo, V., Holzer, T., Brachvogel, B., Stange, R., Pap, T., Esko, J. D., Hoffmann, D., Vortkamp, V., 2020, *An altered heparan sulfate structure in the articular cartilage protects against osteoarthritis*, Osteoarthritis and Cartilage

Severmann, A.C., und Vortkamp, A., 2015, *Hypertrophe Chondrozyten: Programmierter Zelltod oder Stammzellreservoir?,* Review, Zeitschrift für Rheumatologie 10

8.2. Presentations

Severmann, A.C., Vortkamp, A., 2019, *Interaction of Extracellular Heparan Sulfate Proteoglycans and Integrin Signalling in Cell Mobility and Adhesion*, Young Scientist Exchange Meeting (German and Japanese Societies of Developmental Biologists)

Severmann, A.C., Vortkamp, A., 2019, Heparan sulfates in osteoarthritis and articular cartilage maintenance, Annual Meeting of the German Society for Matrix Biology (special session ExCarBon research consortium)

Severmann, A.C., Vortkamp, A., 2019, *Interaction of Heparan Sulfate and Integrin Signalling in Maintaining the Articular Cartilage*, Annual Meeting of the ExCarBon research consortium

Severmann, A.C., Vortkamp, A., 2019*, Interaction of Heparan Sulfates and Integrin Signalling in Maintaining the Articular Cartilage*, "Lunch Talk", Institute Seminar Centre for Medical Biotechnology

Severmann, A.C., Vortkamp, A., 2018, *Interaction of Heparan Sulfate and Integrin Signalling in Maintaining the Articular Cartilage*, Summer School of the ExCarBon research consortium

Severmann, A.C., Vortkamp, A., 2018*, Interaction of Heparan Sulfate and Integrin Signalling in Maintaining the Articular Cartilage*, Annual Meeting of the ExCarBon research consortium

Severmann, A.C., Vortkamp, A., 2017*, Interaction of Heparan Sulfate and Integrin Signalling in Maintaining the Articular Cartilage*, Annual Meeting of the ExCarBon research consortium

Severmann, A.C., Vortkamp, A., 2017*, Interaction of Heparan Sulfate and Integrin Signalling in Maintaining the Articular Cartilage*, "Lunch Talk", Institute Seminar Centre for Medical Biotechnology

Severmann, A.C., 2017*, Animal Model Systems: Mus Musculus*, BIOME Student Review Talk

Severmann, A.C., 2016*, Heparan Sulfate as a Regulator of Indian Hedgehog Signalling*, BIOME Student Progress Talk

Severmann, A.C., Vortkamp, A., 2016*,* Heparan Sulfate as a Regulator of Indian Hedgehog Signalling, “Lunch Talk”, Institute Seminar Centre for Medical Biotechnology

Severmann, A.C., 2016*, Heparan Sulfates and Embryonic Development*, Annual Retreat of the BIOME core “Genetics and Cell Biology”

Severmann, A.C., 2015*, Sugar and Bone: Heparan Sulfates and Embryonic Development*, Annual Retreat of the BIOME core “Genetics and Cell Biology”

Severmann, A.C., 2015*, Heparan Sulfate as a Regulator of Indian Hedgehog Signalling*, BIOME Student Progress Talk

8.3. Posters

Severmann, A.C., Vortkamp, A., 2019, *Interaction of heparansulfate and integrin signaling in maintaining the articular cartilage,* Evaluation Meeting ExCarBon research consortium

Severmann, A.C., Jochmann, K., Zuk, M., Brachvogel, B., Vortkamp, A., 2019, *Interaction of extracellular heparan sulfate proteoglycans and integrin signalling in cell mobility and adhesion*, Annual Meeting of the Japanese Society of Developmental Biologists

Severmann, A.C., Jochmann, K., Feller (neé Papachristou), K., Vortkamp, A., 2019, *Heparan sulfates in osteoarthritis and articular cartilage maintenance*, Annual Meeting of the German Society for Matrix Biology

Severmann, A.C., Jochmann, K., Zuk, M., Brachvogel, B., Vortkamp, A., 2018, *Interaction of extracellular heparan sulfate proteoglycans and integrin signalling in cell mobility and adhesion*, GfE School 2018 - "Imaging and Modeling Development"

Severmann, A.C., Jochmann, K., Zuk, M., Vortkamp, A., 2018*, Heparan sulfates in osteoarthritis and articular cartilage maintenance*, Gordon Research Conference “Proteoglycan”

Severmann, A.C., Jochmann, K., Vortkamp, A., 2017*, Investigating the role of heparan sulfate proteoglycans and integrin signals in the progression of osteoarthritis*, Annual Retreat of the BIOME core “Genetics and Cell Biology”

9. Annex

9.1. Statistical data

Table 6: Statistical evaluation of degradation signals from gelatine zymography The mean changer factor, its 90% HDI and the according p+-value are displayed for each enzyme in the presence or absence of RA. The respective results are displayed in Fig. 10.

protease	treatment	factor	90% HDI		p^+	stable
proMmp2	-RA	1,018707	0,985581	1,05236791	0,827625	FALSE
active Mmp2		1,01759811	0,98631883	1,04951577	0,827625	FALSE
proMmp9		1,0185035	0,98798052	1,05034204	0,841625	FALSE
active Mmp9						
proMmp2	+RA	0,9383165	0,82979692	1,05091279	0,169125	FALSE
active Mmp2		0,94607946	0,85166359	1,04523739	0,169125	FALSE
proMmp9		0,90065096	0,81715909	0,98874053	0,03475	TRUE
active Mmp9		0,8836855	0,7863978	0,9863651	0,03475	TRUE

Table 7: Statistical evaluation of OARSI scores resulting from DMM surgery at different post-operative time points The mean effect of the time point, its 90% HDI and the according p+-value are displayed. The respective data is show in Fig. 13.

base_time	target_time	effect	90% HDI		p^+	stable
2w	4w	0,22802515	-0,16051306	0,61680967	0,83775	FALSE
2w	8w	1,69745519	1,31797989	2,07586763	1	TRUE
2w	12w	2,23066865	1,8475573	2,61072296	1	TRUE
4w	8w	1,46943004	1,09825852	1,83743981	1	TRUE
4w	12w	2,0026435	1,62991197	2,38146004	1	TRUE
8w	12w	0,53321346	0,1809429	0,88348014	0,994	TRUE

Table 8: Statistical evaluation of OARSI scores from *Glce* and *Hs2st1* mice The mean effect of mutant genotype, its 90% HDI and the according p+-value are displayed. The respective data is show in Fig. 14.

Strain	Surgery	mean	lower	upper	p^+	stable
Glce	DMM	-0,22292715	-0,93213897	0,48207104	0,30225	FALSE
	Sham	-0,3347516	-0,65432601	-0,0080278	0,046	TRUE
Hs2st1	DMM	0,09098315	-0,68097174	0,86531177	0,2845	FALSE
	Sham	0,70690301	0,32580542	1,08681546	0,49975	FALSE

Table 9: Statistical evaluation of cell adhesion in presence of Surfen For each time point (0.5, 1, 2, 16, 24h) the change factors between the different concentrations are displayed, including their 90% HDIs and the respective p^+-values. The experimental results are shown in Fig. 19.

Time Point	Base_conc	Target_conc	factor	90% HDI		p+	stable
0.5h	DMSO	2.5µM Surfen	0.70391811	0.5058272	0.93889033	0.023375	TRUE
	DMSO	5µM Surfen	0.49276821	0.35340109	0.66393687	0.00025	TRUE
	DMSO	10µM Surfen	0.28769229	0.20513639	0.38885727	0	TRUE
	2.5µM Surfen	5µM Surfen	0.71194238	0.51493326	0.95458804	0.029875	TRUE

	2.5µM Surfen	10µM Surfen	0.41563435	0.29893025	0.56167265	0	TRUE
	5µM Surfen	10µM Surfen	0.59583174	0.41777227	0.81361288	0.003875	TRUE
1h	DMSO	2.5µM Surfen	0.5628941	0.42995107	0.71718908	0	TRUE
	DMSO	5µM Surfen	0.47477937	0.3747285	0.59251317	0	TRUE
	DMSO	10µM Surfen	0.33770707	0.26512761	0.42166744	0	TRUE
	2.5µM Surfen	5µM Surfen	0.85636353	0.65292175	1.10088659	0.148375	FALSE
	2.5µM Surfen	10µM Surfen	0.60772938	0.47201464	0.76681112	5.00E-04	TRUE
	5µM Surfen	10µM Surfen	0.71849819	0.55894472	0.89845993	0.010125	TRUE
2h	DMSO	2.5µM Surfen	0.8767484	0.77366454	0.98811213	0.0355	TRUE
	DMSO	5µM Surfen	0.85711151	0.75208337	0.97291797	0.0215	TRUE
	DMSO	10µM Surfen	0.59958016	0.52466991	0.68205009	0	TRUE
	2.5µM Surfen	5µM Surfen	0.98019201	0.86088883	1.10749189	0.385875	FALSE
	2.5µM Surfen	10µM Surfen	0.68560996	0.60192536	0.77399745	0	TRUE
	5µM Surfen	10µM Surfen	0.70134259	0.62072039	0.78838364	0	TRUE
16h	DMSO	2.5µM Surfen	0.84626129	0.72614523	0.97770369	0.030875	TRUE
	DMSO	5µM Surfen	0.93879824	0.80391344	1.08585951	0.2275	FALSE
	DMSO	10µM Surfen	0.79326292	0.68060939	0.91976526	0.006375	TRUE
	2.5µM Surfen	5µM Surfen	1.11395509	0.95734454	1.28612437	0.877875	FALSE
	2.5µM Surfen	10µM Surfen	0.94124349	0.80596033	1.09074422	0.238875	FALSE
	5µM Surfen	10µM Surfen	0.84860856	0.72504546	0.98441994	0.035625	TRUE
24h	DMSO	2.5µM Surfen	0.98547438	0.89269606	1.08562028	0.386375	FALSE
	DMSO	5µM Surfen	0.90183261	0.81386961	0.99571062	0.043125	TRUE
	DMSO	10µM Surfen	0.6915657	0.62521714	0.76241327	0	TRUE
	2.5µM Surfen	5µM Surfen	0.91676427	0.82779038	1.01145757	0.0725	FALSE
	2.5µM Surfen	10µM Surfen	0.70299252	0.6359192	0.77456672	0	TRUE
	5µM Surfen	10µM Surfen	0.76832542	0.69329689	0.84843116	0	TRUE

Table 10: Statistical evaluation of life cell imaging data For each feature the mean change factor between 5µM Surfen and the DMSO control, its 90% HDI and the respective p^+-value are displayed. The results are shown in Fig. 20.

Feature	**Time Point**	**factor**	**90% HDI**		**p^+**	**stable**
Lamellipodium	Start	0,74742916	0,66026849	0,83844644	0	TRUE
Pseudopodia		0,95316939	0,83504662	1,08038124	0,26	FALSE
Filopodia		1,41599438	1,16617623	1,69648944	0,998875	TRUE
Protrusions		1,03225929	0,91273395	1,16429169	0,652125	FALSE
Lamellipodium	End	0,81090022	0,74066011	0,8821882	0	TRUE
Pseudopodia		0,96400913	0,87276048	1,05971755	0,26	FALSE
Filopodia		1,34034281	1,13783772	1,56329261	0,998875	TRUE
Protrusions		1,02313766	0,9347931	1,11891894	0,652125	FALSE
migratory	Full video	0,34281463	0,15015971	0,60957269	0,001375	TRUE
polarised		0,66715062	0,49952811	0,86156371	0,0055	TRUE
not viable		1,53484824	0,92378402	2,37113755	0,91375	FALSE

Table 11: Statistical evaluation of the formation of FA and SF in presence of Surfen For each condition (1h adhesion, 24h adhesion, 1h addition) the mean change factor between DMSO and 5µM

Surfen is given, as well as its 90% HDI and the according p^+-value. The experimental results are shown in Fig. 21.

	condition	factor	90% HDI		p^+	stable
FA (Paxillin)	Adhesion 1h	0,50857943	0,35396726	0,65844501	0	TRUE
	Adhesion 24h	0,84077727	0,50492036	1,2901228	0,22275	FALSE
	Addition 1h	1,55710469	1,1937106	2,08040778	0,99925	TRUE
SF (Actin)	Adhesion 1h	0,412475889	0,286034011	0,552712849	0	TRUE
	Adhesion 24h	0,92545559	0,776718492	1,088443434	0,198375	FALSE
	Addition 1h	1,27557423	1,118692995	1,488456424	0,99975	TRUE

Table 12: Statistical evaluation of YAP localisation in Surfen-treated cells For each condition (1h adhesion, 24h adhesion, 1h addition) the change factor between DMSO and 5µM Surfen, its 90% HDI and the respective p+-value are given. The experimental results are shown in Fig. 23.

	condition	factor	90% HDI		p^+	stable
nuclear YAP	Adhesion, 1h	0,81075655	0,67820429	0,95127717	0,01575	TRUE
	Adhesion, 24h	0,56430739	0,4523305	0,67965617	0	TRUE
	Addition, 1h	0,92833318	0,82728508	1,03336704	0,125125	FALSE

9.2. Acknowledgements

First of all, I would like to thank Andrea Vortkamp for giving me the opportunity to work in her lab and for her supervision and support during my time spend in her department.

A particularly big thank you goes to Katja Jochmann, Melanie Zuk and Manuela Wülling, who were not only always ready to discuss data and scientific ideas, but also participated in uncountable peculiar activities inside and outside the lab.

Of course, I would like to thank everyone from the Vortkamp lab for the great time spend at work, and I'm especially thankful to the other, smaller Tina, and Meike for their practical help getting all my experiments done. Additionally, I would like to express my gratitude to our animal care takers, particularly Peppi, for keeping up with my mice.

Christoph Waterkamp did a great job performing the Bayesian statistic for all my data (in quite a short time) and I owe him a lot of cake.

I would also like to thank my colleagues from the ExCarBon network – Dominique for teaching me the DMM technique, Lutz for doing the AFM analysis, and also Shahed and Matthias for the great collaboration and fun time spend at meetings.

Last but not least, I want to thank my family for their support during my Bachelor's, Master's and Doctoral degrees. And my friends Linda, Ceci and Gesche (for scientific AND non-scientific support) and Christoph Hruschka (for non-scientific support).

Curriculum Vitae

The CV is not included in the online version due to data protection regulations.

Der Lebenslauf ist in der Online-Version aus Gründen des Datenschutzes nicht enthalten.

Statutory declarations

Declaration:

In accordance with § 6 (para. 2, clause g) of the Regulations Governing the Doctoral Proceedings of the Faculty of Biology for awarding the doctoral degree *Dr. rer. nat.*, I hereby declare that I represent the field to which the topic “Heparan sulfates as regulators of articular cartilage integrity and cell-matrix interactions” is assigned in research and teaching and that I support the application of Ann-Christine Severmann.

_____

Name of the scientific supervisor/member of the University of Duisburg-Essen

Essen, date _____, _____

Signature of the supervisor/member of the University of Duisburg-Essen

Declaration:

In accordance with § 7 (para. 2, clause d and f) of the Regulations Governing the Doctoral Proceedings of the Faculty of Biology for awarding the doctoral degree *Dr. rer. nat.*, I hereby declare that I have written the herewith submitted dissertation independently using only the materials listed, and have cited all sources taken over verbatim or in content as such.

Essen, date _____, _____

Signature of the doctoral candidate

Declaration:

In accordance with § 7 (para. 2, clause e and g) of the Regulations Governing the Doctoral Proceedings of the Faculty of Biology for awarding the doctoral degree *Dr. rer. nat.*, I hereby declare that I have undertaken no previous attempts to attain a doctoral degree, that the current work has not been rejected by any other faculty, and that I am submitting the dissertation only in this procedure.

Essen, date _____, _____

Signature of the doctoral candidate